# Novel regulatory mechanisms of the RhoGAP tumor suppressor proteins Deleted in Liver Cancer 1 & 3

Von der Fakultät Energie-, Verfahrens- und Biotechnik
der Universität Stuttgart zur Erlangung der Würde eines Doktors der Naturwissenschaften (Dr. rer. nat.) genehmigte Abhandlung

Vorgelegt von

**Yannick Frey**

aus Ludwigsburg

Hauptberichter: Prof. Dr. Monilola Olayioye

Mitberichter: Prof. Dr. Hesso Farhan

Tag der mündlichen Prüfung: 25.04.2023

Institut für Zellbiologie und Immunologie der Universität Stuttgart

2024

# Table of content

## Declaration / Erklärung

I, Yannick Frey, hereby assure that I performed this work independently without further help or other materials than stated. Passages and ideas from other sources have been clearly indicated.

Hiermit erkläre ich, Yannick Frey, dass ich die vorliegende Arbeit selbstständig angefertigt habe. Es wurden nur die in der Arbeit ausdrücklich benannten Quellen und Hilfsmittel benutzt. Wörtlich oder sinngemäß übernommenes Gedankengut habe ich als solches kenntlich gemacht.

Stuttgart, _____ _____

Place, Date Yannick Frey

## List of figures

## List of tables

## Abbreviations

| | |
|---|---|
| 3D | three dimentional |
| aa | amino acid |
| AJ | adherens junction |
| AKT | protein kinase B |
| AP-1 | adaptor protein complex 1 |
| aPKC | atypical protein kinase C |
| APS | ammonium persulfate |
| ArfGEF | ADP ribosylation factor GEF protein |
| ARHGEF | Rho guanine nucleotide exchange factor |
| Arp2/3 | actin-related protein 2/3 |
| BC | breast cancer |
| BSA | bovine serum albumin |
| BTZ | bortezomib |
| Cdc | cell division control protein |
| CDK5 | cyclin-dependent kinase 5 |
| cDNA | complementary DNA |
| ceRNA | competing endogenous RNA |
| CHX | cycloheximide |
| COSMIC | Catalogue Of Somatic Mutations In Cancer |
| CRC | colorectal cancer |
| CRL4A | cullin 4A-RING ubiquitin ligase |
| CTEN | C-terminal tensin-like |
| cv-c | crossveinless-c |
| DAPI | 4′,6-diamidino-2-phenylindole |
| Dbs | DBL's big sister (Dbl family RhoGEF) |
| DCAF7 | DDB1- and CUL4-associated factor 7 |
| DDB1 | DNA damage-binding protein 1 |

| | |
|---|---|
| ddH2O | double deionized water |
| Dia1 | diaphanous homolog 1 |
| DLC | Deleted in Liver Cancer |
| Dlg | discs large |
| DMEM | Dulbecco's Modified Eagle Medium |
| DMSO | dimethyl sulfoxide |
| DUB | deubiquitinase |
| E1 | ubiquitin-activating enzyme |
| E2 | ubiquitin-conjugating enzyme |
| E3 | ubiquitin ligase |
| Ect2 | epithelial cell-transforming sequence 2 oncogene |
| EDTA | ethylenediaminetetraacetic acid |
| EEA1 | early endosome antigen 1 |
| EF1A1 | eukaryotic elongation factor 1A1 |
| EGF | epidermal Growth Factor |
| EGFR | epidermal Growth Factor Receptor |
| EMT | epithelial-to-mesenchymal transition |
| ER/PR | estrogen and progesterone receptors |
| ErbB2 | receptor tyrosine-protein kinase erbB-2 |
| ERC | endocytic recycling compartment |
| ERK1/2 | extracellular signal-regulated kinase 1/2 (alternative names MAPK1/2) |
| EZH2 | enhancer of zeste homolog 2 |
| FA | focal adhesion |
| Fab1p | FYVE finger-containing phosphoinositide kinase |
| FAK | focal adhesion kinase |
| FAPP1 | four-phosphate-adaptor protein 1 |
| FAT | focal adhesion targeting |

| | |
|---|---|
| FBXW5 | F-box/WD repeat-containing protein 5 |
| FCS | fetal calf serum |
| FOXK1 | forkhead box protein K1 |
| FP | forward primer |
| GAP | GTPase-activating protein |
| GDI | guanine nucleotide dissociation inhibitor |
| GDP | guanosine diphosphate |
| GEF | guanine nucleotide exchange factor |
| GFP | green fluorescent protein |
| Grp1 | general receptor for phosphoinositides isoform 1 |
| GST | glutathione S-transferase |
| GTP | guanosine triphosphate |
| GTPase | GTP hydrolase |
| h | hour |
| H2SO4 | sulfuric acid |
| H3K27me3 | histone 3 lysine 27 trimethylation |
| HA tag | hemagglutinin tag |
| HCC | hepatocellular carcinoma |
| HECT family | homologous to the E6-AP Carboxyl Terminus |
| HECTD1 | HECT domain protein 1 |
| HER2 | receptor tyrosine-protein kinase erbB-2, ErbB2 |
| HPLC | high-performance liquid chromatography |
| HRP | horseradish peroxidase |
| ICGC | The International Cancer Genome Consortium |
| IDR | intrinsically disordered region |
| IF | immunofluorescence |
| IPTG | isopropyl β-d-1-thiogalactopyranoside |
| IQGAP1 | Ras GTPase-activating-like protein IQGAP1 |

| | |
|---|---|
| JNK | c-Jun N-terminal kinase |
| K48 | lysine 48 |
| kb | kilobase |
| KH2PO4 | potassium dihydrogen phosphate |
| Kif1B | kinesin-like protein KIF1B |
| LB | lysogeny broth |
| LD motif | leucine-aspartate motif |
| Lgl | lethal giant larvae |
| LOH | loss of heterozygosity |
| LTP | lipid transfer protein |
| LUAD | lung adenocarcinoma |
| mAb | Monoclonal antibody |
| MACC1 | Metastasis-associated in colon cancer protein 1 |
| Mdm2 | E3 ubiquitin-protein ligase Mdm2 |
| MEK | Dual specificity mitogen-activated protein kinase kinase |
| MEM | Minimal Essential Medium |
| MFI | mean fluorescence intensity |
| MgCl2 | magnesium chloride |
| Min | minute(s) |
| miRNA | microRNA |
| MLC | myosin light chain |
| MMP9 | matrix metalloproteinase-9 |
| mRNA | messenger RNA |
| mTOR | mammalian target of rapamycin |
| Na2HPO4 | disodium hydrogen phosphate |
| Na3VO4 | sodium orthovanadate |
| NaDOC | sodium deoxychylate |
| NaH2PO4 | sodium dihydrogen phosphate |

| | |
|---|---|
| NaHCO3 | sodium hydrogen carbonate |
| nanoLC-MS/MS | nano-liquid chromatography tandem mass spectrometry |
| NaOH | sodium hydroxide |
| NEB | NP-40/EDTA buffer |
| NES | nuclear export signal |
| Ni-NTA beads | nickel Nitriloacetic acid beads |
| NLS | nuclear localization signal |
| NMR | nuclear magnetic resonance |
| NSCLC | non-small cell lung cancer |
| P-Rex1 | phosphatidylinositol 3,4,5-trisphosphate-dependent Rac exchanger 1 protein |
| P-Rex2a | phosphatidylinositol 3,4,5-trisphosphate-dependent Rac exchanger 2a protein |
| pAb | polyclonal antibody |
| PAK kinase | P21-activated kinase |
| Pals1 | protein associated with Lin seven 1 |
| Par | partitioning defective |
| PATJ | pals1-associated tight junction protein |
| PBS | phosphate buffered saline |
| PBST | PBS-Tween |
| PCR | polymerase chain reaction |
| PDZ domain | PSD-95, ZO-1 and discs large domain |
| PDZL | PDZ ligand motif |
| PFA | paraformaldehyde |
| PH domain | pleckstrin homology domain |
| PI3K | phosphoinositide 3-kinase |
| PIP2 | phosphatidylinositol 4,5-bisphosphate |
| PIP3 | phosphatidylinositol (3,4,5)-trisphosphate |

| | |
|---|---|
| PKA | protein kinase A |
| PKD | protein kinase D |
| pLDDT | predicted local distance difference test |
| PMSF | phenylmethanesulfonyl fluoride |
| PP2A | protein phosphatase 2 A |
| PRC2 | polycomb repressive complex 2 |
| PTB domain | phosphotyrosine-binding domain |
| PTM | post-translational modification |
| PUM2 | pumilio RNA Binding Family Member 2 |
| PVDF | polyvinylidinedifluoride |
| qRT-PCR | real-time quantitative Reverse Transcription PCR |
| Rab8 | Ras-associated binding (Rab) protein 8 |
| Ras | "Rat sarcoma virus", small GTPase family |
| Rho | ras homologous protein family |
| RIAM | rap1-GTP-interacting adaptor molecule |
| RING family | Really Interesting New Gene domain family |
| RIPA | radioimmunoprecipitation assay buffer |
| RISC | RNA-induced silencing complex |
| RNAi | RNA interference |
| ROCK | Rho-associated kinase |
| ROI | regions of interest |
| RP | reverse primer |
| RPLP0 | Ribosomal Protein Lateral Stalk Subunit P0 |
| rpm | revolutions per minute |
| RPMI | Roswell Park Memorial Institute Medium |
| SAM | sterile α-motif |
| s.d. | standard deviation |
| SDS-PAGE | sodium dodecyl sulfate–polyacrylamide gel electrophoresis |

| | |
|---|---|
| s.e.m. | standard error of the mean |
| SH2/3 domain | Src homology 2/3 domain |
| SH2B1β | Src homology 2 (SH2) B adaptor protein 1 |
| shRNA | short hairpin RNA |
| siRNA | small interfering RNA |
| SNP | single nucleotide polymorphism |
| SNX27 | sorting nexin 27 |
| Src | proto-oncogene tyrosine-protein kinase Src, short for Sarcoma |
| StAR domain | steroidogenic acute regulatory domain |
| STARD | START-domain-containing protein |
| START | StAR protein-related lipid transfer |
| TAZ | transcriptional coactivator with PDZ-binding motif |
| TCGA | The Cancer Genome Atlas |
| TEB | Tris/EDTA buffer |
| TEM4 | tumor endothelial marker 4 |
| TEMED | tetramethyldiethyldiamine |
| TIAM1 | t-lymphoma invasion and metastasis-inducing protein 1 |
| TNA | triple negative A |
| TNB | triple negative B |
| TNBC | triple-negative breast cancer |
| Tris | tris-(hydroxymethyl)-aminomethane |
| Ub | ubiquitin |
| USP7 | ubiquitin-specific-processing protease 7 |
| UTR | untranslated region |
| V/v | volume per volume |
| Vac1p | vacuolar protein-targeting protein |
| Vav1, 2 and 3 | proto-oncogene vav 1, 2 and 3 |

| | |
|---|---|
| VEGF | vascular endothelial growth factor |
| W/w | weight per weight |
| WASP complex | Wiskott-Aldrich syndrome proteins |
| WAVE complex | WASP-family verprolin homologous protein complex |
| WB | Western Blot |
| YAP | Yes-associated protein 1 |
| βPIX | PAK-interacting exchange factor beta |

## Summary

Rho family small GTPases are key regulators of cytoskeletal remodeling, thereby controlling a number of important cellular processes such as cell adhesion and migration, cell cycle progression, and vesicular transport. Rho GTPases act as molecular switches that can be activated by guanine nucleotide exchange factors (GEFs) and deactivated by GTPase-activating proteins (GAPs) to ensure their spatially and temporally fine-tuned activation. During cancer progression, the loss of cell polarity and cell-cell contacts, as well as the acquisition of a more motile phenotype, allows epithelial cells to invade into adjacent tissues. These phenotypic changes are facilitated by aberrant Rho signaling, often caused by altered expression or activity of Rho GTPase regulators.

The three structurally related members of the DLC (deleted in liver cancer) family of RhoGAP proteins have emerged as important tumor suppressors that are frequently downregulated in various malignancies. In many cases, DLC1 and DLC3 expression is impaired by genetic or epigenetic means. However, post-translational regulation of these proteins in tumors that retain transcript expression is insufficiently understood.

In this study, dysregulation of DLC1 expression on the protein level via rapid turnover through the ubiquitin-proteasome system was demonstrated in breast cancer cells. Using mass spectrometry, two novel DLC1 interaction partners were identified, the ubiquitin-ligase HECTD1 and the deubiquitinating enzyme ubiquitin-specific-processing protease 7 (USP7). Pharmacological inhibition of USP7 led to a rapid decrease in DLC1 protein levels, while siRNA-mediated HECTD1 depletion increased DLC1 expression markedly and impaired its degradation. In addition, DLC1 abundance at focal adhesions, its primary site of action, was altered as observed by immunofluorescence microscopy. These results suggest opposing roles for USP7 and HECTD1 in DLC1 protein homeostasis and may provide avenues to address downregulation of DLC1 protein levels in cancer.

In the second part of this work, a nuclear export sequence (NES) in DLC1 was identified, the mutation of which entraps the protein in the nucleus. This will aid to study the regulation of DLC1 translocation between the cytoplasm and the nucleus and its function in the latter compartment.

Finally, I characterized a novel polybasic region (PBR) in DLC3 responsible for binding to membranes, identified by *in silico* sequence analysis and validated it *in cellulo*. Furthermore, a potential phosphorylation-dependent mechanism that regulates DLC3 membrane association was uncovered. I postulate that disruption of this regulatory mechanism by cancer-associated mutations could prevent the correct subcellular positioning of DLC3, leading to its functional inactivation.

## Zusammenfassung

Die kleinen GTPasen der Rho-Familie sind wichtige Regulatoren für den Umbau des Zytoskeletts und steuern damit eine Reihe wichtiger zellulärer Prozesse wie Zelladhäsion und -migration, den Verlauf des Zellzyklus und den vesikulären Transport. Rho-GTPasen fungieren als molekulare Schalter, die durch Guaninnukleotid-Austauschfaktoren (GEFs) aktiviert und durch GTPase-aktivierende Proteine (GAPs) deaktiviert werden können, um ihre räumlich und zeitlich fein abgestimmte Aktivierung zu gewährleisten. Während der Krebsentwicklung ermöglicht der Verlust der Zellpolarität und der Zell-Zell-Kontakte sowie der Erwerb eines motileren Phänotyps den Epithelzellen, in angrenzendes Gewebe einzudringen. Diese phänotypischen Veränderungen werden durch eine gestörte Rho-Signalgebung begünstigt, die häufig durch eine veränderte Expression oder Aktivität von Rho-GTPase-Regulatoren verursacht wird.

Die drei strukturell verwandten Mitglieder der DLC-Familie (deleted in liver cancer) von RhoGAP-Proteinen haben sich als wichtige Tumorsuppressoren erwiesen, die bei verschiedenen malignen Erkrankungen häufig herunterreguliert werden. In vielen Fällen ist die Expression von DLC1 und DLC3 durch genetische oder epigenetische Faktoren beeinträchtigt. Die posttranslationale Regulation dieser Proteine in Tumoren, die ihre Transkription aufrechterhalten, ist jedoch nur unzureichend verstanden.

In dieser Studie wurde in Brustkrebszellen eine Dysregulation der DLC1-Expression auf Proteinebene durch schnellen Umsatz über das Ubiquitin-Proteasom-System nachgewiesen. Mithilfe von Massenspektrometrie wurden zwei neue DLC1-Interaktionspartner identifiziert: die Ubiquitin-Ligase HECTD1 und das deubiquitinierende Enzym ubiquitin-specific-processing protease 7 (USP7). Die pharmakologische Hemmung von USP7 führte zu einer raschen Abnahme des DLC1-Proteinspiegels, während die siRNA-vermittelte Depletion von HECTD1 die DLC1-Expression deutlich erhöhte und seinen Abbau beeinträchtigte. Außerdem veränderte sich die DLC1-Konzentration an fokalen Adhäsionen, dem primären Wirkungsort von DLC1, wie durch Immunfluoreszenzmikroskopie festgestellt wurde. Diese Ergebnisse deuten auf eine gegensätzliche Rolle von USP7 und HECTD1 bei der DLC1-Proteinhomöostase hin und könnten Wege aufzeigen, wie die Herabregulierung des DLC1-Proteinspiegels bei Krebs angegangen werden kann.

Im zweiten Teil dieser Arbeit wurde eine Kernexportsequenz (NES) in DLC1 identifiziert, deren Mutation das Protein im Zellkern zurückhält. Dies wird dazu beitragen, die Regulierung der Translokation von DLC1 zwischen dem Zytoplasma und dem Zellkern und seine Funktion in letzterem Kompartiment zu untersuchen.

Schließlich habe ich eine neuartige polybasische Region (PBR) in DLC3 charakterisiert, die für die Bindung an Membranen verantwortlich ist und durch *in silico* Sequenzanalyse identifiziert und *in cellulo* validiert wurde. Darüber hinaus wurde ein potenzieller phosphorylierungsabhängiger Mechanismus aufgedeckt, der die DLC3-Membranassoziation reguliert. Ich postuliere, dass eine Störung dieses Regulationsmechanismus durch krebsassoziierte Mutationen die korrekte subzelluläre Positionierung von DLC3 verhindern könnte, was zu seiner funktionellen Inaktivierung führt.

# 1 Introduction

## 1.1 The Rho GTPase protein family

### 1.1.1 General cellular functions of Rho GTPases

Rho GTPases are a subgroup of the Ras superfamily of small GTPases, besides the Ras, Rab, Arf and Ran families. The group itself comprises some 20 proteins which can be further subdivided in 8 subgroups, with RhoA, Rac1 and Cdc42 as the best characterized family members (Boureux et al. 2007; Wherlock and Mellor 2002). Through their more than 60 downstream effectors, they integrate a wide range of extracellular stimuli and translate them into local changes in cytoskeleton dynamics (Etienne-Manneville and Hall 2002). Because the actin and microtubule cytoskeleton acts as the structural backbone for cell morphology, polarity and several dynamic processes, Rho GTPases are directly and indirectly regulating most cellular processes, such as cell adhesion, migration, gene transcription, cell cycle progression and secretion (Boureux et al. 2007). More specifically, the Rho GTPase effectors include serine/threonine kinases, tyrosine kinases, lipid kinases, lipases, oxidases, and scaffold proteins which themselves can in turn trigger a plethora of signaling cascades (Jaffe and Hall 2005). The vast possibilities of downstream signaling necessitate tightly controlled regulation of Rho activation and inactivation (see section 1.1.2). In addition, they also make a certain degree of specialization of the individual Rho family members appear highly plausible.

Indeed, the activation of certain Rho GTPase subfamilies happens in different cellular contexts and results in differing phenotypes of actin cytoskeleton changes. For example, RhoA activation is associated with bundling of actin and myosin filaments, leading to stress fiber formation, as well as the clustering of integrins and associated proteins, which form focal adhesions (Hall 1998). Rac1 activation leads to the assembly of peripheral actin networks forming lamellipodia and membrane ruffles, whereas Cdc42 activity is characterized by enhanced filopodia formation (Hall 1998). These complex actin phenotypes are mediated by distinct actin-remodeling GTPase effector proteins: Downstream of RhoA, the activation Rho-associated kinase (ROCK) mediates phosphorylation of myosin light chain (MLC), which in turn promotes the assembly of actomyosin filaments. In cooperation with the activity of actin-bundling formins like Dia1, this increases stress fiber formation and cellular tension (Bishop and Hall 2000; Jaffe and Hall 2005). Cdc42 and Rac1 signal through the WASP and WAVE complexes, respectively, to activate actin polymerization via the actin-related protein 2/3 (Arp2/3) complex (Jaffe and Hall 2005). Further, via PAK kinase induced inactivation of MLC kinase, their activity can lead to reduced MLC phosphorylation and thus inhibition of actomyosin assembly (Bishop and Hall 2000). This illustrates the often antagonistic regulatory behavior of certain competing Rho GTPase downstream signaling pathways.

Even closely related subfamily members can take on both redundant and divergent roles. For instance, the highly homologous Rho subfamily members of Rho GTPases RhoA, RhoB and RhoC, show some differences in binding of key effector proteins (Wheeler and Ridley 2004). Additionally, whereas RhoA and RhoC reside exclusively on the plasma membrane, two distinct RhoB pools exist at the plasma membrane and the endolysosomal compartment (Gong et al. 2018). In accordance with this, RhoB has a unique role in vesicular trafficking as a regulator of actin assembly on endosomes. Hyperactivation of RhoB leads to the formation of an actin coat around the endosomes and reduces endosomal motility by their strong association with subcortical actin fibers (Fernandez-Borja et al. 2005).

### 1.1.2 Regulation of Rho GTPases

As outlined above, Rho GTPases require multilevel spatial and temporal control to fulfill their manifold functions. Generally, Rho GTPases act as molecular switches between an active GTP-bound state and an inactive GDP-bound state. They are targeted to the plasma membrane or other endomembranes by C-terminal prenylation, which acts as a lipid anchor. Additionally, their activity is directly controlled by three distinct protein classes of regulators. Activation is mediated by guanine nucleotide exchange factors (GEFs) which exchange the bound GDP for GTP, thus enabling the binding of downstream effectors. Conversely, GTPase-activating proteins (GAPs) catalyze the low intrinsic GTPase activity of the Rho GTPase, resulting in GTP hydrolysis and signal termination. The class of guanine nucleotide dissociation inhibitors (GDIs) was classically thought of as passive shuttles, which extract the inactive GTPase from the membrane and sequester it in a soluble cytoplasmic pool (Garcia-Mata et al. 2011). However, recent evidence suggests that these regulators can also extract and consequently redistribute GTPases in their active state from membranes, ascribing them a more active role in regulating Rho signaling (Golding et al. 2019). The Rho GTPase activity cycle is schematically depicted below in Fig. 1. In mammals, the number of GEFs and GAPs identified is much larger than the number of Rho GTPases, approximately 80 and 70, respectively. In addition to their catalytic domains, interaction and activation domains provide possibilities for a large and precisely tunable regulatory network (Vigil et al. 2010).

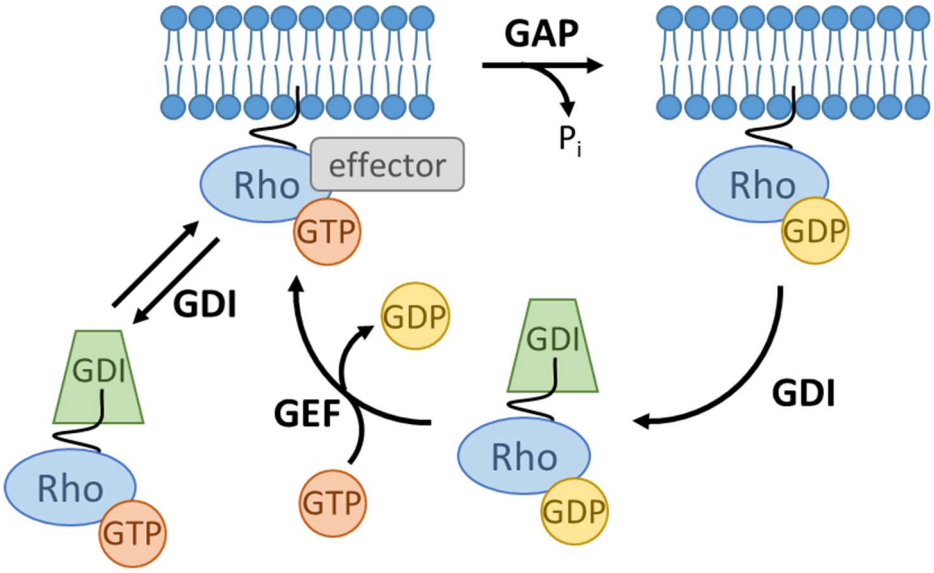


**Figure 1: Regulation of Rho GTPase activity by GAPs, GEFs and GDIs.** Schematic representation of the Rho GTPase activity cycle by guanine nucleotide exchange factors (GEFs) GTPase-activating proteins (GAPs) and guanine nucleotide dissociation inhibitors (GDIs). Modified from (Golding et al. 2019).

On the molecular level, prenylation is carried out by three classes of enzymes that attach either farnesyl or geranylgeranyl groups to cysteine residues in their target proteins. Substrates of farnesyltransferase and geranylgeranyltransferase undergo modification with a single prenyl group and are characterized by a C-terminal CAAX motif, whereby C represents the cysteine residue, A any aliphatic amino acid and X an arbitrary amino acid (Reiss et al. 1990).

When Rho GTPases change their activation status, they undergo a universal conformational change depending on the switch I and II regions, which show increased flexibility (Milburn et al. 1990). The proposed mechanism relies on a conserved threonine residue, that coordinates $Mg^{2+}$ via its side chain, and a glycine residue as part of a conserved DXXG motif (Farrar et al. 1997; Vetter and Wittinghofer 2001). GEF proteins catalyze the intrinsically slow release of the GDP from the GTPase by interaction with both switch domains (Klebe et al. 1995) This involves a series of reaction steps, eventually leaving a binary nucleotide-free GEF-GTPase complex to which then the higher concentrated GTP is preferentially bound back (Vetter and Wittinghofer 2001). The catalytic function of GAPs is canonically mediated by a highly conserved arginine residue in a loop structure referred to as arginine finger (Scheffzek et al. 1997; Ahmadian et al. 1997). Its insertion into the GTPase active site stabilizes the position of the GTPase glutamine residue that coordinates the water molecule required for GTP hydrolysis (Scheffzek et al. 1997). Furthermore, this causes a crucial charge shift towards the β-phosphate in the GTP (Allin et al. 2001). After GTP hydrolysis, the release of the γ-phosphate allows the two switch regions to fall back into their GDP-specific conformation (Vetter and Wittinghofer 2001).

### 1.1.3 Rho GTPases in epithelial cell polarity

From an evolutionary perspective, epithelial tissues in multicellular organisms arose from the requirement for a partition of their internal contents from the outer surroundings (Cereijido et al. 2004). Consequentially, apical-basolateral cell polarity is necessary for the directional tissue morphogenesis and cellular transport, and is thus a major characteristic of higher epithelial tissues. Furthermore, the spatial organization of signaling pathways allows for the differential interpretation and integration of cues from the extracellular microenvironment and their translation into appropriate downstream signaling pathways with respect to control of cell proliferation, apoptosis, metabolism, differentiation and motility (Rodriguez-Boulan and Macara 2014). Epithelial cells adequately meet these requirements through special provisions. As these cells grow in uniformly polarized epithelial sheets, they are kept together by adherens junctions, whereas tight junctions seal the interior from the outside environment. Furthermore, the distinct apical and basolateral membranes with asymmetric composition of receptors, transporter proteins, lipids and other signaling molecules, are maintained by a polarized trafficking machinery. This includes secretory organelles and endolysosomal compartments (Rodriguez-Boulan and Macara 2014).

Three major protein complexes have been identified to play essential roles in the maintenance of polarized signaling. Originally discovered in *C. elegans*, the partitioning defective (Par) protein family contains among others the protein kinases Par1 and Par4, as well as the multidomain adaptor proteins Par3 and Par6, which act in a complex with atypical protein kinase C (aPKC). The Crumbs complex was identified in *Drosophila* and includes the transmembrane protein Crumbs3, as well as Pals1 (Protein associated with Lin seven 1) and Pals1-associated tight junction protein (PATJ) (Ellenbroek et al. 2012). Both of these complexes define the apical membrane compartment and thus act in an antagonistic manner towards the Scribble complex. This protein assembly, also first described in *Drosophila*, entails Scribble, Discs large (Dlg) and Lethal giant larvae (Lgl).and localizes to basolateral membranes. A defining motif in cell polarity regulation is the mutual exclusion between protein complexes from their respective domains. Commonly, this is achieved by phosphorylation of trespassing proteins either by aPKC for the apical side or by Par1 at the basolateral cortex (Rodriguez-Boulan and Macara 2014).

For the establishment of cell polarity, cells have to undertake extensive cytoskeletal rearrangements and organelle repositioning. Therefore, crosstalk between polarity proteins and Rho GTPases is required (Iden and Collard 2008). A key step in polarization is the formation of cell-cell junctions through calcium-dependent cell adhesion molecules, such as E-cadherin. During this process, lamellipodia and filopodia, controlled by Cdc42 and Rac1, respectively, assemble into nascent adhesions which contain E-Cadherin and tight-junction

proteins (Ebnet 2008). In return, the E-Cadherin clustering and ligation of intercellular nectins can further activate Rac1 and Cdc-42 (Nakagawa et al. 2001; Kim et al. 2000; Fukuhara et al. 2004). As polarity is established and later maintained, polarity proteins often serve as scaffolds for specific GEF and GAP proteins, which enable the precise spatial and temporal control of Rho GTPase activity. As a consequence of the exclusive localization of polarity proteins, there are antagonistic Rac and RhoA activity gradients along the apical-basal axis of epithelial cells. The ongoing development of genetically encoded biosensors for Rho GTPase activity has allowed visualization of, and furthered our understanding of, the spatiotemporal Rho crosstalk in cell polarity (Yamada and Nelson 2007). The recruitment of the Rac1 GEF TIAM1 to Par3 is essential for polarization and the formation of functional tight junctions and further couples Rac1 and aPKC activation (O'Brien et al. 2001; Mertens et al. 2005). With the progression of cell-cell junction stabilization, Rac1 antagonizes basolateral RhoA signaling by the recruitment of p190RhoGAP to p120 catenin which is bound to E-cadherin (Noren et al. 2001; Wildenberg et al. 2006). The cytokinetic regulator Centralspindilin performs extramitotic functions by recruiting the RhoGEF Ect2 to interphase zonula adherens while simultaneously inhibiting the junctional localization of p190RhoGAP (Ratheesh et al. 2012). The crosstalk between the Crumbs polarity complex and Rho signaling includes the association of p114RhoGEF with PATJ, which is impaired through aPKC phosphorylation. In this way, contractility of the circumferential actomyosin belt is regulated via RhoA signaling (Nakajima and Tanoue 2011). Specifically, p114RhoGEF was found to be essential for the proper formation of tight junctions and forms a complex with the Rho effectors ROCK II, myosin II and the adaptor protein cingulin (Terry et al. 2011). Its activity is additionally regulated by the Ser/Thr kinase LKB1 (Xu et al. 2013). Further RhoGEFs involved in myosin signaling at cell junctions include TEM4, ARHGEF11 and ARHGEF18 (Ngok et al. 2013; Itoh et al. 2012; Herder et al. 2013). On the one hand, apical inhibition of Rac and Cdc42 signaling is mediated by the recruitment of the Rac/Cdc42 GAP protein Rich1 to Crumbs members Pals1 and PATJ via the adaptor protein angiomoetin (Wells et al. 2006). On the other hand, a Cdc42 GEF, Tuba, regulates tight junction configuration and nascent adherens junctions, via N-WASP-mediated actin polymerisation downstream of Cdc42 (Otani et al. 2006).

The basolaterally located Scribble polarity complex plays an important role in the maintenance of adherens junction integrity. Specifically, E-cadherin binding to p120-catenin is stabilized, whereas the endocytosis and retromer-mediated diversion of E-Cadherin to the Golgi apparatus is inhibited (Qin et al. 2005; Lohia et al. 2012). Independently, the Scribble protein contains multiple PDZ domains and thus can act as an assembly platform for various signaling complexes. In this way, Scribble interacts with the RacGEF βPIX and mediates its recruitment to adherens junctions (Audebert et al. 2004; Frank et al. 2012). In 3D cultures of MCF10A breast epithelial cells, this interaction was reported to be necessary for the process of myc-

induced lumen formation by local Rac activation (Zhan et al. 2008). Besides its role at adherens junctions, Scribble is essential for the control of polarity in epithelial cell migration (Dow et al. 2007). Here, the recruitment of βPIX to the leading edge controls the activity of Cdc42 and Rac and subsequently lamellipodia formation (Dow et al. 2007; Osmani et al. 2006). More recently, work from our lab has identified the RhoGAP DLC3 as another Rho regulator that is targeted to cell-cell contacts by Scribble in a mutually dependent way (see also section 1.2.3). DLC3 locally regulates RhoA-ROCK signaling, thereby ensuring adherens junction integrity as well as polarized morphogenesis in 3D culture (Hendrick et al. 2016). Taken together, polarity protein complexes together with Rho GTPases and their regulators generate complex interaction and signaling networks, which are necessary to regulate the numerous characteristics defining epithelial cell architecture.

### 1.1.4 Rho GTPases in tumor development

The malignant transformation of healthy cells is a multi-step process involving several genetic alterations (Hanahan and Weinberg 2000). While the individual genes involved differ from case to case, the resulting acquired capabilities can be summarized into eight distinct hallmarks of carcinogenesis. These include sustained proliferative signaling, evasion of growth suppressors, resistance to cell death, enabling of replicative immortality, induction/access to vasculature, activation of invasion and metastasis, reprogramming of cellular metabolism, and avoidance of immune destruction (Hanahan 2022). Owing to their multifaceted role in the regulation of cytoskeletal remodeling, aberrant Rho GTPase signaling facilitates many of these hallmarks. Overexpression of several Rho GTPases, likely corresponding to higher activated Rho GTPase total levels, was frequently observed in various tumor entities (Karlsson et al. 2009). However, whereas activating mutations in Ras GTPase family members are common drivers of tumorigenesis, such mutations in Rho GTPases appear only in a small subset of patients (Haga and Ridley 2016). In particular, the fast-cycling Rac1 P29L mutation was found in melanoma, breast cancer, and head and neck cancer samples (Alan and Lundquist 2013). Additionally, RhoA gain-of-function mutations have been described in gastric cancer and T cell lymphoma (Kakiuchi et al. 2014; Sakata-Yanagimoto et al. 2014; Wang et al. 2014b; Yoo et al. 2014). Analyses of human cancer sample databases suggested recurring hot-spot mutations also for other Rho GTPases, such as RhoB, RhoC, RhoT1 and Cdc42, however their functional relevance has not been studied in detail (Porter et al. 2016).

As outlined above, Rho GTPases play a crucial role in the maintenance of cell polarity, morphogenesis and intracellular trafficking. Therefore, misregulation of Rho signaling contributes to the breakdown of epithelial cell polarity and the adoption of a more motile phenotype in cells, a process termed epithelial-to-mesenchymal transition (EMT). During EMT, immotile epithelial cells acquire traits such as motility, invasiveness, and resistance to

apoptosis or the ability to adapt to environmental changes (Parri and Chiarugi 2010). Elevated Rho activity has often been associated with increased proliferation and cell survival as well as higher cell migration and invasion (Sahai and Marshall 2002). However, depending on the context, Rho GTPases may also act in a tumor suppressive manner (Svensmark and Brakebusch 2019). As a prominent example of this duality, RhoB was assigned either tumor suppressive or oncogenic functions in patient samples and *in vivo* models of the same tumor entities in different studies (Ju and Gilkes 2018). Besides Rho copy number alteration, altered expression or activity of GEFs and GAPs is a major cause of deregulated Rho signaling in cancer.

Although this again depends on the entity and tumor progression, GEFs are commonly overexpressed or hyperactivated in cancer samples, suggesting that increased Rho signaling mostly has a positive impact on carcinogenesis (Barrio-Real and Kazanietz 2012; Porter et al. 2016). The GEF Ect2 is frequently overexpressed or mislocalized in various tumors and can therefore be classified as an oncogene (Fields and Justilien 2010). Further examples include the overexpression of the hematopoetic-specific RhoGEF Vav1 in neuroblastoma, lung and pancreatic cancer, and metastatic melanoma (Hornstein et al. 2003; Fernandez-Zapico et al. 2005; Lazer et al. 2009; Bartolomé et al. 2006), while its orthologues Vav2 and Vav3 have been implicated in breast cancer metastasizing to the lung (Citterio et al. 2012). The RacGEFs P-Rex1 and P-Rex2a are frequently overexpressed or mutated, respectively, in melanoma (Lindsay et al. 2011; Berger et al. 2012) and high TIAM1 levels were found to be important for metastasis of T-cell lymphoma, breast and lung cancer (Habets et al. 1994; Adam et al. 2001; Liu et al. 2014).

In contrast, RhoGAP proteins often show decreased expression or activity in cancer, although recent studies have revealed some contextual oncogenic functions (Kreider-Letterman et al. 2022; Porter et al. 2016). Among the best-studied RhoGAPs associated with cancer progression are the p190RhoGAP orthologs p190A and p190B. The gene encoding for p190A was reported to be lost in various tumors (Tikoo et al. 2000; Zack et al. 2013). Moreover, it is the target of frequent cancer-associated mutations which can translate into a protein that is GAP-impaired or truncated and mislocalized (Kandoth et al. 2013; Lawrence et al. 2014; Campbell et al. 2016; Binamé et al. 2016; Wen et al. 2020). However, reports of high p190A expression associated with poorer outcomes in colorectal cancer (CRC), breast cancer (BC), and lung adenocarcinoma (LUAD) paint an unclear picture of its tumor suppressive role (Notsuda et al. 2013; Chiu et al. 2017; Li et al. 2016a). For p190B, results from loss-of-function studies suggest a pro-oncogenic function in various cell lines of nasopharyngeal, lung, and breast cancer (Fang et al. 2015; Wang et al. 2014a; Heckman-Stoddard et al. 2009; Wu et al. 2014). Conversely, another well-characterized RhoGAP, DLC1, together with its orthologues

DLC2 and DLC3, appears to exert mainly tumor suppressive functions which will be further described below (see section 1.2). Overall, the role of Rho signaling in carcinogenesis often depends on the tumor entity and progression stage. The ambiguity about tumor-promoting or -suppressing outcomes reflects its different roles in cellular processes and needs further investigation for a mechanistic understanding.

## 1.2 The Deleted in Liver Cancer family of RhoGAP proteins

### 1.2.1 DLC family members in cancer and development

The Deleted in Liver Cancer (DLC) family comprises three structurally related RhoGAP proteins in humans, DLC1, DLC2 and DLC3, which are often downregulated in various types of cancer. Orthologues of the genes encoding these three proteins are present in all vertebrates and likely arose from gene duplication events, while lower multicellular organisms, such as *C. elegans* or *D. melanogaster*, only contain a single DLC related gene (Kawai et al. 2007). In *Drosophila*, the DLC homologue RhoGAP88C has prominent functions in wing development. While several mutant alleles are lethal, viable mutations show prominent phenotypes including loss of the wing crossvein (Denholm et al. 2005). Consequently, the gene was named as crossveinless-c (cv-c). RhoGAP88C was further shown to play important roles in several fly tissues undergoing embryonal morphogenesis, such as Malpighian tubules, midgut, head, posterior spiracles, the epidermis during dorsal closure and epidermal tracheal invagination (Denholm et al. 2005; Brodu and Casanova 2006). The first family member discovered in higher mammals, rat RhoGAP p122, was reported as a phospholipase C delta 1 interacting protein with GAP activity towards RhoA, but not Rac1 (Homma and Emori 1995).

Later, its human orthologue DLC1 was identified as a candidate tumor suppressor exhibiting frequent loss of heterozygosity (LOH) in primary hepatocellular carcinomas (HCCs) and HCC cell lines, thus coining the corresponding gene name (Yuan et al. 1998). Subsequent studies reported frequent DLC1 copy number loss in various solid tumor entities, including breast, lung, nasopharyngeal and prostate cancer (Plaumann et al. 2003; Yuan et al. 2003; Yuan et al. 2004; Peng et al. 2006; Guan et al. 2006). The *DLC1* gene was mapped to chromosome 8 (8p21.3-22), a region known to undergo frequent allelic loss in several cancer types (Yuan et al. 1998; Anbazhagan et al. 1998). Moreover, *DLC1* lies in close proximity to a chromosomal breakpoint in the mouse/human synteny and could thus be predisposed to deletions, as the breakpoints often coincide with regions of instability in tumours (Durkin et al. 2007b). However, other studies concluded that *DLC1* was likely not the primary target for deletions on chromosome arm 8p22 in head and neck squamous cell carcinoma and in CRC and ovarian tumours (Hewitt et al. 2004; Wilson et al. 2000). Indeed, besides genomic deletions, *DLC1* expression is often downregulated by transcriptional or post-transcriptional mechanisms, and the DLC1 protein is further subjected to extensive post-translational regulation (see sections

1.2.4 and 1.2.5, respectively). Additionally, several cancer-associated point mutations can functionally inactivate DLC1 on the protein level (Wang et al. 2020). The first direct evidence for the tumor suppressive role came from mouse tumor models, in which reconstitution of DLC1 in breast cancer cells lacking endogenous DLC1 expression abrogated *in vivo* tumorigenicity (Yuan et al. 2003). In further studies, restoration of DLC1 expression in HCC or BC cell lines resulted in reduced motility and invasiveness *in vitro* as well as impaired tumorigenicity and metastasis formation, respectively, *in vivo*. (Wong et al. 2005; Goodison et al. 2005). Conversely, DLC1 depletion in a mouse HCC model using liver progenitor cells lacking p53 with myc overexpression promoted tumor formation, confirming DLC1 as a *bona fide* tumor suppressor (Xue et al. 2008). Mechanistically, loss of DLC1 expression is associated with aberrant RhoA signaling and activation of downstream effectors such as Dia1, resulting in increased stress fiber formation and accumulation of focal adhesions (Holeiter et al. 2008). These cytoskeletal changes culminate in a more motile and invasive cell phenotype. Interestingly, in addition to early studies in *Drosophila*, subsequent work has revealed that DLC1 also plays a role in vertebrate developmental processes. DLC1 knockout in mice results in embryonic lethality by midgestation, likely due to severe cardiac, neural and placental defects (Durkin et al. 2005; Sabbir et al. 2010). In an avian model, trunk neural crest cell directional delamination and migration, which in turn is essential for peripheral nervous system development, was severely disrupted upon DLC1 depletion (Liu et al. 2017). Moreover, recent work implicated an essential role for DLC1 in the cardiac and vascular development in zebrafish (Linnerz and Bertrand 2021).

The *DLC2* gene (also referred to as *STARD13*) was discovered at chromosome 13q12.3 in proximity to the known tumor suppressor gene BRCA2 (Ching et al. 2003). Like DLC1, DLC2 shows substantial expression in a wide range of healthy tissues, while loss of expression could be observed in several tumor entities (Ullmannova and Popescu 2006). A tumor suppressive function is supported by *in vitro* studies, showing suppression of cell proliferation, motility and transformation upon overexpression of DLC2, partly through RhoA-ROCK signaling (Ching et al. 2003; Leung et al. 2005). However, loss of DLC2 expression in an *ErbB2* induced mouse tumor model, resulted in increased lung metastasis but showed no effect on tumor growth (Basak et al. 2018). In contrast to DLC1, *DLC2* knockout mice are viable and show no enhanced susceptibility to hepatocarcinogenesis (Yau et al. 2009). Although the animals appear otherwise healthy, they display enhanced angiogenic responses induced by matrigel and by tumor cells, but not by wounds (Lin et al. 2010). These studies suggest that DLC2 is not required for normal mouse development. However in *Xenopus* developmental models, DLC2 also plays an essential role during gastrulation, by regulating RhoA-ROCK dependent actomyosin contractility, thus decreasing cortical actin tension and conferring motility in the mesoderm (Kashkooli et al. 2021). Furthermore, DLC2 has been implicated in the regulation

of spindle positioning and cell-cell adhesion by the attenuation of Cdc42 activity during cell division (Vitiello et al. 2014).

The gene encoding DLC3, referred to as *STARD8*, was originally identified as KIAA0189 from clones of a human myeloid cDNA library (Nagase et al. 1996). As for DLC1 and DLC2, DLC3 expression was detectable in a large number of healthy human tissue samples, but it was reduced in various primary tumors and cancer cell lines (Nagase et al. 1996; Durkin et al. 2007a). *In vitro*, DLC3 overexpression is associated with inhibition of cell proliferation, colony formation and growth in soft agar in breast and prostate cancer cells and with decreased GAP-dependent stress fiber formation in HeLa cells (Durkin et al. 2007a; Kawai et al. 2007). In contrast, DLC3 depletion resulted in impaired endocytic membrane trafficking, decreased cell-cell adhesion and enhanced cell motility in HeLa and MCF7 breast cancer cells, respectively (Holeiter et al. 2012; Braun et al. 2015). In a xenograft mouse model of gastric cancer cells, DLC3 depletion accelerated tumor growth, while also increasing lung metastasis after tail vein injection and colonization of the liver, gut and peritoneum after intrasplenic transplantation (Lin et al. 2019). These effects are mediated by DLC3 through the transcriptional inhibition of MACC1 expression via RhoA/JNK/AP-1 signaling, and thus suppression of cell glycolysis and survival under metabolic stress (Lin et al. 2019). In summary, these results point toward a tumor-suppressive role for DLC3 as well.

### 1.2.2 Multi-domain organization of DLC proteins

The three DLC family members share a similar structural organization that includes three major functional domains. These are from N-terminus to C-terminus: A sterile α-motif (SAM), the catalytic GAP domain and a StAR (steroidogenic acute regulatory protein)-related lipid transfer (START) domain. Moreover, for all DLC proteins, multiple isoforms have been described in the literature and annotated in sequence databases as a result of alternative splicing or alternate transcription start sites with several more transcripts predicted computationally. Many of these alternative transcripts result in the loss of one or multiple domains in the encoded proteins (Fig. 2). However, detailed experimental exploration of possibly divergent functions of different DLC isoforms is lacking.

The N-terminal SAM domain stretches over approximately 70 amino acids. In general, SAM domains can form homomeric or heteromeric protein-protein interactions but also bind DNA, RNA or lipid molecules (Qiao and Bowie 2005). Structural studies of the DLC1 and DLC2 SAM domains by NMR spectroscopy revealed a monomeric four α-helical bundle fold stabilized by interhelix hydrophobic interactions and is distinct from other SAM domains (Zhong et al. 2009; Li et al. 2007). For DLC1, it was suggested that the SAM domain serves an autoinhibitory function towards the intrinsic RhoGAP activity (Kim et al. 2008a). Intriguingly, SAM domain-binding peptides promoted the RhoGAP function of DLC1, leading to decreased RhoA

activation, cell migration and growth in soft agar *in vitro* (Joshi et al. 2020). Transcript variants leading to protein isoforms lacking the SAM domain have been described for all members of the DLC family but their relevance has not yet been studied in detail (Lin et al. 2014; Ching et al. 2003; Durkin et al. 2007a).

The RhoGAP domains of the DLC family members each comprise around 200 amino acids. They are the most conserved regions among the DLC proteins and show sequence identity of about 70%, including the catalytic arginine finger. Therefore, they also share a similar GAP affinity spectrum towards specific Rho GTPases, with a strong preference in GAP activity for RhoA, and its subfamily members, *in vitro* and in cellular assays (Healy et al. 2008; Kawai et al. 2007; Müller et al. 2020; Ching et al. 2003). Moreover, a weak GAP activity towards Cdc42 but not towards Rac1 has been reported (Healy et al. 2008; Kawai et al. 2007; Müller et al. 2020; Wong et al. 2003; Ching et al. 2003).

At the C-terminus, all three DLC proteins contain a START domain of around 200 amino acids length and are therefore also classified in the family of StAR proteins as StarD12 (DLC1), StarD13 (DLC2) and StarD8 (DLC3). Many StAR proteins act as lipid transfer proteins (LTPs), and are able to extract and bind lipids in a deep binding pocket covered by a hydrophobic lid, thus protecting them from the hydrophilic cytosolic environment (Alpy and Tomasetto 2005). Besides the transfer of these lipids to other membranes, LTPs can also fulfill a lipid chaperone function and present their lipids to other proteins (Wong et al. 2017; Chiapparino et al. 2016). However, the role of DLC proteins in cellular lipid metabolism, transport and signaling remains rather elusive. In a recent report, binding of phosphatidylserine to the START domain was shown to be important for DLC1 interaction with other proteins (Sanchez-Solana et al. 2021). Additionally, cancer-associated mutations in the START domain resulted in reduced inhibition of cell migration and anchorage-independent growth, while retaining DLC1 GAP activity. This highlights the importance of the DLC START domains for their tumor suppressive function.

The long linker region between the SAM and the GAP domain, also termed serine-rich region for the relatively high abundance of this amino acid, has the lowest overall conservation among the three DLC family members (Durkin et al. 2007b). Nevertheless, short, locally conserved amino acid stretches can be found, including an eight amino acid long LD-motif (position 469-476 in DLC1) that is important for DLC1 activity by mediating protein binding to ensure correct DLC1 localization (Li et al. 2011). Moreover, N-terminally adjacent to the GAP domain a polybasic region is situated that has been shown to mediate the binding of DLC1 to negatively charged phospholipids such as phosphatidylinositol (4,5)-bisphosphate ($PIP_2$) and thus stimulating its RhoGAP activity (Erlmann et al. 2009). Earlier *in silico* structure analysis based on the amino acid sequence of DLC1 suggested that large parts of the serine rich region would not adopt a defined secondary structure but remain unfolded (Durkin et al. 2007b). The

relatively low sequence similarity of this region among DLC proteins may partially explain some of their non-redundant functions.

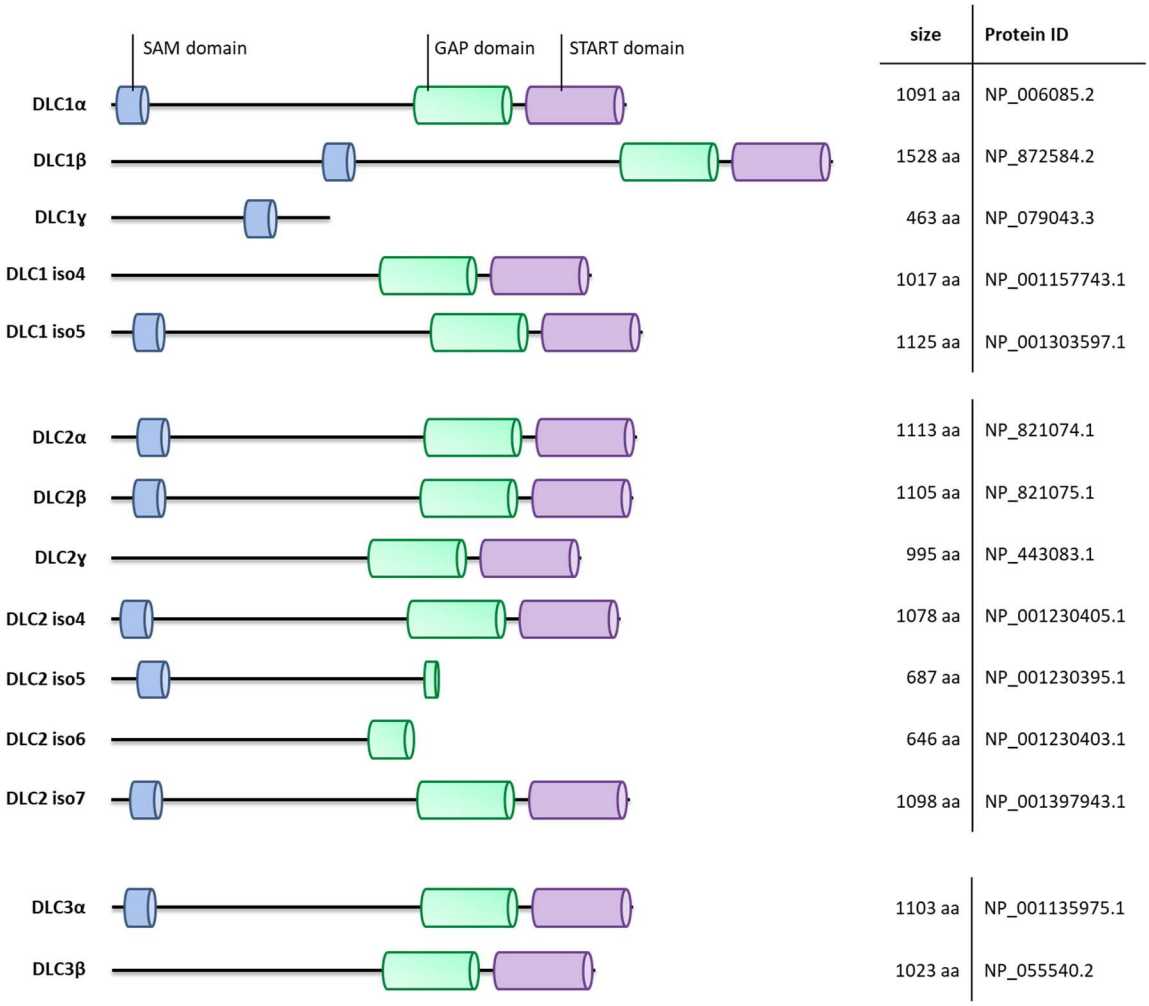


**Figure 2: The human DLC protein family.** Schematic overview of different DLC proteins, including a sterile α-motif (SAM) domain, the catalytic RhoGAP domain and a steroidogenic acute regulatory protein-related lipid transfer (START) domain, as annotated in the NCBI Reference Sequence (RefSeq) database, with their RefSeq identifiers given. Predicted proteins and transcripts were not included. Size and localization of domains are drawn to scale. Adapted and updated from Braun and Olayioye 2015.

### 1.2.3 Subcellular localization and interaction partners of DLC proteins

Because Rho GTPases are usually membrane-bound while in their active state, the RhoGAP proteins must be targeted to the same site in order to properly exert their regulatory function. Several protein interaction partners mediating recruitment to specific subcellular localizations have been described for members of the DLC family, which will be summarized below. Perhaps best understood is the localization of the DLC proteins at focal adhesion sites and their involvement in FA turnover. As mentioned above, FAs provide the cell with the ability to sense the surrounding matrix by linking integrin molecules to the actin cytoskeleton.

An early study of the rat DLC1 homolog p122RhoGAP showed its co-localization and co-immunoprecipitation with the FA adaptor protein vinculin, deeming the N-terminal half of the protein responsible for this localization (Kawai et al. 2004). Later studies showed that members

of the tensin family mediate this recruitment and mapped their interaction with so-called focal adhesion targeting (FAT) regions in the DLC proteins. Specifically, tensin1 and cten bind DLC1 through the interaction of their Src homology 2 (SH2) and phosphotyrosine-binding (PTB) domains with the binding motif SIYDNV at amino acid position 440-445 within DLC1 (Liao et al. 2007; Qian et al. 2007). This interaction is dependent on the tyrosine residue within the ligand motif; however, in contrast to other SH2 and PTB domain binders, binding does not require its phosphorylation. With its PTB domain, Tensin2 is able to bind DLC proteins through an alternative mechanism, also phosphorylation-independent, involving the FAT subdomain comprising amino acids 359–397 in DLC1 (Kawai et al. 2009; Kawai et al. 2010). The last tensin family member, tensin3, associates with DLC1 through its actin-binding domain, a region absent in cten, and thereby resulting in the release of an autoinhibitory interaction between the SAM and GAP domains of DLC1 (Cao et al. 2012). The interaction of DLC1 with cten and tensin3, respectively, is additionally regulated via a phosphorylation-mediated molecular switch in binding partners, enabling precise spatiotemporal Rho activation to control directional cell migration (Cao et al. 2015). This highlights that the interactions between the various DLC and tensin proteins form a complex, interdependent regulatory network.

Once recruited to FAs, DLC1 further interacts with the signaling protein focal adhesion kinase (FAK) and the mechanosensing adaptor molecule talin. Both of these FA-associated proteins bind at the LD motif in DLC1, which is required to exert its full tumor-suppressive activity (Li et al. 2011). The interaction with talin is mediated through its R8 domain, for which DLC1 competes with LD domain-containing proteins such as paxillin (Zacharchenko et al. 2016). The R8 domain is part of the so-called talin rod, a force-sensing module composed of 13 compact four- or five-helical bundles connected by short linkers (Goult et al. 2013). These bundles can undergo unfolding upon contractile forces from the actomyosin machinery during focal adhesion maturation, resulting in a change in the talin interactome. For example, several of the rod domains contain cryptic vinculin binding sites that allow talin to engage with the cytoskeleton via vinculin (Papagrigoriou et al. 2004; Fillingham et al. 2005; Atherton et al. 2015). Thus, the talin rod plays a major role in regulating the assembly and maturation of adhesion complexes. Specifically, DLC1 interacts with talin when the R8 domain is folded (Haining et al. 2018; Dahal et al. 2022). This led to the hypothesis of a switch-like DLC1-mediated regulation of actomyosin contractility during focal adhesion maturation. Initial contractile forces impair DLC1 binding, allowing for force amplification through increased Rho activity and vinculin binding, whereas in matured focal adhesions, the presence of increasing numbers of mechanical linkages reducing the individual force load would re-allow for DLC1 binding (Haining et al. 2018). Alternatively, a recent study suggested that DLC1 binding locks the R8 domain in a mechanically stable state, thus precluding interaction with the talin recruitment factor RIAM and other proteins, and possibly favoring binding of talin to the

microtubule over the actin cytoskeleton (Dahal et al. 2022). Both models can partially explain earlier findings that show preferential DLC1 localization at the inner, more mature adhesions during fibroblast adhesion, as well as the GAP-independent DLC1-mediated downregulation of paxillin turnover (Kaushik et al. 2014). Future studies will further elucidate the detailed regulatory mechanisms and the potential roles of DLC2 and DLC3 in these processes.

All DLC family members have also been implicated in the regulation of cell-cell adhesion at adherens junctions (AJ). As outlined previously, the precise spatiotemporal activation of Rho GTPases is necessary for the formation and the maintenance of the cadherin-catenin complexes, which are attached to the cytoskeleton. Early circumstantial evidence for DLC1 involvement in AJ regulation was derived from non-small cell lung cancer (NSCLC) cell lines overexpressing E-Cadherin, which decreased active RhoA levels and inhibited anchorage independent growth and cell migration (Asnaghi et al. 2010). This phenotype could be partially mitigated by the siRNA-mediated depletion of DLC1. Later, it was shown that DLC1 associates with the AJ complex members E-Cadherin and β-catenin through the direct interaction of the N-terminal amino acids 340 to 435 of DLC1 with the N-terminal amino acids 117 to 161 of α-catenin (Tripathi et al. 2012). In a follow-up study, DLC1 overexpression in prostate cancer cells led to the transcriptional upregulation of E-cadherin expression, in a GAP-dependent but α-catenin-independent manner, and further resulted in an elevated rate of cell–cell aggregation (Tripathi et al. 2014b). Mechanistically, these effects can be explained by inactivation of RhoA and RhoC, as the phenotype mimicked RhoA and RhoC depletion or ROCK inhibition. While DLC2 depletion showed only mild effects on junction formation in differentiating intestinal epithelial Caco-2 cells (Elbediwy et al. 2012), a subsequent study observed defects in the integrity of tight and adherens junctions in mitotic cells (Vitiello et al. 2014). Their data suggest the formation of a complex including DLC2, p120 catenin, E-Cadherin and the kinesin Kif1B, which would ensure spindle positioning and cell junction maintenance through the regulation of microtubular growth and crosstalk (Vitiello et al. 2014). Research from our group established a clear role for DLC3 as a regulating factor of adherens junction integrity. In breast epithelial and BC cell lines, DLC3 co-localizes with E-Cadherin at cell–cell contact sites and its overexpression impairs breast epithelial cell differentiation (Holeiter et al. 2012). Depletion of DLC3 leads to impaired recruitment of E-Cadherin and catenins to cell-cell contacts, resulting in AJ instability and increased cell migration (Holeiter et al. 2012). The proper localization of DLC3 to cell-cell junctions is dependent on its interaction with the scaffold polarity protein Scribble, mediated by Scribble's PDZ domain and a C-terminal PDZ ligand motif in DLC3, which is not shared with the other DLC family members (Hendrick et al. 2016). Experiments using ROCK inhibition or a targeted DLC3 GAP domain could rescue DLC3 depletion phenotypes, indicating that its primary mode of action is exerted via the Rho-ROCK signaling axis (Holeiter et al. 2012; Hendrick et al. 2016). In summary, the recruitment of DLC proteins

to cell-cell contacts through various mechanisms enables the correct assembly of AJ complexes and ensures the spatial regulation of Rho signaling, thus maintaining the integrity of cell-cell adhesions.

In addition to their common functions at cell-cell or cell-matrix adhesion sites, non-redundant localizations of the DLC family members have been described. Utilizing its aforementioned unique PDZ ligand motif, DLC3 can interact with the sorting nexin 27 (SNX27) adaptor protein, which mediates its recruitment to the endosomal compartment in breast cancer cell lines (Noll et al. 2019). Here, it is involved in recycling and trafficking of matrix metalloproteinases through the regulation of endosomal actin via RhoB, which results in increased matrix degradation upon DLC3 depletion (Noll et al. 2019). In HeLa cells, DLC3 also localizes to endomembranes at the endocytic recycling compartment (ERC) in the form of Rab8-positive recycling tubules. Depletion of DLC3 causes fragmentation of these structures as well as the Golgi apparatus (Braun et al. 2015). Moreover, in the absence of DLC3, trafficking of internalized transferrin to the ERC and lysosomal degradation of activated epidermal growth factor receptor is impaired (Braun et al. 2015). Recent work has further uncovered a RhoGEF that appears to be a direct counterpart for DLC3 to locally balance Rho GTPase activation cycles in the regulation of endocytic trafficking (Lungu et al. 2023). However, while many aspects of DLC3 regulation have been uncovered, it remains unclear whether Scribble and SNX27 compete for a single DLC3 pool using their common PDZ-dependent binding strategy, or whether additional regulation specifying the DLC3 target membrane is in place. Furthermore, molecular mechanisms regulating DLC3 binding to and detachment from the respective membrane sites are still elusive.

The observation that DLC1 is the only member of the family capable of translocating from the cytoplasm to the nucleus has long raised puzzles about its role in this compartment. Generally, proteins as large as DLC1 require active transport into the nucleus through the nuclear pore complex, involving binding of importins to a nuclear localization signal (NLS) while binding of exportins to nuclear export signals (NES) leads to shuttling of the protein back to the cytoplasm (Fu et al. 2018). While overexpressed DLC1 is predominantly located in the cytoplasm, in NSCLC cell lines its translocation into the nucleus shortly before apoptosis was described (Yuan et al. 2007). Work from our group showed that DLC1 is rapidly accumulating in the nucleus upon inhibition of exportins, which points to a continuous nucleocytoplasmic shuttling mechanism (Scholz et al. 2009). Moreover, an NLS motif spanning amino acid residues 423–429, a region not conserved in DLC2 and DLC3, was uncovered and a phosphorylation-dependent regulatory mechanism was revealed (see also section 1.2.5). So far, however, none of the presumptive NES motifs examined has proven functional (Chan et al. 2011; Theil 2008). Targeting ectopic DLC1 to the nucleus by the addition of an artificial NLS resulted in reduced

suppression of colony formation and actin stress fiber formation *in vitro* and abrogated suppressive activity *in vivo,* when compared with wild-type DLC1, respectively (Chan et al. 2011). Recently, Yang *et al.* reported that in melanoma, DLC1 was retained in the nucleus by binding to the transcription factor FOXK1 and that this interaction mediates transcription of oncogenic target genes (e.g. MMP9) independent of the RhoGAP activity of DLC1 (Yang et al. 2020). However, the extracellular stimuli and signaling pathways that trigger the translocation of DLC1 into the nucleus and the regulation of its export as well as the detailed role of its functions in the nucleus in a broader context are still insufficiently understood and thus require further research.

Finally, there have been isolated reports of interaction partners or distinct subcellular localizations for specific DLC family members. The eukaryotic elongation factor 1A1 (EF1A1) is able to bind to the SAM domain of DLC1, but not DLC2, and this interaction facilitates EF1A1 distribution to the plasma membrane periphery (Zhong et al. 2009). The DLC1 START domain interacts with Caveolin-1, the principal structural component of caveolae (Du et al. 2012). Cancer-associated START domain mutants with reduced Caveolin-1 binding showed reduced inhibition of cell growth and migration, and thus suggest a GAP-independent contribution of this interaction to the tumor suppressive functions of DLC1 (Wang et al. 2020). An early study reported the localization of DLC2 via its START domain at mitochondria in HeLa and Huh-7 cells (Ng et al. 2006). For DLC1, an isoform harboring an N-terminal putative mitochondrial targeting sequence has been described (Low et al. 2011). However, potential interactors or functions of the DLC proteins at this organelle have not been studied in detail. Conversely, for some of the proposed regulatory DLC interactors no specific subcellular localization has been reported. DLC1 interaction with S100A10, a member of the S100 family of small dimeric EF-hand-type $Ca^{2+}$-binding proteins, was shown to inhibit cell growth, invasion and migration in a GAP-independent manner in NSCLC cell lines (Yang et al. 2011). Until now, the only known direct regulator of DLC1 RhoGAP activity is p120RasGAP. Its N-terminal SH3 domain directly binds to the DLC1 GAP domain, resulting in reduced growth suppression by DLC1 and increased RhoA activity upon p120RasGAP overexpression (Yang et al. 2009). Recently, a co-crystal structure of these interaction domains has been solved, demonstrating that the p120RasGAP SH3 domain obstructs the RhoA binding site and impinges on the catalytic arginine finger (Chau et al. 2022). At this point, other DLC1 interactors that are specifically responsible for or interact with post-translational modifications of DLC1 should also be mentioned; these will be discussed in more detail in section 1.2.5. Collectively, DLC family members are involved in multiple protein-protein interactions that allow spatiotemporal control of their localization and activity.

### 1.2.4 Transcriptional and post-transcriptional regulation of DLC expression

While the genes encoding for the DLC proteins often undergo copy loss, in many tumor entities and cell lines the genes are retained, but transcriptionally inactive (Ullmannova and Popescu 2006; Wang et al. 2016). Evidence from numerous studies in the last two decades suggests that *DLC1* is subject to extensive transcriptional and post-transcriptional regulation, whereas *STARD13* and *STARD8* have not been studied in such detail in this context. On the epigenetic level, gene expression can be silenced by hypermethylation of CpG islands in the promoter region. Indeed, higher *DLC1* promoter methylation was detected in various primary tumor samples such as prostate, colon, lung, pancreas, nasopharynx, esophagus, cervix, and kidney cancers compared to healthy tissues. (Guan et al. 2006; Peng et al. 2013; Dammann et al. 2005; Wang et al. 2016; Xue et al. 2013; Seng et al. 2007; Zhang et al. 2007). Analyses of TCGA datasets showed that methylation of *STARD13* and *STARD8* is only modestly increased in lung cancer samples (Wang et al. 2016). In contrast, *STARD8* was found to be highly methylated in primary CRC samples (Mokarram et al. 2009). Besides DNA methylation, transcriptional silencing can be mediated by repressive histone modifications, such as histone 3 lysine 27 trimethylation (H3K27me3). EZH2, the catalytic subunit of the polycomb repressive complex 2 (PRC2) responsible for setting this epigenetic mark has previously been shown to be overexpressed in a variety of cancers. EZH2 expression in several cancer tissues was found to be inversely correlated with DLC1 expression (Au et al. 2013; Zhou et al. 2020). Moreover, studies in HCC and esophageal cancer cell lines demonstrated a link between EZH2 recruitment and H3K27me3 deposition at the *DLC1* promoter (Au et al. 2013; Qin et al. 2022). Another mechanism for suppression of *DLC1* gene expression is the removal of activating epigenetic marks such as histone acetylation by histone deacetylases. In this context, treatment with histone deacetylase inhibitors was shown to increase *DLC1* expression in prostate, gastric and liver cancer cell lines (Kim et al. 2003; Guan et al. 2006; Kim et al. 2008b; Zhou et al. 2010).

Regulation of gene expression on the post-transcriptional level involves all processes from the modulation of the pre-mRNA after transcription over the distribution and degradation of the mature mRNA until translation. As mentioned earlier, all members of the DLC family exhibit different transcript variants, some of which are due to alternative splicing. However, the underlying regulation of this alternative splicing has not yet been investigated. Several recent studies have shown that especially *DLC1* and *STARD13* transcripts appear to be the target of microRNA (miRNA) mediated degradation. The RNA-induced silencing complex (RISC) uses miRNAs to bind and subsequently degrade complementary mRNAs in a process termed RNA interference (RNAi). Table 1 shows all miRNAs for which the direct binding to DLC transcripts and a resulting change in DLC expression levels was validated experimentally in dual luciferase assays and immunoblot or quantitative PCR, respectively. While the downregulation

of DLC proteins was mostly studied in the cell-autonomous context, there is evidence that at least some of these miRNAs are also secreted in exosomes and thus may play a role in paracrine signaling within the tumor microenvironment (Liu et al. 2020). Additionally, the RNA-binding protein PUM2 was shown to regulate *STARD13* transcript stability by competitive binding to the 3' untranslated region (UTR), thereby attenuating cell migration and proliferation in osteosarcoma cells (Hu et al. 2018). Moreover, the *STARD13* 3' UTR plays a role in a network involving multiple competing endogenous RNAs (ceRNA) that regulates epithelial to mesenchymal transition (EMT), metastasis and stemness in breast cancer (Li et al. 2016b; Zheng et al. 2018). In summary, loss of DLC1 expression in many tumor entities is often due to epigenetic suppression in addition to genomic deletion. Furthermore, *DLC1* and *STARD13* transcripts are subject to extensive post-transcriptional regulation, whereas no such mechanisms have been described for *STARD8*. However, for a subset of cancers, suppression of DLC family member expression on both the genomic and (post-) transcriptional levels are not commonly observed. Thus, different post-translational regulatory mechanisms may be in place to perturb their function.

**Table 1: List of miRNAs regulating DLC expression.** Shown are miRNAs that have been experimentally validated to directly target DLC transcripts in cell lines or primary samples from the respective tissue of origin, as described in the literature. PC: prostate cancer, BC: breast cancer, LUAD: lung adenocarcinoma, CRC: colorectal carcinoma, MYO: myocardium, NPC: nasopharyngeal cancer, HCC: hepatocellular carcinoma, GC: gastric cancer, SOC: serous ovarian cancer, NSCLC: non small-cell lung cancer, MM: multiple myeloma, OS: osteosarcoma, PA: pancreatic cancer

| Name | Target | Tissue origin | Sequence (5' → 3') | Reference |
|---|---|---|---|---|
| miR-9-5p | *STARD13* | PC, BC, LUAD | ucuuugguuaucuagcuguauga | Chen et al. 2019; Li et al. 2016b; Lu et al. 2022 |
| miR-10-5p | *STARD13* | BC | uacccuguagaaccgaauuugug | Li et al. 2016b |
| miR-106b-5p | *DLC1* | CRC | uaaagugcugacagugcagau | Zhang et al. 2015 |
| miR-106b-3p | *DLC1* | CRC | ccgcacuguggguacuugcugc | Liu et al. 2020 |
| miR-125b-5p | *STARD13* | MYO, BC | ucccugagacccuaacuuguga | Jin et al. 2022; Tang et al. 2012; Li et al. 2016b |
| miR-141-3p | *DLC1* | CRC, NPC | uaacacugucugguaaagaugg | Wu et al. 2015; Mu et al. 2020. |
| miR-182-5p | *STARD13* | LUAD, HCC | uuuggcaaugguagaacucacacu | Wu et al. 2021; Zhang et al. 2022 |
| miR-186-5p | *DLC1* | CRC | caaagaauucuccuuuugggcu | Guo et al. 2022 |
| miR-200a-3p | *DLC1* | GC | uaacacugucugguaacgaugu | Li et al. 2022 |
| miR-200c-3p | *DLC1* | SOC | uaauacugccggguaaugaugga | Ankasha et al. 2021 |
| miR-301a-3p | *DLC1* | CRC, NSCLC | cagugcaauaguauugucaaagc | Zhang et al. 2019; Wu et al. 2017 |

| | | | | |
|---|---|---|---|---|
| miR-301b-3p | *DLC1, STARD13* | LUAD | cagugcaaugauauugucaaagc | Liu et al. 2021; Qian et al. 2021 |
| miR-483-3p | *DLC1* | CRC | ucacuccucuccucccgucuu | Cui et al. 2016 |
| miR-561-5p | *DLC1* | MM | aucaaggaucuuaaacuuugcc | Wang et al. 2022 |
| miR-590-3p | *STARD13* | OS | uaauuuuauguauaagcuagu | Hu et al. 2018 |
| miR-873-5p | *DLC1* | HCC | gcaggaacuugugagucuccu | Li et al. 2021a |
| miR-887-3p | *STARD13* | PA | gugaacgggcgccaucccgagg | Xu and Zheng 2020 |

### 1.2.5 Post-translational regulation of DLC proteins

After mRNA translation, protein activity can be functionally regulated by post-translational modifications (PTMs) which induce altered subcellular localization, conformational changes or a change in protein stability. Generally, protein degradation is most commonly mediated by the ubiquitin-proteasome-system, whereby addition of multiple moieties of the small protein ubiquitin (Ub), interlinked on their lysine 48 (K48) residue, to lysine residues of target proteins serves as a recognition signal by the proteasomal degradation machinery. Alternatively, poly-Ub chains that are linked through other residues, e.g. K63, or addition of a single Ub can alter protein localization, activity and binding to other proteins. Ubiquitination is a multistep process involving a ubiquitin-activating enzyme (E1), a ubiquitin-conjugating enzyme (E2) and an E3 ubiquitin ligase that transfers the Ub to the target protein. The E3 ligase interacts with both the target protein and the E2 enzyme and thus is the key player in mediating specificity of the degradation process. Therefore, while in humans there are only two E1 enzymes and about fifty E2 enzymes, the ubiquitination cascade culminates in a large number of E3 ligases, with over 600 members of the RING family and over 30 members of the HECT family (Zheng and Shabek 2017; George et al. 2018). In NSCLC cells, it was described that DLC1 degradation occurs after ubiquitination by the cullin 4A-RING ubiquitin ligase (CRL4A) complex, consisting of cullin 4A, DDB1 and the FBXW5 substrate receptor (Kim et al. 2013). Moreover, a recent study reported that EZH2, besides its function in regulating DLC1 expression on the transcriptional level, is able to interact with DLC1 in the cytoplasm, resulting in methylation of DLC1 at lysine 678 (Tripathi et al. 2021). Methylation of the protein resulted in enhanced binding of the CRL4A complex and thus a faster degradation. However, molecular details of this regulatory interaction such as ubiquitination sites within DLC1 and the subcellular site where ubiquitination takes place are still unknown. Additionally, the mechanisms of DLC1 degradation in other tumor entities and DUBs that counteract its ubiquitination have not yet been investigated.

Contrastingly, many recent studies have shed a light on the extensive regulation of DLC1 through phosphorylation of serine, threonine and tyrosine residues. As mentioned before, DLC1 activity can be attenuated by an autoinhibitory interaction between the N-terminal SR

region and the GAP domain. Phosphorylation of four serine residues (S120, S205, S422, and S509) in DLC1 by CDK5 (Cyclin-dependent kinase 5) decreases this interaction and results in DLC1 adopting an open confirmation that increases the binding to tensin and talin, its localization to focal adhesions and its Rho-GAP activity (Tripathi et al. 2014a). In H358 NSCLC cells, phosphodeficient DLC1 mutants, in which these serines were exchanged for alanines, failed to suppress anchorage independent growth and cell migration as well as tumor growth in an *in vivo* mouse model. Neither the interaction with CDK5 nor the phosphorylation sites are conserved for DLC2 or DLC3.

On the contrary, phosphorylation of serine residues S298, S329, and S567 by Akt strengthens the autoinhibitory interaction and thereby leads to a reduction in RhoGAP activity and attenuation of the tumor suppressor activity (Tripathi et al. 2017). Similarly, an earlier study reported that Akt phosphorylation of serine S567 in DLC1 abrogates the suppression of tumorigenesis and metastasis a mouse model of oncogenically transformed hepatoblasts (Ko et al. 2010). In a closely related mechanism, ERK1/2 was found to phosphorylate serine S129 in DLC1, which serves as a binding site for Src kinase (Tripathi et al. 2019). Subsequent phosphorylation by Src on tyrosines Y451 and Y701 again favored the adoption of the autoinhibitory closed confirmation, thereby restricting DLC1 functions. Previously, threonine T301 and serine S308 were identified as phosphorylation sites by MEK/ERK after EGF stimulation in HeLa JW cells (Ravi et al. 2015). Phosphorylation at these positions allows for the binding of protein phosphatase 2 A (PP2A) and subsequent dephosphorylation of DLC1, which is necessary, but not sufficient for its RhoGAP activity. Additionally, while active FAK was proposed to inhibit the DLC1-PP2A interaction, EGF stimulation resulted in FAK inactivation, thereby relieving the inhibition (Ravi et al. 2015). Together, these studies demonstrate how receptor kinase downstream signaling can control Rho activation through DLC1 and provide possible strategies to reactivate DLC1 activity in cancer therapy. In DLC1-positive transgenic mouse models, treatment with Akt and Src inhibitors showed a cooperative potent antitumor response (Tripathi et al. 2017; Tripathi et al. 2019). Of note, Akt and Src interaction and phosphorylation were observed to a lesser degree for DLC2 and DLC3, and it is unclear whether this would result in an analogous autoinhibitory confirmation (Tripathi et al. 2017; Tripathi et al. 2019).

Moreover, DLC1 can be stabilized in the active, open protein confirmation by protein kinase A (PKA) mediated phosphorylation on serine S549, which enables its dimerization (Ko et al. 2013). This phosphorylation induced enhanced RhoGAP activity and stronger suppression of hepatoma cell growth and cell motility *in vitro* and tumor growth and metastasis *in vivo*. Interestingly, artificial dimerization could rescue the diminished tumor suppression and Rho hydrolysis activities of a DLC1 S549A phosphodeficient mutant (Ko et al. 2013). The phosphorylation site is conserved in DLC2 and DLC3, and DLC1-DLC2 heterodimerization as

well as PKA-dependent DLC2 homodimerization was observed. Furthermore, our group could show that DLC1 is phosphorylated by protein kinase D (PKD) on serine S807 (Scholz et al. 2011). While this did not alter *in vitro* GAP activity towards RhoA, the phosphodeficient mutant was more potent in inhibiting colony formation of MCF7 breast cancer cells. Additionally, phosphorylation by PKD on serine residues S329 and S431 enables binding of 14-3-3 adaptor proteins to DLC1 (Scholz et al. 2009). This leads to the masking of the nearby NLS and thus the sequestration of DLC1 in the cytoplasm, while also inhibiting DLC1 RhoGAP activity, possibly through the masking of the dimerization region (Scholz et al. 2009; Ko et al. 2013).

## 1.3 Aims of the thesis

As important regulators of cytoskeleton remodeling, Rho GTPases are required for diverse biological processes ranging from cell morphology and polarity, organelle positioning and membrane transport, cell division and motility. Disruption of the finely tuned regulatory mechanisms of spatiotemporal Rho activation facilitates transformation of epithelial cells. The three members of the Deleted in Liver Cancer (DLC) protein family of RhoGAP proteins have emerged as important tumor suppressors. In various cancer settings, DLC expression is lost due to genomic deletion or transcriptional downregulation, but many tumors retain DLC transcript expression. Thus, additional post-translational regulation of the DLC proteins likely occurs.

While a pathway mediating the turnover of DLC1 through the ubiquitin-proteasome system has recently been described in NSCLC, the DLC1 protein homeostasis in cellular systems of other origins has not been studied. In the first part of this work, I investigated DLC1 protein degradation in breast cancer cells. After identification of novel ubiquitination-related proteins as DLC1 interaction partners, I assessed their effect on DLC1 turnover, ubiquitination and abundance at focal adhesions using small molecule inhibition or siRNA-mediated depletion.

Furthermore, DLC1 is known to shuttle between the cytoplasm and the nucleus, but its role in the latter compartment and the mechanisms of nuclear export are unclear. The goal of the second part of this work was to identify the nuclear export sequence of DLC1, the mutation of which would facilitate preferential localization of the protein to the nucleus and thus allow further studies of its function there.

In the third part of the thesis, I focused on DLC3 for which non-redundant functions in the maintenance of adherens junctions integrity and endocytic membrane trafficking have been established in previous work. However, molecular mechanisms regulating DLC3 binding of and detachment from the respective membrane sites are still elusive. Therefore, a putative membrane-binding polybasic region in DLC3 was to be characterized by bioinformatical sequence analysis and validated *in cellulo*. Finally, I investigated a potential phosphorylation-dependent regulatory mechanism of DLC3 membrane interaction and its potential disruption by cancer-associated mutations.

# 2 Material and methods

## 2.1 Material

### 2.1.1 Equipment

**Table 2: List of equipment used in this thesis**

| Equipment | Supplier |
|---|---|
| CASY® cell counter | Roche Diagnostics, Basel, Switzerland |
| Curix 60 x-ray film processor | Agfa, Düsseldorf, Germany |
| Eppendorf Centrifuge 5415D | Eppendorf, Hamburg, Germany |
| Eppendorf Centrifuge 5415R | Eppendorf, Hamburg, Germany |
| EPS 301 Power Supply | GE Healthcare Life Science, Uppsala, Sweden |
| EVOS fl., Digital Inverted Microscope | AMG, Life technologies, Carlsbad, CA, USA |
| FACSAria II cell sorter | BD Biosciences, San Jose, CA, USA |
| Gel Documentation Camera Felix 2000, Dark hood DH-50, transilluminator UST-20M-8R | Biostep, Jahnsdorf, Germany |
| Infinite 200M (96-well plate fluorescence reader) | Tecan, Crailsheim, Germany |
| Laminar flow class 2 work bench | Varolab, Gießen, Germany |
| Mastercycler gradient | Eppendorf, Hamburg, Germany |
| NanoDrop® ND-1000 (Spectrophotometer) | Thermo Fisher Scientific, Waltham, USA |
| Varocell 2460, CO2 Incubator | Varolab, Gießen, Germany |
| Pipettes (1 – 20 µl / 20 – 200 µl / 100 – 1000 µl) | Eppendorf, Hamburg, Germany |
| Quantitative PCR Cfx96 | Bio-Rad, Hercules, USA |
| Semi Dry Blotter PEGASUS | Phase, Lübeck, Germany |
| Thermoshaker MKR 13 | HLC BioTech, Bovenden, Germany |
| Vortex Genie 2 | Scientific Industries, Bohemia, NY, USA |
| PhosphoImager | Molecular Dynamics, Sunnyvale, USA |
| Axio Observer Z1/7 microscope | Carl Zeiss, Oberkochen, Germany |
| LSM710 confocal laser scanning microscope | Carl Zeiss, Oberkochen, Germany |
| Plan-Apochromat 63x/1.40 DIC M27 | Carl Zeiss, Oberkochen, Germany |

### 2.1.2 Consumables

**Table 3: List of consumables used in this thesis**

| Consumable | Supplier |
|---|---|
| Cell culture flasks, plates, centrifuge tubes, cryo vials (1 ml), glass-bottom dishes & pipette tips | Greiner BioOne, Frickenhausen, Germany |
| glass cover slips 18 mm x 18 mm | Carl Roth, Karlsruhe, Germany |
| Microscopy slides | Carl Roth, Karlsruhe, Germany |
| Fluoromount-G® | SouthernBiotech, Birmingham, USA |
| Reaction tubes 1.5 ml/2 ml, standard & safe-lock | Eppendorf, Hamburg, Germany |

| | |
|---|---|
| Replica Dishes | Sterilin Ltd, Newport, UK |
| Roti-PVDF transfer membrane | Carl Roth, Karlsruhe, Germany |
| Whatman® cellulose chromatography papers | Sigma-Aldrich, Munich, Germany |
| Glutathione sepharose 4B beads | GE Healthcare, Piscataway, USA |
| GFP-Trap agarose beads | Chromotek, Martinsried, Germany |
| Ni-NTA-Agarose | Qiagen, Hilden, Germany. |
| Protein G agarose | Thermo Fisher Scientific, Waltham, USA |
| Flag M2 agarose | Sigma-Aldrich, Munich, Germany |

### 2.1.3 Chemicals and reagents

**Table 4. List of chemicals and reagents used in this thesis**

| Chemical/reagent | Supplier |
|---|---|
| Acetic acid | Carl Roth, Karlsruhe, Germany |
| Acrylamide (Rotiphorese Gel 30) | Carl Roth, Karlsruhe, Germany |
| Agarose | Invitrogen, Karlsruhe, Germany |
| Ammonium persulfate (APS) | Carl Roth, Karlsruhe, Germany |
| Ammonium bicarbonate | Carl Roth, Karlsruhe, Germany |
| Blocking solution | Roche Diagnostics, Basel, Switzerland |
| Bromophenol blue | Serva, Heidelberg, Germany |
| Complete protease inhibitor cocktail | Roche Diagnostics, Basel, Switzerland |
| Dimethyl sulfoxide (DMSO) | Carl Roth, Karlsruhe, Germany |
| Disodium hydrogen phosphate ($Na_2HPO_4$) | Carl Roth, Karlsruhe, Germany |
| Dithiothreitol | Sigma-Aldrich, Munich, Germany |
| Ethanol | Carl Roth, Karlsruhe, Germany |
| Ethidium bromide | Roche Diagnostics, Basel, Switzerland |
| Ethylenediaminetetraacetic acid (EDTA) | Carl Roth, Karlsruhe, Germany |
| Fluoromount-G | Southern Biotech, Birmingham, USA |
| GeneRuler 1 kb DNA Ladder | Thermo Fisher Scientific, Waltham, USA |
| Glycerol | Carl Roth, Karlsruhe, Germany |
| Glycine | Carl Roth, Karlsruhe, Germany |
| Goat serum | Invitrogen, Karlsruhe, Germany |
| Guanidinium-HCl | Carl Roth, Karlsruhe, Germany |
| Imidazole | Invitrogen, Karlsruhe, Germany |
| Isopropanol | Carl Roth, Karlsruhe, Germany |
| Isopropyl β-d-1-thiogalactopyranoside (IPTG) | Carl Roth, Karlsruhe, Germany |
| Magnesium chloride ($MgCl_2$) | Carl Roth, Karlsruhe, Germany |
| Methanol | Carl Roth, Karlsruhe, Germany |
| NP-40 | Sigma-Aldrich, Munich, Germany |
| PageRuler prestained protein ladder | Thermo Fisher Scientific, Waltham, USA |
| Paraformaldehyde | Carl Roth, Karlsruhe, Germany |

| | |
|---|---|
| Phenylmethanesulfonyl fluoride (PMSF) | Sigma-Aldrich, Munich, Germany |
| Potassium chloride | Carl Roth, Karlsruhe, Germany |
| Potassium dihydrogen phosphate ($KH_2PO_4$) | Carl Roth, Karlsruhe, Germany |
| Protein G Sepharose beads | KPL, Gaithersburg, USA |
| Sodium azide | Sigma-Aldrich, Munich, Germany |
| Sodium chloride | Carl Roth, Karlsruhe, Germany |
| Sodium deoxychylate (NaDOC) | Carl Roth, Karlsruhe, Germany |
| Sodium dihydrogen phosphate ($NaH_2PO_4$) | Carl Roth, Karlsruhe, Germany |
| Sodium dodecyl sulfate (SDS) | Carl Roth, Karlsruhe, Germany |
| Sodium fluoride | Carl Roth, Karlsruhe, Germany |
| Sodium hydrogen carbonate ($NaHCO_3$) | Sigma-Aldrich, Munich, Germany |
| Sodium hydroxide (NaOH) | Carl Roth, Karlsruhe, Germany |
| Sodium orthovanadate ($Na_3VO_4$) | Sigma-Aldrich, Munich, Germany |
| Sulfuric acid ($H_2SO_4$) | Carl Roth, Karlsruhe, Germany |
| Tetramethyldiethyldiamine (TEMED) | Carl Roth, Karlsruhe, Germany |
| Thimerosal | Sigma-Aldrich, Munich, Germany |
| Tris-(hydroxymethyl)-aminomethane (Tris) | Carl Roth, Karlsruhe, Germany |
| Triton X-100 | Carl Roth, Karlsruhe, Germany |
| Tween-20 | Carl Roth, Karlsruhe, Germany |
| β-glycerophosphate | Sigma-Aldrich, Munich, Germany |
| β-mercaptoethanol (β-ME) | Carl Roth, Karlsruhe, Germany |
| [γ-32P]ATP | Hartmann Analytic, Braunschweig, Germany |

### 2.1.4 Buffers and Solutions

**Table 5: List of buffers and solutions used in this thesis**

| Buffer/solution | Composition |
|---|---|
| ***Agarose gel electrophoresis*** | |
| Agarose gel solution | 1% or 2% (w/v) agarose, 0.6 µg/ml ethidium bromide in TAE |
| TAE buffer | 40 mM Tris acetate, 1 mM EDTA in ddH2O, pH 8.0 |
| ***Cell lysis, SDS-PAGE and Western Blotting*** | |
| Blocking solution (WB) | 0.5% (v/v) blocking solution (Roche Diagnostics), 0.05% (v/v) Tween-20, 0.01% (v/v) thimerosal in PBS |
| Blotting buffer | 200 mM glycine, 25 mM Tris base, 20% (v/v) methanol in $ddH_2O$ |
| Laemmli protein loading buffer (5x) | 400 mM Tris pH 6.8, 500 mM dithiothreitol, 50% (v/v) glycerol, 10% (w/v) SDS, 0.2% (w/v) bromophenol blue in $ddH_2O$ |

| | |
|---|---|
| NEB lysis buffer (0.5% or 1%) | 0.5% or 1% (v/v) NP-40, 50 mM Tris (pH 7.5), 150 mM NaCl, 1 mM EDTA, 1 mM $Na_3VO_4$, 10 mM NaF, 0.5 mM PMSF, 20 mM β-glycerophosphate, Complete protease inhibitor cocktail in $ddH_2O$ |
| PBS | 140 mM NaCl, 2.7 mM KCl, 8 mM $Na_2HPO_4$, 1.5 mM $KH_2PO_4$ in $ddH_2O$, pH 7.4 |
| PBS-Tween | 0.05% (v/v) Tween-20 in PBS |
| RIPA lysis buffer | 50 mM Tris pH 7.5, 150 mM NaCl, 10 mM NaF, 20 mM ß-glycerophosphate, 1 mM EDTA, 1% (v/v) NP-40, 0.1% (v/v) SDS, 0.25% (v/v) NaDOC, 1 mM $Na_3VO_4$, 0.5 mM PMSF, protease inhibitor cocktail (Roche Diagnostics) in $ddH_2O$ |
| Hypotonic lysis buffer | 50mM Hepes (pH 7.4), 100 mM NaCl, 5 mM MgCl2, 5mM EDTA, 1mM DTT, 0.5 mM PMSF, 1 mM Na3VO4, Complete protease inhibitor cocktail without EDTA (Roche Diagnostics) |
| SDS-PAGE running buffer | 25 mM Tris pH 8.8, 192 mM glycine, 0.1% (v/v) SDS in $ddH_2O$ |
| SDS-PAGE running gel solution | 8% and 10% (v/v) acrylamide, 375 mM Tris pH 8.8, 0.1% (w/v) SDS, 0.1% APS, 0.06% TEMED in $ddH_2O$ |
| SDS-PAGE stacking gel solution | 5% (v/v) acrylamide, 130 mM Tris pH 6.8, 0.1% (w/v) SDS, 0.1% APS, 0.1% TEMED in $ddH_2O$ |
| ***Flag pulldown*** | |
| 1% TEB buffer (lysis) | RIPA buffer without sodium deoxycholate and SDS |
| Wash buffer | 50 mM ammonium bicarbonate buffer |
| ***His-Ub pulldown*** | |
| denaturing lysis buffer | 8 M urea, 0.1 M Na2HPO4, 0.1 M NaH2PO4, 0.01 M Tris-HCl (pH 8), 10 mM β-ME, 10mM imidazole and 1% Triton X-100 |
| First washing buffer | 6 M guanidinium-HCl, 0.1 M Na2HPO4, 0.1 M NaH2PO4, 0.01 M Tris-HCl (pH 8) and 10 mM β-ME |
| Second washing buffer | 8 M urea, 0.1 M Na2HPO4, 0.1 M NaH2PO4, 0.01 M Tris-HCl (pH 8), 10 mM β-ME, 10mM imidazole |
| Elution buffer | 5x SDS-sample (1M Tris (pH 6.8), 50% glycerol, 0.5 M DTT, 10% SDS) plus 200 mM imidazole |
| ***Immunofluorescence*** | |
| Blocking solution (IF) | 5% (v/v) goat serum, 0.1% (v/v) Tween-20 in PBS |
| PBS | 140 mM NaCl, 2.7 mM KCl, 8 mM $Na_2HPO_4$, 1.5 mM $KH_2PO_4$ in $ddH_2O$, ph 7.4 |
| PBS-Tween | 0.1% (v/v) Tween-20 in PBS |

| | |
|---|---|
| Permeabilizing solution | 0.2% (v/v) Triton X-100 in PBS |
| PFA fixing solution | 4% (v/v) PFA in PBS |
| ***Bacterial culture*** | |
| Lysogeny broth (LB) medium | 10 g/l peptone, 5 g/l yeast extract, 5 g/l NaCl in dd$H_2O$ |
| LB agar plates | LB medium + 14 g/l agar |
| ***GST-tagged protein purification*** | |
| Lysis | PBS containing protease inhibitors (Roche Diagnostics) and Triton X-100 to a final concentration of 1% (v/v) |
| Elution buffer | 50 mM Tris, 10 mM reduced glutathione in ddH2O, pH 8.0 |
| ***In-vitro kinase assay*** | |
| Kinase buffer | 50 mM Tris-HCl, pH 7.4, 10 mM MgCl2, 1 mM DTT |

### 2.1.5 Bacterial strains

The competent *Escherichia coli* DH5 α strain, used for cloning and amplification of mammalian expression constructs, was purchased from Invitrogen (Karlsruhe, Germany). For recombinant protein production, the *E. coli* strain BL21 (DE3) (Thermo Fisher Scientific, Waltham, United States) was used.

### 2.1.6 Plasmids

**Table 6: List of plasmids used in this thesis**

| Plasmid | Source |
|---|---|
| FLAG-DLC1 | Described in Scholz et al. 2009 |
| pCI-neo Flag HAUSP (Flag-USP7) | A gift from Bert Vogelstein (Addgene plasmid #16655 (Cummins and Vogelstein 2004)) |
| pCMV-HA-HECTD1 | Kindly provided by Irene Zohn (Center for Genetic Medicine Research, Children's National, Washington, DC) (Sarkar and Zohn 2012) |
| pCR.V62-Met-Flag-DLC3 | Described in Braun et al. 2015 |
| pCR.V62-Met-Flag-DLC3 S208/215A | Generated in this work |
| pCR.V62-Met-Flag-DLC3 S208/215D | Generated in this work |
| pEGFP-C1 DLC1 | Described in Holeiter et al. 2008 |
| pEGFP-C1 DLC1 K714E | Described in Holeiter et al. 2008 |
| pEGFP-C1 DLC1 K714E NES1* | Generated in this work |
| pEGFP-C1 DLC1 K714E NES1+2* | Generated in this work |
| pEGFP-C1 DLC1 K714E NES2* | Generated in this work |
| pEGFP-C1 DLC1 K714E S236A | Described in Scholz et al. 2009 |
| pEGFP-C1 DLC1 K714E S236D | Generated in this work |

| | |
|---|---|
| pEGFP-C1 DLC1 K714E S236E | Generated in this work |
| pEGFP-C1 DLC1 NES1* | Generated in this work |
| pEGFP-C1 DLC3 K725E | Described in Holeiter et al. 2012 |
| pEGFP-C1 DLC3 S208/215A | Generated in this work |
| pEGFP-C1 DLC3 S208/215D | Generated in this work |
| pEGFP-C1 DLC3 wt | Described in Holeiter et al. 2012 |
| pEGFP-C1 DLC3α K725E ΔPBR | Described in Braun 2015 |
| pEGFP-C1-hScrib (GFP-Scribble) | Kindly provided by Jean-Paul Borg, Centre de Recherche en Cancérologie de Marseille, France |
| pEGFP-N1 DLC1 | Described in Holeiter et al. 2008 |
| pGEX6P1-GFP-Nanobody | A gift from Kazuhisa Nakayama (Addgene plasmid #61838 (Katoh et al. 2015)) |
| pGEX–DLC3-(2-232) | Described in Braun 2015 as pGEX–DLC3α-SAM-(81-232) |
| pGEX–DLC3-(2-232) R205C | Generated in this work |
| pGEX–DLC3-(2-232) R205H | Generated in this work |
| pGEX–DLC3-(2-232) S208/215A | Generated in this work |
| pGEX–DLC3-(2-232) S208A | Generated in this work |
| pGEX–DLC3-(2-232) S208A | Generated in this work |
| pGEX–DLC3-(2-232) S215A | Generated in this work |
| pMT107 (His-ubiquitin plasmid) | Kindly provided by Reinhard Fässler (MPI of Biochemistry, Martinsried, Germany) |

### 2.1.7 Enzymes

**Table 7: List of enzymes used in this thesis**

| Enzyme | Supplier |
|---|---|
| PfuUltra™ High-Fidelity DNA Polymerase | Stratagene, La Jolla, USA |
| Q5® High-Fidelity DNA Polymerase | NEB, Frankfurt a. M., Germany |
| T4 DNA ligase | Thermo Fisher Scientific, Waltham, USA |
| FastAP Thermosensitive Alkaline Phosphatase | Thermo Fisher Scientific, Waltham, USA |
| BamHI | Thermo Fisher Scientific, Waltham, USA |
| DpnI | Thermo Fisher Scientific, Waltham, USA |

### 2.1.8 Oligonucleotides

Primers listed below were purchased from Eurofins Genomics (Ebersberg, Germany)

**Table 8: List of primers used in this thesis**

| Primer name | Sequence (5' to 3') |
|---|---|
| DLC1 NES1* FP | GACGCGCAGTCTGGCGAAACGGATGGAGAGCGCGAAGCTCAAGA GCTC |
| DLC1 NES1* RP | GAGCTCTTGAGCTTCGCGCTCTCCATCCGTTTCGCCAGACTGCGCGT C |
| DLC1 S236D FP | GCTGAAACGGATGGAGGACCTGAAGCTCAAGAGC |
| DLC1 S236D RP | GCTCTTGAGCTTCAGGTCCTCCATCCGTTTCAGC |
| DLC1 S236E FP | CTGCTGAAACGGATGGAGGAGCTGAAGCTCAAGAGCTC |
| DLC1 S236E RP | GAGCTCTTGAGCTTCAGCTCCTCCATCCGTTTCAGCAG |
| DLC3 S208A FP | GCGCCATCGTAACCGTGCCTTCCTCAAGCACC |
| DLC3 S208A RP | GGTGCTTGAGGAAGGCACGGTTACGATGGCGC |
| DLC3 S215A FP | CAAGCACCTTGAAGCTCTGAGGCGGAAGG |
| DLC3 S215A RP | CCTTCCGCCTCAGAGCTTCAAGGTGCTTG |
| DLC3 S208D FP | GCGCCATCGTAACCGTGACTTCCTCAAGCACC |
| DLC3 S208D RP | GGTGCTTGAGGAAGTCACGGTTACGATGGCGC |
| DLC3 S215D FP | CTTCCTCAAGCACCTTGAAGATCTGAGGCGGAAGGAAAAG |
| DLC3 S215D RP | CTTTTCCTTCCGCCTCAGATCTTCAAGGTGCTTGAGGAAG |
| DLC3 R205H FP | CCAAGAAGCGCCATCATAACCGTAGCTTCCTC |
| DLC3 R205H RP | GAGGAAGCTACGGTTATGATGGCGCTTCTTGG |
| DLC3 R205C FP | CCAAGAAGCGCCATTGTAACCGTAGCTTCCTC |
| DLC3 R205C RP | GAGGAAGCTACGGTTACAATGGCGCTTCTTGG |

**Table 9: List of qRT-PCR primers used in this work**

| Amplicon name | Forward Primer Sequence (5' to 3') | Reverse Primer Sequence (5' to 3') |
|---|---|---|
| DLC1 | TGAAGATTTCCTGTTCCCCATC | AGTATTTAGACGCCTGCATAGAG |
| HECTD1 | ATTGCTGGAATGGCTACAGATG | AAGGGCTGGTAAGAAAGTGCG |
| RPLP0 | CTCTGCATTCTCGCTTCCTGGAG | CAGATGGATCAGCCAAGAAGG |

### 2.1.9 Kits

**Table 10: List of kits used in this work**

| Kit | Supplier |
|---|---|
| DC Protein Assay | BioRad, Hercules, USA |
| HRP SuperSignal®West substrate pico | Thermo Fisher Scientific, Waltham, USA |
| HRP SuperSignal®West substrate dura | Thermo Fisher Scientific, Waltham, USA |
| NucleoSpin RNA kit | Macherey-Nagel, Düren, Germany |
| SYBR® Green RNA-to-CT 1-Step kit | Thermo Fisher Scientific, Waltham, USA |

| | |
|---|---|
| 4-12% NuPAGE® Novex Bis-Tris gels | Invitrogen, Karlsruhe, Germany |
| NuPAGE™ MOPS SDS-Buffer kit (for Bis-Tris-Gels) | Invitrogen, Karlsruhe, Germany |
| iBlot®Gel Transfer Stacks | Invitrogen, Karlsruhe, Germany |
| NucleoSpin Plasmid | Macherey-Nagel, Düren, Germany |
| NucleoBond Xtra Midi | Macherey-Nagel, Düren, Germany |
| NucleoSpin Gel and PCR Clean-up | Macherey-Nagel, Düren, Germany |

### 2.1.10 Cell culture media, additives and reagents

**Table 11: List of cell culture media, additives and reagents used in this thesis**

| Medium/additive/reagent | Supplier |
|---|---|
| Collagen R | Serva, Heidelberg, Germany |
| Dulbecco's Phosphate-Buffered Saline, with (DPBS+) or without (DPBS-) Calcium, Magnesium | Invitrogen, Karlsruhe, Germany |
| Fetal calf serum (FCS) | PAA Laboratories, Pasching, Austria |
| Lipofectamine LTX | Invitrogen, Karlsruhe, Germany |
| Lipofectamine RNAiMAX | Invitrogen, Karlsruhe, Germany |
| Opti-MEM | Invitrogen, Karlsruhe, Germany |
| Polyethylenimine | Sigma-Aldrich, St. Louis, USA |
| RPMI 1640, L-Glutamine, with or without phenol red indicator | Invitrogen, Karlsruhe, Germany |
| DMEM/F-12 | Invitrogen, Karlsruhe, Germany |
| DMEM, high glucose | Invitrogen, Karlsruhe, Germany |
| Trypsin/EDTA (10x) | Invitrogen, Karlsruhe, Germany |

### 2.1.11 Inhibitors

**Table 12: List of inhibitors used in this thesis**

| Inhibitor | Supplier |
|---|---|
| Bortezomib | UBPBio, Dallas, USA |
| MG-132 | Selleck Chemicals Houston, USA |
| PR-619 | Cayman Chemicals, Ann Arbor, USA |
| HBX 41108 | Cayman Chemicals, Ann Arbor, USA |
| P5091 | Cayman Chemicals, Ann Arbor, USA |
| Cycloheximide | Santa Cruz, Dallas, USA |

### 2.1.12 Cell lines

**Table 13: List of cell lines used in this thesis**

| Cell line | | obtained from/ kindly provided by |
|---|---|---|
| BT-474 | human breast ductal carcinoma cell line | Nancy Hynes, FMI, Basel, Switzerland |
| BT-549 | human breast ductal carcinoma cell line | Cell Lines Service GmbH CLS, Eppelheim, Baden-Württemberg |
| HCC1806 | human breast squamous cell carcinoma cell line | ATCC, Manassas, USA |
| Hs 578T | human breast carcinoma cell line | Bernhard Lüscher, RWTH Aachen, Germany |
| MDA-MB-231 | human breast adenocarcinoma cell line | Cell Lines Service GmbH CLS, Eppelheim, Baden-Württemberg |
| MDA-MB-436 | human breast adenocarcinoma cell line | Institute of Clinical Pharmacology, Stuttgart, Germany |
| MDA-MD-453 | human breast metastatic carcinoma cell line | Jane Visvader, Walter and Eliza Hall Institute of Medical Research, Melbourne, Australia |
| MDA-MB-468 | human breast adenocarcinoma cell line | Cell Lines Service GmbH CLS, Eppelheim, Baden-Württemberg |
| SUM159PT | human breast carcinoma cell line | DKFZ, Heidelberg, Germany |
| SKBR3 | human breast adenocarcinoma cell line | Cell Lines Service GmbH CLS, Eppelheim, Baden-Württemberg |
| T-47D | human breast ductal carcinoma cell line | Bernhard Lüscher, RWTH Aachen, Germany |
| ZR-75-1 | human breast ductal carcinoma cell line | Bernhard Lüscher, RWTH Aachen, Germany |
| ZR-75-30 | human breast ductal carcinoma cell line | Bernhard Lüscher, RWTH Aachen, Germany |
| HEK 293T | human embryonic kidney cell line transformed with large T antigen | ATCC, Manassas, USA |
| MCF7 | human breast adenocarcinoma cell line | Cornelius Knabbe, Institute of Clinical Pharmacology, Stuttgart, Germany |
| MCF7 GFP-DLC3 K725E | MCF7 cells stably expressing GFP-DLC3 K725E | Generated in this work |
| MCF7 GFP-DLC3 K725E ΔPBR | MCF7 cells stably expressing GFP-DLC3 K725E ΔPBR | Generated in this work |

### 2.1.13 siRNAs for transient knockdown

The siRNAs used were the following: negative control siRNA (siCtrl, ON-TARGETplus® non-targeting control pool D-001810-10; Dharmacon, Lafayette, CO), siHECTD1#1 (Silencer® Select HECTD1 s24575; ambion life technologies), siHECTD1#2 (Silencer® Select HECTD1

s24576; ambion life technologies), custom designed Silencer® Select human DLC1 siRNA (siDLC1, s530697, ambion life technologies).

### 2.1.14 Antibodies and fluorescent dyes

All antibodies used in western blotting were diluted in blocking solution for WB (Table 5). Primary antibody solutions were used multiple times and stored at 4 °C with 0.01% (v/v) sodium azide added. The antibodies used in immunofluorescence assays were diluted in blocking solution for IF (Table 5).

**Table 14: List of primary antibodies used in this thesis**

| Primary antibody | Species | Dilution | Supplier |
|---|---|---|---|
| anti-GAPDH (G9545) | mAb, rabbit | 1:15000 (WB) | Sigma-Aldrich, St. Louis, USA |
| anti-α-tubulin (05-829) | mAb, mouse | 1:10000 (WB) | Sigma-Aldrich, St. Louis, USA |
| anti-FLAG M2 (F1804) | mAb, mouse | 1:1000 (WB) | Sigma-Aldrich, St. Louis, USA |
| anti-GFP (2956) | mAb, rabbit | 1:1000 (WB) | Cell Signaling Technologies, Danvers, USA |
| anti-GFP (11814460001) | mAb, mouse | 1:250 (IF)<br>1:1000 (WB) | Roche Biosciences, Basel, Switzerland |
| anti-GST (GE27-4577-01) | pAb, goat | 1:5000 (WB) | GE Healthcare, Piscataway, USA |
| anti-His (sc-8036) | mAb, mouse | 1:200 (WB) | Santa Cruz Biotechnology, Dallas, USA |
| anti-HA (3724) | mAb, rabbit | 1:1000 (WB) | Cell Signaling Technologies, Danvers, USA |
| anti-DLC1 (612021) | mAb, mouse | 1:500 (WB and IF) | BD Biosciences, Heidelberg, Germany |
| anti-HECTD1 (20605-1-AP) | pAb, rabbit | 1:1000 (WB) | Proteintech, Manchester, UK |
| anti-vinculin (V9131) | mAb, mouse | 1:500 (WB) | Sigma-Aldrich, St. Louis, USA |
| anti-FAK (610088) | mAb, mouse | 1:1000 (WB) | BD Biosciences, Heidelberg, Germany |
| anti-paxillin (sc-5574) | pAb, rabbit | 1:500 (WB and IF) | Santa Cruz Biotechnology, Dallas, USA |
| anti-E-cadherin (3195) | mAb, rabbit | 1:200 (IF) | Cell Signaling Technologies, Danvers, USA |

**Table 15: List of secondary antibodies and fluorescent dyes used in this thesis**

| Secondary antibody | Source | Dilution | Supplier |
|---|---|---|---|
| Alexa Fluor® 488/546 anti-mouse | goat | 1:500 (IF) | Invitrogen, Karlsruhe, Germany |
| Alexa Fluor® 488/546 anti-rabbit | goat | 1:500 (IF) | Invitrogen, Karlsruhe, Germany |

| | | | |
|---|---|---|---|
| horseradish peroxidase (HRP)-anti-mouse IgG | goat | 1:10000 (WB) | Dianova, Hamburg, Germany |
| HRP-anti-rabbit IgG | goat | 1:10000 (WB) | Dianova, Hamburg, Germany |
| Dye | - | Dilution | Supplier |
| DAPI | - | 1:5000 | Sigma-Aldrich, St. Louis, USA |

## 2.2 Methods

### 2.2.1 Cloning strategies

The provenance of the different expression vectors previously described in other sources is detailed in Table 6.

All oligonucleotide sequences used for subcloning or mutagenesis are listed in Table 8. The *E. coli* strain used for plasmid propagation was generally DH5α.

The generation of the phosphodeficient S208A and S215A mutations or phosphomimic S208D and S215D mutations or cancer-associated R205H and R205C mutations was achieved by site-directed PCR mutagenesis using the S208A, S215A, S208D, S215D, R205H or R205C forward and reverse primers with the corresponding DLC3 expression constructs as templates, respectively. The methylated template DNA was digested with DpnI. Similarly, DLC1 NES mutations and phosphomimetic S236D and S236E mutations were introduced by site-directed PCR mutagenesis using the NES1*, NES2*, S236D or S236E primer pairs and pEGFP-C1 DLC1 as template. The PCR program for site-directed mutagenesis with Pfu Polymerase is given in Table 16.

All constructs were verified using Sanger sequencing (Microsynth Seqlab, Göttingen, Germany).

**Table 16: PCR program for site-directed mutagenesis**

| step | temperature | time | cycles |
|---|---|---|---|
| initial denaturation | 95 °C | 90 s | 1 |
| denaturation | 95 °C | 45 s | 18 |
| annealing | 55 °C | 45 s | |
| elongation | 72 °C | 2 min/kb | |
| final elongation | 72 °C | 10 min | 1 |
| hold | 4 °C | ∞ | |

### 2.2.2 Transformation of *Escherichia coli*

The competent *Escherichia coli* strain (depending on application, DH5α or BL21 (DE3)) was transformed via heat shock with the target recombinant plasmids. After thawing on ice, 3 µl of PCR mixture from site-directed mutagenesis was added. After 30 min incubation on ice, a heat shock for 1 min at 42 °C was applied and the bacteria were cooled on ice for 3 min. For outgrowth 500 µl LB medium was added and the bacteria were incubated with shaking at 37 °C before plating on LB agar plates containing the appropriate antibiotic.

### 2.2.3 Isolation of plasmid DNA

To amplify recombinant plasmids during the cloning procedure, a single *E. coli* colony was collected from the plate using a sterile pipette tip and was then inserted in a sterile tube containing 2 ml LB medium with antibiotic, to be incubated overnight with shaking at 37 °C. After overnight incubation, 1.5 ml of the culture were centrifuged for 2 min at 13,000 rpm and the supernatant was discarded. For DNA isolation, the NucleoSpin Plasmid kit was used according to the manufacturer instructions.

To obtain higher plasmid DNA yields, as well as high purity grade preparations used in mammalian cell transfections, 100 µl of the 2 ml overnight culture were used to inoculate 100 ml of LB medium containing selection antibiotics and the flask culture was incubated overnight with shaking at 37°C. The manufacturer´s instructions were followed for plasmid isolation and purification with the NulceoBond Xtra Midi plasmid DNA purification kit. The obtained DNA pellet was resuspended in 200 µl sterile dd$H_2O$ and the DNA concentration of the solution was determined using a NanoDrop® ND-1000 spectrophotometer (Thermo Fisher Scientific, Waltham, USA).

### 2.2.4 Production of recombinant GST-DLC3-fusion proteins

*Escherichia coli* BL21 (DE3) were transformed with the respective pGEX expression vectors and grown in LB medium to an optical density at 600 nm of 0.6. 0.5 mM IPTG was used to induce protein expression for 4 h at 37°C or 30°C. Harvested bacteria were resuspended in PBS containing protease inhibitors (Roche Diagnostics) and disrupted by sonification, followed by addition of Triton X-100 to a final concentration of 1% (v/v). Lysates were incubated on ice for 15 min, and GST-fusion proteins were purified from clarified lysates by binding to glutathione sepharose 4B (GE Healthcare) beads. After three washing steps, GST-fusion proteins were eluted by incubation of the beads with elution buffer (50 mM Tris, 10 mM reduced glutathione in ddH2O, pH 8.0).

### 2.2.5 In-vitro kinase assay

Equal amounts of the purified GST-DLC3 proteins were mixed with kinase buffer containing 2 µCi [γ-$^{32}$P]-ATP and incubated for 15 minutes at 37 °C in the presence of recombinant Akt

or PKCζ. Samples were then resolved by SDS-PAGE, transferred to PVDF membranes and the ionizing radiation was recorded on a PhosphoImager (Molecular Dynamics), followed by immunoblotting of the membrane.

### 2.2.6 Cell culture

All cell lines were cultured without antibiotics under sterile conditions at 37 °C in a humidified atmosphere of 5% CO2. Cell provenance is described in detail in Table 13. BT-20 were cultivated in DMEM/F12 medium supplemented with 5% fetal calf serum. BT-474, BT-549, HCC1806, Hs 578T, MDA-MB-231, MDA-MB-436, MDA-MD-453, MDA-MB-468, SUM159PT were cultured in DMEM supplemented with 10% FCS. HEK293T, MCF7, SKBR3, T-47D, ZR-75-1 and ZR-75-30 were cultured in RPMI 1640 supplemented with 10% FCS.

All cell lines were authenticated by SNP analysis and regularly tested for mycoplasma contamination. Cells were harvested when reaching 70% to 90% confluence by aspirating the medium, washing once with PBS, adding 1x Trypsin/EDTA and incubating at 37 °C for five to ten minutes until cell detachment was visible. Cells were collected in growth medium supplemented with FCS and centrifuged for 5 min at 1,500 rpm. The supernatant was discarded, and the cell pellet was resuspended in an appropriate volume of growth medium. For appropriate passaging or seeding, the cell number in the suspension was determined using a Casy® cell counter or cells were directly passaged at a ratio of 1:5 to 1:10. Long term storage of the cell lines in liquid nitrogen was ensured using cell suspensions in 90% (v/v) FCS and 10% (v/v) DMSO.

### 2.2.7 Cell transfections

Plasmid transfection of MCF7 cells was achieved using Lipofectamine LTX with Plus Reagent (Invitrogen) according to manufacturer's instructions. HEK293T cells were transfected using a 1:3 (w/w) mixture of DNA to polyethylenimine (Sigma Aldrich). In case of RNAi, transfection with siRNA was performed for 72 h using Lipofectamine RNAiMAX (Invitrogen) according to manufacturer's instructions.

### 2.2.8 Generation of stable cell lines

MCF7 cells stably expressing GFP-DLC3 K725E or GFP-DLC3 K725E ΔPBR were generated by transfection of the expression vectors using Lipofectamine LTX followed by selection with 1 mg/ml G418 (Calbiochem) and FACS sorting of GFP-positive cells. Briefly, 1.6 million cells were seeded in 10 cm-dish 24 h prior to transfection. A transfection mix was prepared by diluting 20 µg plasmid DNA and 70 µl Lipofectamine LTX in 4 ml Opti-MEM. After 25 min incubation at room temperature, the mix was added dropwise to the cells. After 48 h, cells were subjected to selection with 1 mg/ml G480 for at least 2 weeks. Stable expression of the GFP-

fusion proteins was verified by FACS analysis, immunoblotting and immunofluorescence microscopy.

### 2.2.9 Cell lysis and protein quantification

For assays other than cellular fractionation, cell lysis was performed as follows. Before cell lysis, cell culture dishes were placed on ice and the culture medium was aspirated. After washing carefully with cold PBS once, cells were lysed using RIPA or 0.5% NEB lysis buffer (Table 5). Cells were incubated for 10 min on ice and collected by scraping. The lysates were then transferred into pre-cooled reaction tubes and clarified by centrifugation (16,000 *g*, 10 min, at 4 °C). Supernatants were transferred into new reaction tubes and protein concentration was measured using the DC Protein Assay (Bio-Rad, Hercules, USA). 5 µl of lysate were transferred in duplicates to 96-well F plate and mixed with 25 µl of a mixture between Reagent A and Reagent S (ratio 50:1) and 200 µl of Reagent B. After 15 min incubation, the absorbance was measured at 750 nm with Infinite-200M (Tecan). The protein concentration was calculated using a BSA standard curve as reference.

### 2.2.10 Immunoprecipitation

Cells were lysed on ice for 10 min in cold 0.5% or 1% NEB buffer and lysates were clarified by centrifugation (16,000 × g, 10 min). To pulldown GFP-tagged protein, equal amounts of protein were incubated for 1 hour at 4 °C with GST-tagged GFP-nanobody coupled to glutathione sepharose beads. Alternatively, the clarified lysates were incubated for 3 hours at 4 °C with specific antibodies and immune complexes were collected using protein G agarose (Thermo Scientific) for 1 hour at 4 °C. In both cases, after three washing steps in lysis buffer, specifically bound proteins were eluted by boiling in SDS-PAGE sample buffer for 5 min.

### 2.2.11 His-Ubiquitin pulldown

The next day after transfection, cells were lysed in denaturing lysis buffer and the lysates were incubated with Ni-NTA-Agarose beads overnight at RT. The beads were washed once with the first wash buffer containing 6 M guanidinium-HCl, 0.1 M $Na_2HPO_4$, 0.1 M $NaH_2PO_4$, 0.01 M Tris-HCl (pH 8) and 10 mM β-ME, and twice with the second washing buffer (8 M urea, 0.1 M $Na_2HPO_4$, 0.1 M $NaH_2PO_4$, 0.01 M Tris-HCl (pH 8), 10 mM β-ME, 10mM imidazole) before elution by boiling in 5x SDS-sample buffer with 200 mM imidazole.

### 2.2.12 SDS polyacrylamide gel electrophoresis (SDS-PAGE) and immunoblotting

Depending on the assay, equal amounts of protein (up to 80 µg) were denatured by boiling in Laemmli buffer for 5 min at 95 °C and subsequently loaded onto Tris/glycine SDS polyacrylamide gels. Electrophoresis was carried out in a vertical electrophoresis chamber (Phase, Lübeck, Germany) in 1x SDS running buffer for approximately 90 min at 55 mA.

The proteins separated by SDS-PAGE were blotted onto a polyvinylidinedifluoride membrane (PVDF; Carl Roth, Karlsruhe, Germany), that has been wetted with Methanol and equilibrated with blotting buffer, using a semi-dry blotting chamber (Phase, Lübeck, Germany) with a current depending on membrane size (1.5 mA/cm$^2$) for 2 h.

Alternatively, lysates were loaded on 4-12% NuPAGE® Novex Bis-Tris gels (Invitrogen) and transferred to nitrocellulose membranes (iBlot®Gel Transfer Stacks; Invitrogen) according to the manufacturer's instructions.

The membrane was subsequently blocked with blocking solution (WB) for 30 min at RT and incubated with the primary antibody solution overnight at 4 °C. After washing three times for 10 min with PBS-T, followed by a 1 hour incubation at RT with HRP-labeled secondary antibody. Following three washing steps with PBS-T, a peroxidase substrate (HRP SuperSignal®West substrate, Thermo Fisher Scientific, Waltham, USA) was added according to the manufacturer's instructions. Signals were visualized with the Amersham600 system (GE Healthcare) or the Fusion Solo (VilberLourmat). Original western blots of all cropped blots are available.

### 2.2.13 NanoLC-MS/MS analysis and MS data processing

To identify interaction partners of DLC1, MCF7 cells expressing GFP-DLC1 or GFP as a control were lysed in 1% TEB buffer (RIPA buffer without sodium deoxycholate and SDS). GFP was immunoprecipitated using GFP-Trap agarose beads (Chromotek). After washing with 1% TEB and PBS, elution followed with 0.1 M glycine (pH 2.5) and neutralization with 1/10 volume of 1 M Tris (pH 8.0). Protein expression and immunopurification were verified in parallel by immunoblotting.

Proteins were purified on a NuPAGE 12% gel (Invitrogen) and Coomassie-stained gel pieces were digested in gel with trypsin as described previously (Borchert et al. 2010). After desalting using C18 stage tips (Rappsilber et al. 2007) peptide mixtures were run on an EasyLC nano-HPLC coupled to an LTQ Orbitrap Elite mass spectrometer (both Thermo Fisher Scientific) as described elsewhere (Franz-Wachtel et al. 2012) with slight modifications: the peptide mixtures were separated using a 127 min segmented gradient from 10-33-50-90% of HPLC solvent B (80% acetonitrile in 0.1% formic acid) in HPLC solvent A (0.1% formic acid) at a flow rate of 200 nl/min. Precursor ions were acquired in the mass range from m/z 300 to 2000 in the Orbitrap mass analyzer at a resolution of 120,000. Accumulation target value of 106 charges was set. The 15 most intense ions were sequentially isolated and fragmented in the linear ion trap using collision-induced dissociation at the ion accumulation target value of 5000 and default CID settings. Sequenced precursor masses were excluded from further selection for 60 s.

Acquired MS spectra were processed with MaxQuant software package version 1.5.2.8 with integrated Andromeda search engine (Cox and Mann 2008; Cox et al. 2011). Database search was performed against a Homo sapiens database containing 91,675 protein entries, and 285 commonly observed contaminants, plus the GFP-DLC1 sequence. Endoprotease trypsin was defined as protease with a maximum of two missed cleavages. Oxidation of methionine, phosphorylation of serine, threonine and tyrosine, methylation on lysine and arginine residues, acetylation of lysine and the protein N-terminus were specified as variable modifications. Carbamidomethylation on cysteine was set as fixed modification. Initial precursor mass tolerance was set to 4.5 parts per million, and at the fragment ion level 0.5 Da was set for CID fragmentation. Peptide, protein and modification site identifications were reported at a false discovery rate of 0.01, estimated by the target-decoy approach (Elias and Gygi 2007). The iBAQ algorithm was enabled to estimate quantitative values by dividing the sum of peptide intensities of all detected peptides by the number of theoretically observable peptides of the matched protein (Schwanhäusser et al. 2011).

For the identification of the phosphorylation sites within the DLC3 PBR region the following modifications were made: HEK293T cells were transfected with constructs encoding FLAG tagged DLC3 and subsequently lysed in 1% TEB buffer. Flag-tagged proteins were immunoprecipitated from cell lysates using Flag M2 agarose (Sigma Aldrich). Next, the beads were washed with lysis buffer three times and with 50 mM ammonium bicarbonate buffer another three times, before tryptic digest on-beads. Enrichment of phosphopeptides by titanium dioxide chromatography was done as described previously (Olsen and Macek 2009) with the following modifications: phosphopeptide elution from the beads was performed three times with 100 µl of 40% ammonia hydroxide solution in 60% acetonitrile at a pH of >10.5.

All mass spectrometry analyses and data processing was conducted by our collaboration partners at the Proteome Center Tübingen, University of Tübingen, Germany.

### 2.2.14 Quantitative Real-Time PCR

Total RNA was isolated from cells using the NucleoSpin RNA kit (Macherey-Nagel) according to the manufacturer's instructions. 100 ng RNA were used as template for real-time PCR, using the Power SYBR® Green RNA-to-CT 1-Step kit (Thermo Fisher) with the the primers described in Table 9. The assay was performed using the CFX96 Touch Real-Time PCR Detection System (Bio-RAD). Changes in the relative expression level were determined using the 2-ΔΔCt method (Biorad CFX manager software 3.1.). RPLP0 served as control gene.

### 2.2.15 Immunofluorescence staining, microscopy and image analysis

In general, for immunofluorescence staining assays, cells grown on glass coverslips coated with 10 µg/ml collagen R (Serva) were fixed with 4% PFA in PBS for 15 min at RT, followed by

PBS washing and a 15-minute incubation in 150 mM glycine in PBS. Then, permeabilization was achieved with 0.2% Triton-X-100 in PBS for 5 min and blocking was performed with 5% goat serum (Invitrogen) in PBS containing 0.1% Tween-20 (PBST) for 30 min.

For analysis of DLC1 at focal adhesions (FAs), cells grown on glass coverslips coated with 10 µg/ml collagen R (Serva) were fixed and permeabilized simultaneously with 4% PFA containing 0.1% Triton X-100 for 10 min at RT. For analysis of FA length, cells were fixed with 4% PFA for 10 min at RT and permeabilized with 0.2% Triton X-100. After PBS washes, cells were incubated for 15 min with 150 mM glycine in PBS and then blocked with 5% goat serum (Invitrogen) in PBST for 30 min at RT.

Samples were incubated with specific primary antibodies diluted in blocking buffer for 2 hours at RT, washed with PBST, followed by incubation with AlexaFluor® (488, 546) labeled secondary antibodies together with DAPI in blocking buffer for 1 hour at RT. Coverslips were mounted in Fluoromount-G® (SouthernBiotech) and analyzed at RT on a spinning disc Axio Observer Z1/7 microscope (Carl Zeiss) or an LSM710 confocal laser scanning microscope (Carl Zeiss), both equipped with a Plan-Apochromat 63x/1.40 DIC M27 (Carl Zeiss) oil immersion objective using 488-, 561-nm laser excitation.

For each set of replicates, images were acquired with the same laser and confocal settings. The ZEN software (Zeiss) was employed to perform maximum intensity projections, linear adjustments of brightness and contrast, as well as the analysis of mean fluorescence intensity (MFI) of junctional and cytoplasmic regions of interest (ROI) in experiments investigating the DLC3 PBR function. For all other analysis the ImageJ software (NIMH; Bethesda, Maryland) was used. For quantification of DLC1 at FAs, focal adhesion areas were defined by paxillin staining, while the mean intensity of the DLC1 signal over the whole image was measured. The length of paxillin-positive focal adhesions was determined manually. Data are presented as SuperPlot (Lord et al. 2020). For quantification of DLC1 nuclear translocation, a nuclear ROI was defined based on the DAPI staining. The cytoplasmic ROI was defined by expanding the nuclear ROI with the “dilate” function three times, or until the cell border, based on the GFP signal, was reached. MFI in each ROI was measured and the ratio of nuclear to cytoplasmic MFI determined.

### 2.2.16 *In silico* sequence analyses

To predict unstructured membrane binding sites in DLC proteins a modified hydrophobicity scale implemented in the BH search program was used (Brzeska et al. 2010). Alignment of DLC protein sequences and DLC3 orthologue sequences from different species was performed using BLAST (https://blast.ncbi.nlm.nih.gov/Blast.cgi). For disorder prediction the ANCHOR and IUPred3 algorithms were used (Mészáros et al. 2009; Erdős et al. 2021). To

further predict the DLC3 protein folding structure, the machine learning model AlphaFold2 as implemented in ColabFold was used (Jumper et al. 2021; Mirdita et al. 2022). Candidate phosphorylation sites and responsible kinases were predicted using Scansite 4.0 and NetPhos 3.1 (Obenauer et al. 2003; Blom et al. 2004). Cancer-associated mutations in DLC3 were extracted from the cBio Cancer Genomics Portal (http://cbioportal.org) and the COSMIC (https://cancer.sanger.ac.uk/cosmic) databases (Gao et al. 2013; Tate et al. 2019).

### 2.2.17 Statistical analysis

Unless otherwise specified, data are shown as mean ± S.E.M. 'N' refers to the total number of sample points and 'n' to the number of independent experiments. GraphPad Prism 9 was used for data analysis, with the statistical tests and p-values detailed in the figure legends.

# 3 Results

## 3.1 Regulation of DLC1 proteasomal turnover by HECTD1 and USP7

### 3.1.1 DLC1 is subject to rapid proteasomal degradation

To date, several studies have systematically investigated DLC1 transcript levels in cultured cell lines of different cancer origins. However, systematic expression data of DLC1 at the protein level is only available for melanoma and gastric cancer cell lines, respectively (Yang et al. 2020; Hinsenkamp et al. 2022). Therefore, the expression levels of the DLC1 protein in a panel of BC cell lines of various subtypes was analyzed by western blot (Fig. 3). In most cell lines of the luminal A/B and HER2 positive subtypes DLC1 levels were barely detectable, while several triple-negative breast cancer cell lines showed robust DLC1 expression.

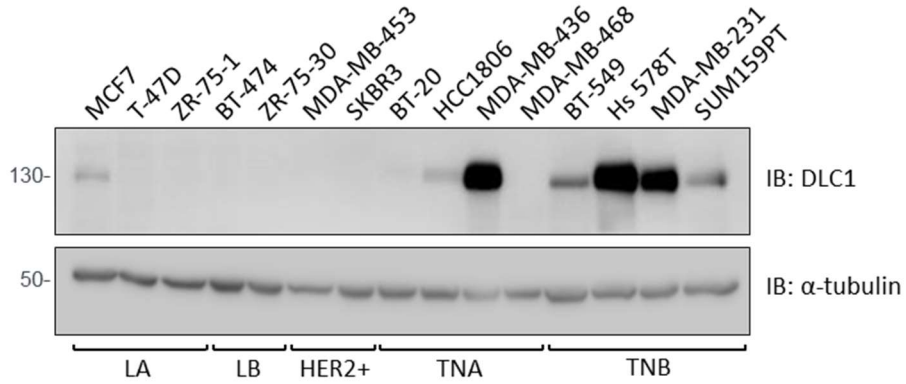


**Figure 3: Differential DLC1 expression in breast cancer cell lines.** Lysates of the indicated cell lines from different breast cancer subgroups (luminal A (LA), luminal B (LB), HER2 positive (HER2+), triple-negative A (TNA), triple-negative B (TNB)) were analyzed by immunoblotting with the indicated antibodies. Shown is a representative blot from two independent experiments.

Generally, cellular protein expression is determined by a fine balance between protein synthesis and protein breakdown rates. To explore to which extent protein degradation plays a role in the maintenance of the low DLC1 levels observed, the effect of the proteasome inhibitors MG-132 and bortezomib (BTZ) on DLC1 expression in several cell lines was monitored (Fig. 4A, B). Treatment of cells for only three or six hours resulted in multifold increased DLC1 protein levels in all cell lines tested. Of note, the protein was also clearly detectable in T-47D and SKBR3 cell lines which have been described previously as DLC1-negative (Tripathi et al. 2017; Yuan et al. 2003). This suggests a high turnover rate of DLC1 in breast cancer cell lines.

The DUB protease family can cleave Ub chains that mark proteins destined for proteasomal degradation. In MCF7 and BT-549 cells, treatment with the pan-DUB inhibitor PR-619 resulted in a sizeable reduction of DLC1 protein levels within a few hours (Fig. 5A, B). During this time,

DLC1 mRNA levels remained largely unchanged (Fig. 5C), further highlighting the role of the Ub-proteasome system in DLC1 turnover.

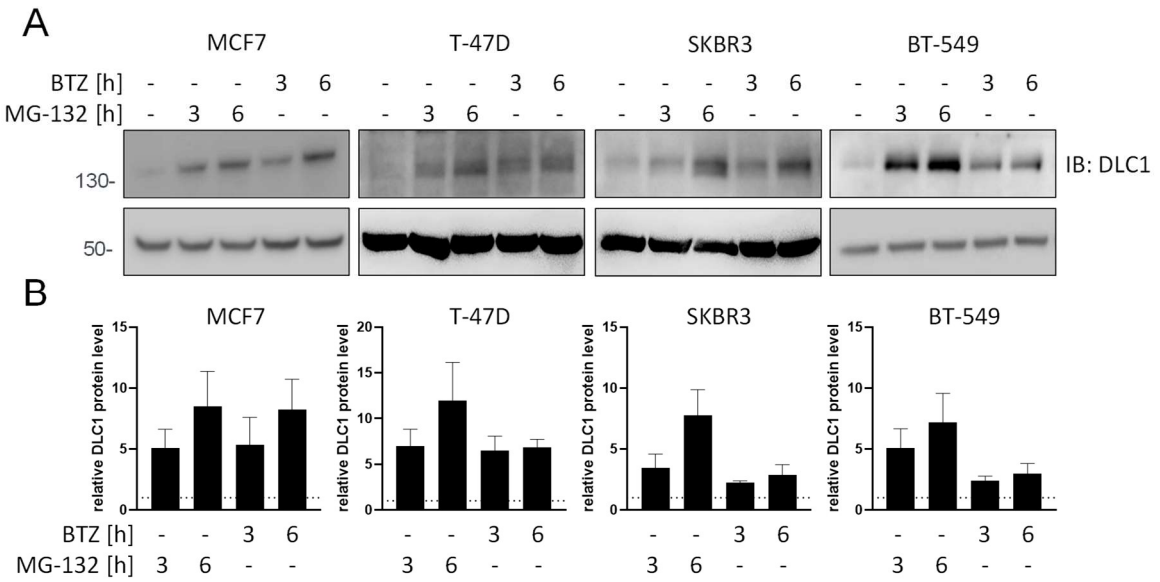


**Figure 4: Proteasomal inhibition rapidly stabilizes DLC1 levels.** (A) Cells were treated with MG-132 (10 μM) or bortezomib (BTZ, 100 ng/ml) as indicated and the lysates were analyzed by immunoblotting with the indicated antibodies. Control sample was treated with DMSO for 6 h. Cropped blots shown from different cell lines are derived from separate blots. (B) Western blots from three independent experiments were analyzed with ImageJ, the fold change in DLC1 expression was determined by normalizing the DLC1/α-tubulin ratio to that of control sample and is presented as mean ±SEM.

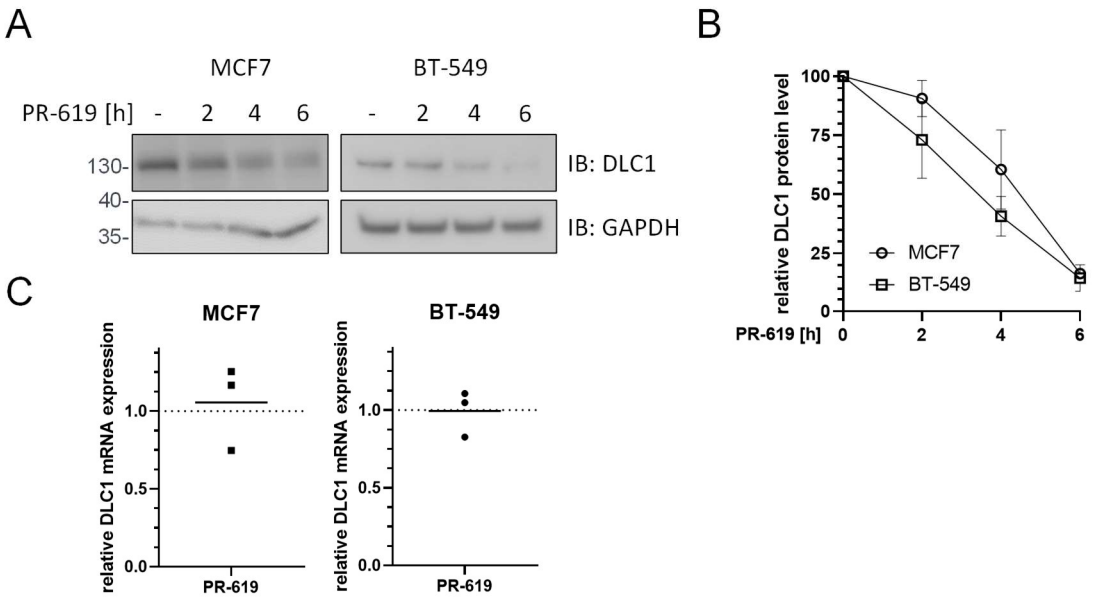


**Figure 5: DUB inhibition results in DLC1 degradation.** (A) Cells were treated with PR-619 (20 μM) as indicated and the lysates were analyzed by immunoblotting with the indicated antibodies. The control sample was treated with DMSO for 6 h. Cropped blots shown from different cell lines are derived from separate blots. (B) Western blots from three independent experiments were analyzed with ImageJ, the fold change in DLC1 expression was determined by normalizing the DLC1/GAPDH ratio to that of control sample and is presented as mean ± SEM. (C) qPCR analysis of DLC1 expression after treatment with PR-619 for 6h. Data are presented as mean mRNA expression of treated cells normalized to DMSO control (n=3).

As DLC1 is known to localize to and signal at FAs, one might speculate that its stability is linked to their constant remodeling and subsequent degradation of FA protein complexes. However, in chase assays with cycloheximide, an inhibitor of protein synthesis, other proteins associated with FAs such as vinculin, FAK and paxillin showed a much longer half-life (Fig. 6A, B). This suggests that rapid DLC1 degradation is independent of general high turnover rates of FA protein complexes.

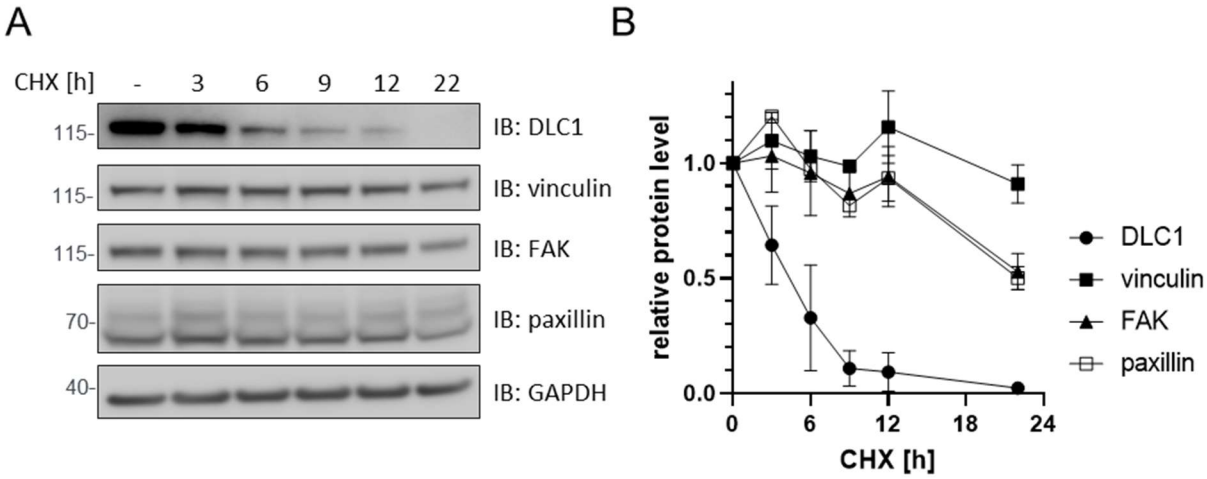


**Figure 6: DLC1 shows a shorter protein half-life than other focal adhesion proteins.** (A) MCF7 cells were treated with cycloheximide (CHX, 60 µg/ml) as indicated, and lysates were analyzed by immunoblotting with the indicated antibodies. (B) Western blots from three independent experiments were analyzed with ImageJ, the fold change in protein expression was determined by normalizing the signal to GAPDH and to the control sample and is presented as mean ± SEM.

### 3.1.2 HECTD1 and USP7 are novel regulators of DLC1 stability

Tight regulatory mechanisms are a necessity to allow for precise and rapid protein degradation. In order to elucidate proteins of this regulatory machinery interacting with DLC1 turnover, an unbiased mass spectrometry was performed. To this end, protein complexes containing GFP-tagged DLC1 were immunopurified from lysates of transiently expressing MCF7 cells and analyzed by nano-liquid chromatography tandem mass spectrometry (nanoLC-MS/MS). Proteins that were identified in the immunoprecipitate from an empty vector control experiment were considered as unspecific binders and thus excluded (Table S1). The resulting list of putative DLC1 interactors contained several proteins that were previously reported to interact with DLC1, such as EEF1A1, PP2A and different isoforms of 14-3-3 (Zhong et al. 2009; Ravi et al. 2015; Scholz et al. 2009). Furthermore, the HECT family E3 ligase HECTD1 and the DUB ubiquitin-specific-processing protease 7 (USP7) were identified as ubiquitination regulating proteins within the candidate DLC1 interactome. HECTD1 was already previously implicated in FA remodeling through the ubiquitination of phosphatidylinositol 4-phosphate 5-kinase type I γ (Li et al. 2013). USP7 has been shown to regulate a plethora of protein

substrates and is perhaps best known for stabilizing the ubiquitin ligase Mdm2, which in turn leads to degradation of the tumor suppressor master regulator p53 (Bhattacharya et al. 2018).

The mass spectrometry results were further validated by co-immunoprecipitation assays. For these experiments, HEK293T cells were used as they allowed for sufficient co-expression of the rather large constructs. GFP-tagged DLC1 was found to specifically bind to FLAG-tagged USP7 (Fig. 7A). Conversely, GFP-DLC1, but not GFP alone, was able to co-immunoprecipitate FLAG-USP7 (Fig. 7B). Similarly, the HA-tagged murine orthologue of HECTD1 showed binding to GFP-DLC1 (Fig. 7C). Unfortunately, co-immunoprecipitation attempts of the endogenous proteins from MCF7 cells were not successful, owing possibly to the very transient nature of interaction and insufficient sensitivity of the antibodies (data not shown).

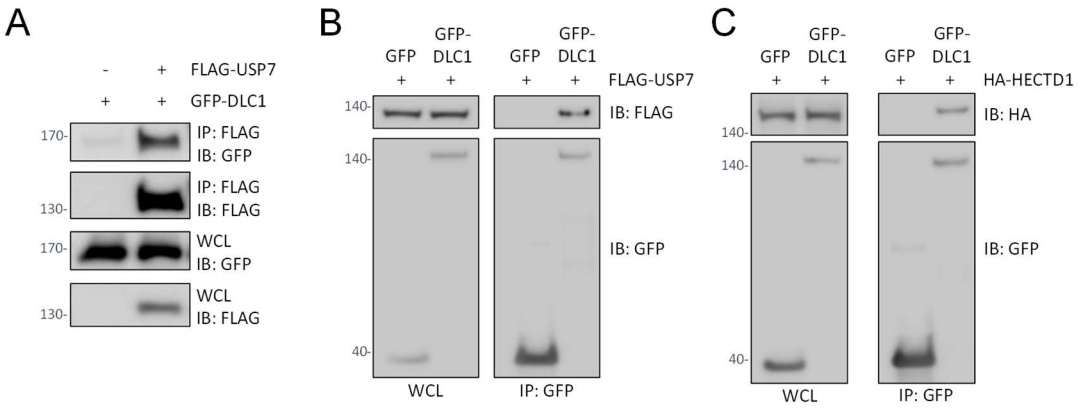


**Figure 7: DLC1 interacts with USP7 and HECTD1.** HEK293T cells were transiently transfected with vectors encoding the indicated fusion proteins or empty vectors. (A) After immunoprecipitation with an anti-FLAG antibody, whole cell lysates (WCL) and immunoprecipitates were analyzed by immunoblotting using the indicated antibodies. Cropped blots showing co-immunoprecipitation signals are derived from blots with different exposure compared to WCL. (B, C) Immunoprecipitation with an anti-GFP-nanobody was performed. Whole cell lysates (WCL) and precipitates were analyzed by immunoblotting using the indicated antibodies. Cropped blots showing co-immunoprecipitation signals are derived from blots with different exposure compared to WCL. Shown are representative blots from two independent experiments.

To elucidate the role of the newly identified interaction partners in DLC1 degradation, MCF7 cells were first treated with two independent small-molecule inhibitors of USP7, P5091 or HBX 41108. Inhibition of USP7 resulted in rapid decrease of DLC1 protein levels (Fig 8A, B). This effect was similar in magnitude and time course to that observed with the pan-DUB inhibitor PR-619, suggesting that USP7 might be the major DUB regulating DLC1 degradation. Importantly, qPCR analysis confirmed that the depletion of DLC1 upon USP7 inhibition did not occur at the transcript levels (Fig. 8C).

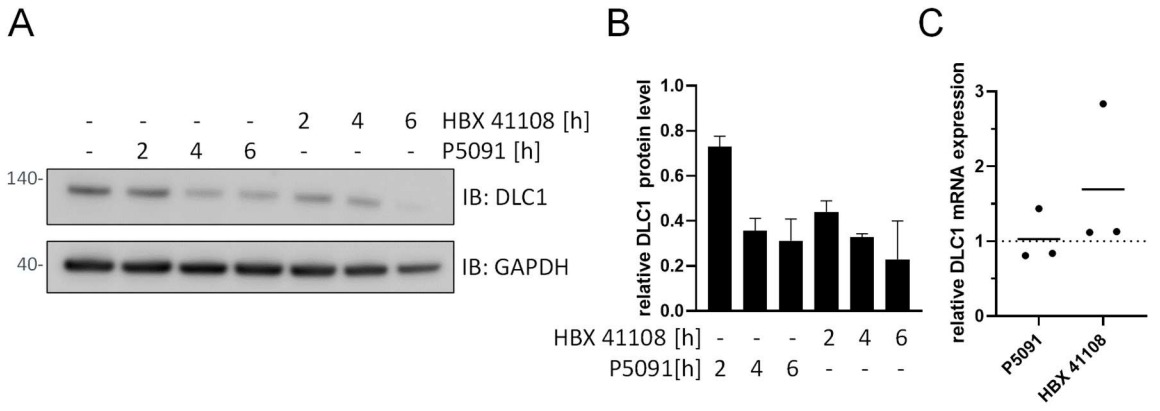


**Figure 8: USP7 inhibition results in DLC1 degradation.** (A) MCF7 cells were treated with P5091 (20 µM) or HBX 41108 (10 µM) as indicated, and lysates were analyzed by immunoblotting with the indicated antibodies. The control sample was treated with DMSO for 6 h. (B) Western blots from three independent experiments were analyzed with ImageJ. The fold change in DLC1 expression was determined by normalizing the DLC1/GAPDH ratio to that of control sample and is presented as mean ± SEM. (C) qPCR analysis of relative DLC1 expression in MCF7 cells after treatment with P5091 or HBX 41108 for 6 h. Data are presented as mean mRNA expression of treated cells normalized to DMSO control (n=3).

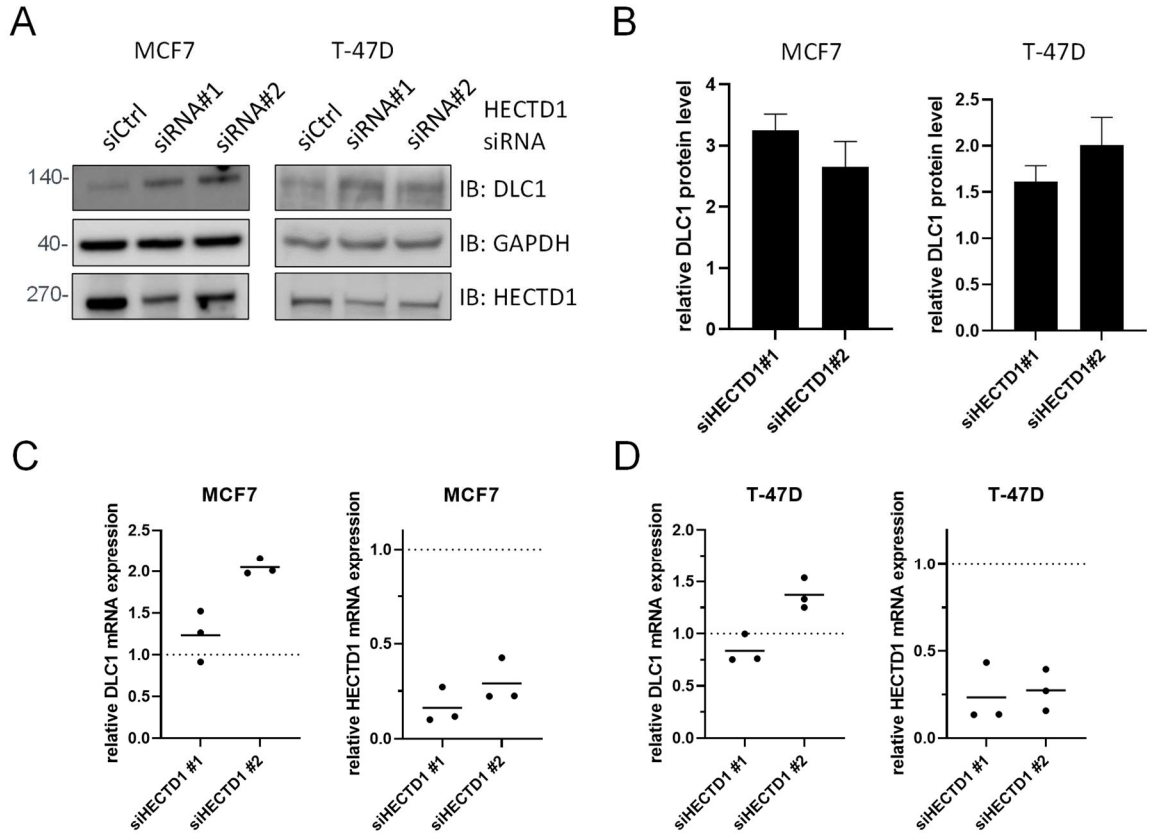


**Figure 9: HECTD1 depletion results in increased DLC1 levels.** (A) Cells were transfected with control siRNA or two independent siRNAs targeting HECTD1. Three days post transfection, cells were lysed and lysates were analyzed by immunoblotting with the indicated antibodies. Cropped blots shown from different cell lines are derived from separate blots. (B) Western blots from three independent experiments were analyzed with ImageJ, the fold change in DLC1 expression was determined by normalizing the DLC1/GAPDH ratio to that of control sample and is presented as mean ± SEM. (C),(D) qPCR analysis of DLC1 and HECTD1 expression in MCF7 or T-47D cells three days after transfection with the indicated siRNAs. Data are presented as mean mRNA expression of treated cells normalized to non-targeting siRNA control (n=3).

Unfortunately, specific inhibitors for HECTD1 enzymatic activity are commercially available. Therefore, to investigate its role in the DLC1 degradation process, two independent specific siRNAs were used to deplete its expression in MCF7 and T-47D cells. Immunoblots revealed an increase in DLC1 abundance and successful HECTD1 knockdown (Fig. 9A, B) three days post transfection. However, on the transcript level, one of the two siRNAs also caused slightly elevated DLC1 mRNA amounts in both cell lines as evident by qPCR analyses (Fig. 9C, D). To verify that the increase in DLC1 protein levels was largely due to impaired degradation upon HECTD1 knockdown, additional CHX chase assays were performed in MCF7 cells. After depletion of HECTD1 with either of the two siRNAs, DLC1 degradation occurred at a markedly reduced rate, but was not completely abrogated (Fig. 10A, B). This may be explained by residual HECTD1 protein as well as different pathways regulating DLC1 turnover independent of HECTD1.

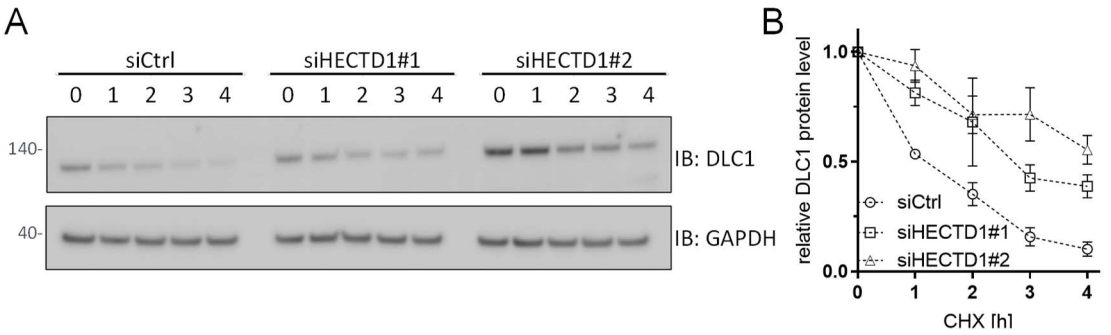


**Figure 10: HECTD1 depletion impairs DLC1 degradation.** (A) MCF7 cells were transfected with control siRNA or two siRNAs targeting HECTD1. Three days post transfection, cells were treated with cycloheximide (CHX, 60 µg/ml) as indicated and lysates were analyzed by immunoblotting with the indicated antibodies. (B) Western blots of four independent experiments were quantified by ImageJ. The fold change in DLC1 expression was determined by normalizing the DLC1/GAPDH ratio to that of control sample. Data are presented as mean ± SEM.

The altered DLC1 stability upon manipulation of USP7 activity and HECTD1 levels, respectively, points towards a role of these proteins in the regulation of DLC1 ubiquitination. To confirm this hypothesis, GFP-tagged DLC1 and either USP7 or HECTD1 were overexpressed together with His-tagged Ub in HEK293T cells. This allowed for enrichment of ubiquitinated proteins by pulldown of His-Ub with Ni-NTA agarose. Following SDS-page and immunoblotting, slower migrating GFP-DLC1 signals could be detected in the pulldown fraction, likely corresponding to polyubiquitinated GFP-DLC1 species. While GFP-DLC1-Ub signals were increased after HECTD1 co-expression signals, USP7 co-expression clearly reduced GFP-DLC1 ubiquitination (Fig. 11A, B). In MCF7 cells, treatment with the USP7 inhibitor P5091 resulted in a slight increase in DLC1 ubiquitination detected (Fig. 11C, D). However, using different experimental strategies of enriching for ubiquitinated proteins in combination with proteasome and DUB inhibitors ubiquitination of endogenous DLC1 could not be shown conclusively, similar to a previous report (Kim et al. 2013).

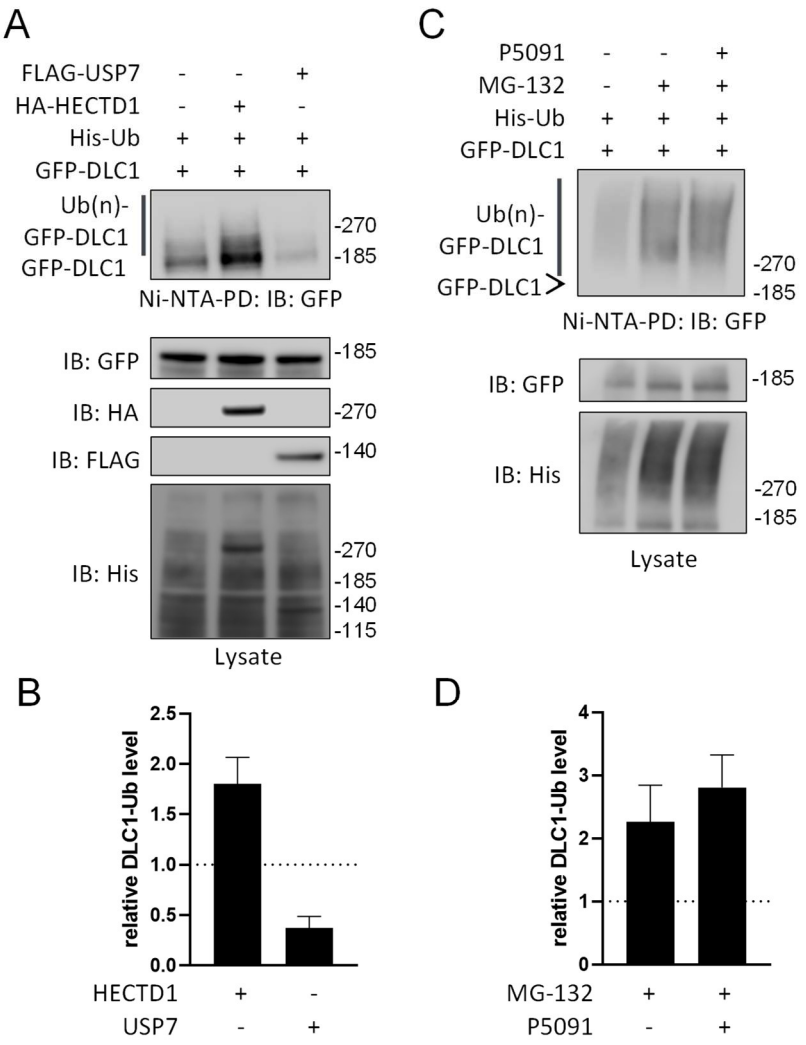


**Figure 11: HECTD1 and USP7 regulate DLC1 ubiquitation.** (A) HEK293T cells were transiently transfected with vectors encoding the indicated constructs, treated with the proteasome inhibitor MG-132 (10 μM) and lysates were subjected to pulldown with Ni–NTA-agarose. Pulldowns and lysates were analyzed by immunoblotting with the indicated antibodies. (B) Western blots from three independent experiments were analyzed with ImageJ. The fold change in ubiquitinated GFP-DLC1 species was determined by normalizing their signal intensity to that of control sample, and is shown as mean ± SEM. (C) MCF7 cells were transiently transfected with vectors encoding the indicated constructs. The next day, cells were treated with MG-132 (10 μM), P5091 (20 μM) as indicated or DMSO as a control for 6 h before lysis. Lysates were subjected to pulldown with Ni–NTA-agarose. Pulldowns and lysates were analyzed by immunoblotting with the indicated antibodies. (D) Western blots from three independent experiments were analyzed with ImageJ. The fold change in ubiquitinated GFP-DLC1 species was determined by normalizing their signal intensity to that of control sample, and is shown as mean ± SEM.

### 3.1.3 HECTD1 and USP7 regulate DLC1 levels at focal adhesions

For its full tumor suppressive activity, DLC1 is dependent on the recruitment to FAs by the binding of tensins (Liao et al. 2007). Here, it interacts with other FA associated proteins such as FAK or talin and is involved in cellular processes such as FA turnover and mechanotransduction (Li et al. 2011; Tripathi et al. 2017; Kaushik et al. 2014). The above biochemical experiments demonstrated a role for HECTD1 and USP7 in the regulation of DLC1 stability but allow for no conclusions whether the active FA-localized DLC1 pool is equally affected or rather maintained irrespective of changes in total protein levels. Thus, to investigate

DLC1 abundance specifically at FAs, immunofluorescence microscopy analyses after HECTD1 depletion or USP7 inhibition were performed in MCF7 cells. The signal intensity of DLC1 staining upon treatment of cells with USP7 inhibitors was significantly reduced at FA areas defined by the adaptor protein paxillin (Fig. 12A, B).

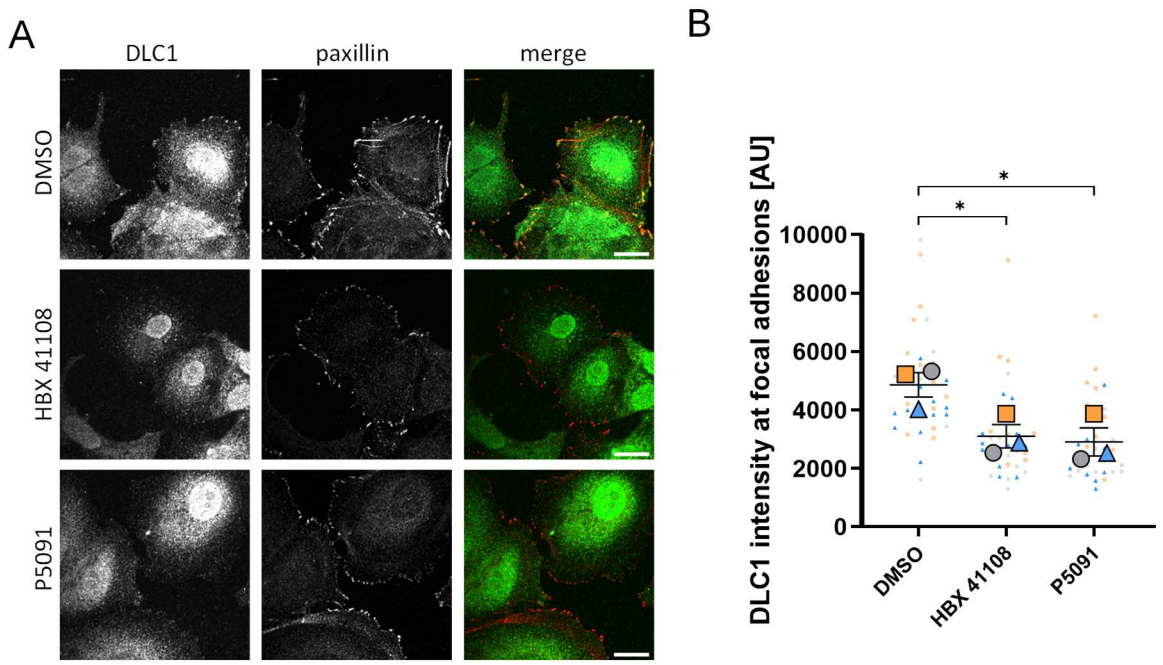


**Figure 12: USP7 inhibition decreases DLC1 levels at focal adhesions.** (A) MCF7 cells were seeded on collagen-coated glass coverslips. The next day, cells were treated with P5091 (20 µM), HBX 41108 (10 µM) or DMSO as a control for 6 h before fixation. Fixed cells were stained for DLC1 (green) and paxillin (red) with specific primary antibodies, followed by AlexaFluor488- and AlexaFluor546-coupled secondary antibodies, respectively. Images show a single basal section, scale bar: 20 µm. (B) The mean intensity of the DLC1 signal at focal adhesions over the whole image was quantified using ImageJ. N = 36 images, n = 3. Statistical comparison of means by RM-ANOVA with Dunnett's multiple comparison test: DMSO vs. HBX41108: p = 0.0252; DMSO vs. P5091: p = 0.0178.

Conversely, depletion of HECTD1 with specific siRNAs resulted in a significant increase of DLC1 detected at focal adhesions (Fig. 13A, B). Nascent adhesions undergo a maturation process during which their size changes depending on mechanical tension forces from actomyosin networks. Actomyosin contractility, in turn, is controlled by local Rho signaling. To this end, DLC1 depletion was previously described to promote the accumulation of smaller paxillin-positive adhesive structures (Holeiter et al. 2008; Kaushik et al. 2014). Looking more closely at adhesion morphology by measuring the length of paxillin structures revealed a significant decrease in mean FA length upon USP7 inhibition, in line with these earlier reports (Fig. 14A). On the contrary, cells depleted of HECTD1 showed on average longer FAs (Fig. 14B). This was likely due to the higher local abundance of DLC1, as its simultaneous depletion abolished the effect.

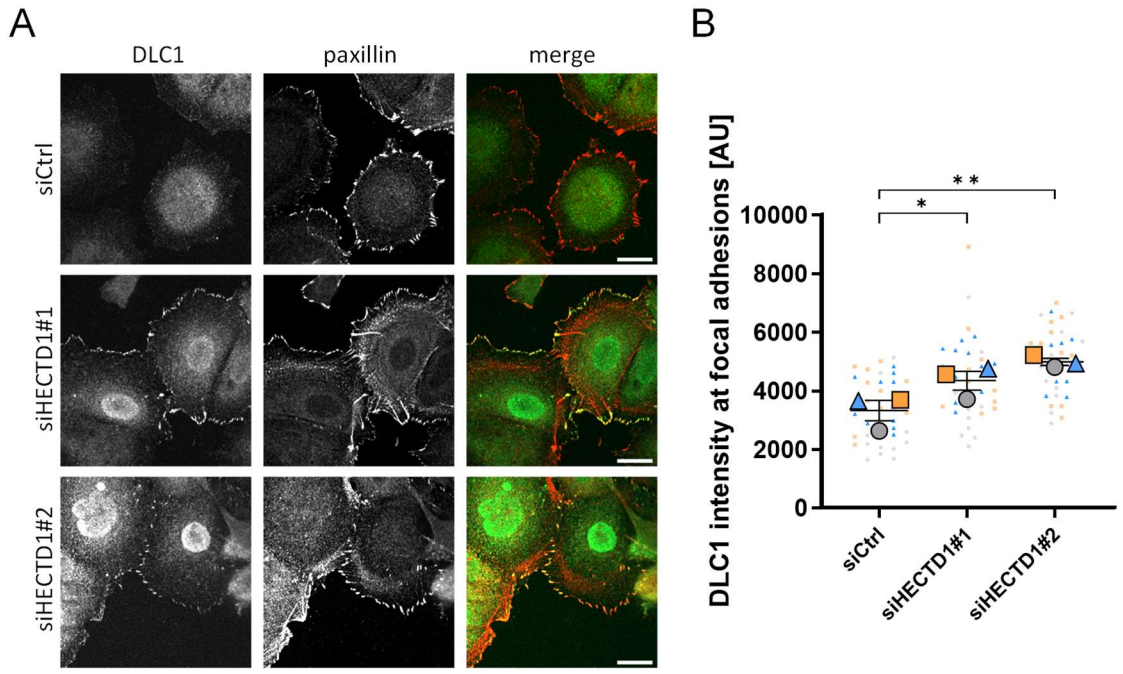


**Figure 13: HECTD1 knockdown increases DLC1 levels at focal adhesions.** (A) MCF7 cells were transfected with the indicated siRNAs, seeded on collagen-coated glass coverslips and fixed after 72 h. Fixed cells were stained for DLC1 (green) and paxillin (red) with specific primary antibodies, followed by AlexaFluor488- and AlexaFluor546-coupled secondary antibodies, respectively. Images show a single basal section, scale bar: 20 µm. (B) The mean intensity of the DLC1 signal at focal adhesions over the whole image was quantified using ImageJ. N = 36 images, n = 3. Statistical comparison of means by RM-ANOVA with Dunnett's multiple comparison test: siCtrl vs. siHECTD1#1: p = 0.0171; siCtrl vs. siHECTD1#2: p = 0.0029.

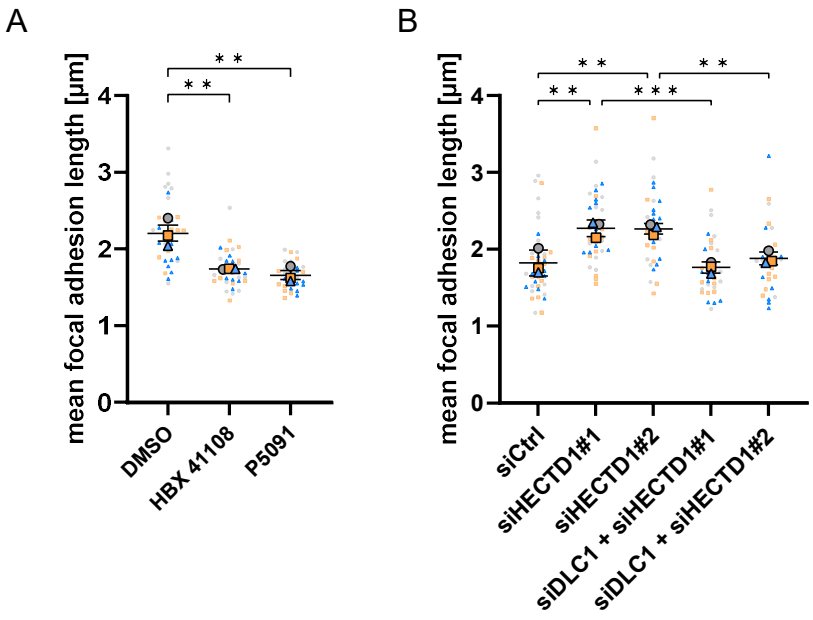


**Figure 14: DLC1 abundance at FAs regulates their morphology**. (A) Mean focal adhesion length per cell in samples from Fig. 13 was analyzed using ImageJ. N = 36, 31, 30; n = 3. Statistical comparison of means by RM-ANOVA with Dunnett's multiple comparison test: DMSO vs. HBX 41108: p = 0.0064; DMSO vs. P5091: p = 0.0036. (B) MCF7 cells were transfected with the indicated siRNAs. After 2 days, cells were seeded on collagen-coated glass coverslips and fixed 16 h later. Cells were stained with paxillin-specific primary antibody followed by AlexaFluor488-coupled secondary antibody. Mean focal adhesion length per cell was analyzed using ImageJ. N = 40, 36, 29, 35, 30; n = 3. Statistical comparison of means by one-way ANOVA with Bonferroni's multiple comparison test: siCtrl vs siHECTD1#1: p = 0.0017; siCtrl vs. siHECTD1#2: p = 0.002; siHECTD1#1 vs. siDLC1 + siHECTD1#1: p = 0.0007; siHECTD1#2 vs. siDLC1 + siHECTD1#2: p = 0.0056.

Taken together, the rapid turnover of DLC1 by the Ub-proteasome machinery in breast cancer cells was demonstrated. HECTD1 and USP7 were identified as novel interaction partners of DLC1. Modulation of HECTD1 levels and USP7 activity was shown to alter DLC1 stability and its abundance at focal adhesions. Thus, opposing regulatory mechanisms of DLC1 protein homeostasis by USP7 and HECTD1 are suggested.

## 3.2 A novel nuclear export sequence in DLC1

Although it has been known for many years that DLC1 shuttles between the cytoplasm and the nucleus, a detailed understanding of the translocation mechanisms of the protein and its function within this compartment is still lacking. Recently, nuclear DLC1 has been proposed to exert an oncogenic role in melanoma through the association with the transcription factor FOXK1 (Yang et al. 2020). When overexpressed in breast cancer cells, DLC1 mostly shows a cytoplasmic localization. However, in order to further elucidate its function in the nucleus, model systems that show preferential nuclear DLC1 localization are required. Therefore, the goal was to identify the region in DLC1 responsible for its nuclear export and to entrap the protein in the nucleus by mutation of this NES. Generally, NESs are characterized by several hydrophobic amino acids with defined spacing (Kosugi et al. 2008). Several candidate sequences were proposed in previous work, but their mutation or deletion did not alter the subcellular localization of the protein (Chan et al. 2011; Theil 2008). Here, I analyzed the DLC1 sequence using LocNES, a bioinformatics tool that was not available at the time of the previous studies, to identify potential NESs (Xu et al. 2015). The top results obtained from the LocNES sequence analysis are shown in Table 16. Notably, the two highest scoring proposed sequences covered a neighboring hydrophobic cluster in the SR region between the SAM and the GAP domain. This amino acid stretch harbored a combination of class 1a, class 1b, and class 3 NES consensus patterns (Kosugi et al. 2008). The third proposed sequence corresponded to a combined class 1d and class 3 motif.

**Table 17: Top candidate NESs predicted by LocNES. Given are the highest scoring regions in the DLC1 sequence predicted as putative NES by the LocNES algorithm and their respective prediction score.**

| Predicted NES Sequence | LocNES score |
|---|---|
| $^{225}$ SKTRSLLKRMESLKL $^{239}$ | 0.709 |
| $^{223}$ AKSKTRSLLKRMESL $^{237}$ | 0.427 |
| $^{55}$ DRDAIEALCRRLNTL $^{69}$ | 0.328 |
| $^{741}$ PKDQRLQAIKAAIML $^{755}$ | 0.195 |
| $^{265}$ GMDEEKLKQLNCVEI $^{279}$ | 0.187 |

Initial focus was placed on the highest scoring putative NES sequences that were altered by point mutations of individual amino acids to alanine such that the prediction of the respective sequence by LocNES was abolished. The mutations are hereafter referred to as NES1* and NES2*, respectively (Fig. 15A). The localization of GFP-tagged NES mutants, based on the

GAP-inactive DLC1 K714E point mutant to conserve cell morphology (Heering et al. 2009), was analyzed by fluorescence microscopy. Fusion proteins harboring the NES1* mutation showed a clear shift in steady-state subcellular localization towards the nucleus as indicated by the significantly increased ratio of nuclear to cytoplasmic mean fluorescence intensity (Fig. 15B, C). On the contrary, NES2* mutation alone or in combination with NES1* showed no alteration in localization.

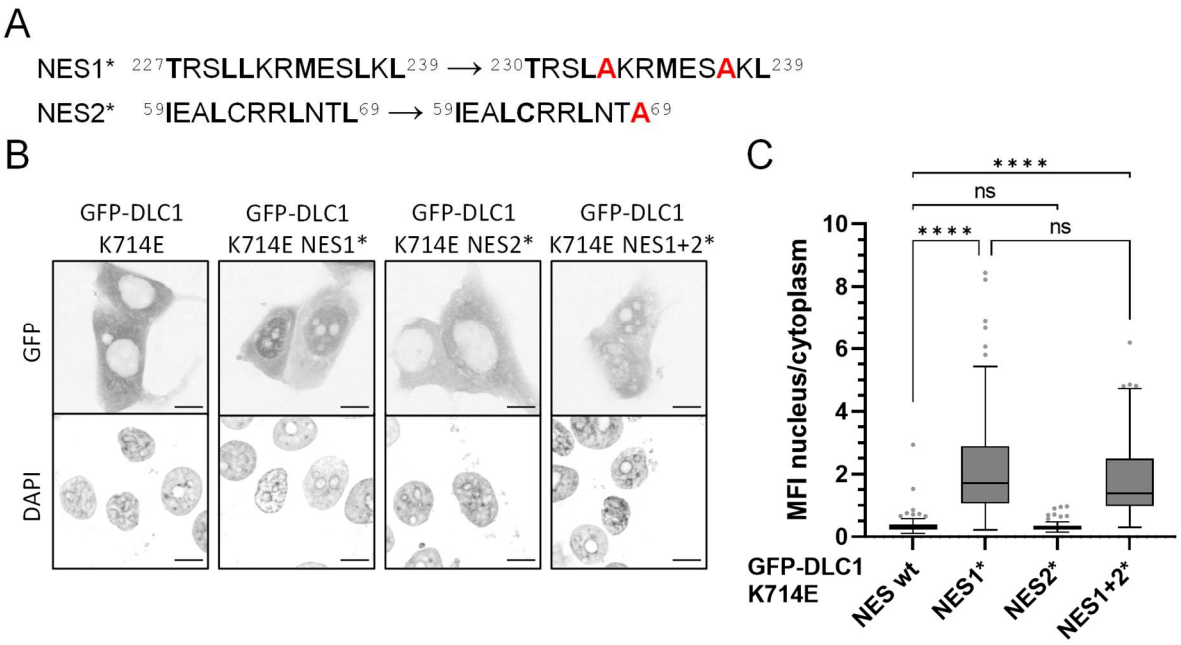


**Figure 15: Mutation in putative NES alters DLC1 localization.** (A) Schematic of the mutations introduced to disrupt putative nuclear export sequences. (B) MCF7 cells were transfected with plasmids encoding the indicated constructs. After fixation, nuclei were counterstained with DAPI and cells were analyzed by fluorescence microscopy. Scale bars: 10 µm (C) Images from (B) were analyzed with ImageJ. Graph shows the ratio of mean fluorescence intensity (MFI) of nuclear to cytoplasmic GFP signal per cell. (Boxplot with Tukey whiskers; N=115, 100, 86, 111 cells; n=3). Statistical comparison by Kruskal-Wallis test with Dunn's multiple comparisons test: NES wt vs NES1*: $p < 0.0001$; NES wt vs. NES2*: $p > 0.9999$; NES wt vs NES1+2*: $p < 0.0001$; NES1* vs NES1+2*: $p > 0.9999$.

To exclude additional effects of the GAP-inactivating K714E point mutation, similar experiments were conducted using GFP-tagged GAP-active constructs in MCF7 cells. Again, in cells expressing constructs harboring the NES1* mutation, GFP signals were clearly stronger in the nucleus (Fig. 16A, B). This suggests that the hydrophobic cluster spanning amino acids 227-239 acts as a bona fide NES, the mutation of which impedes nuclear export, leaving the protein trapped in the nucleus.

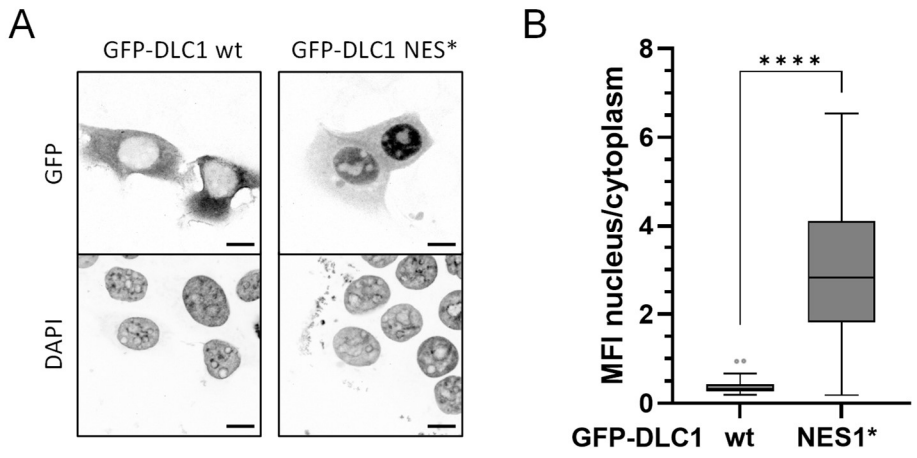


**Figure 16: NES mutation alters DLC1 localization independent of GAP activity.** (A) MCF7 cells were transfected with plasmids encoding the indicated constructs. After fixation, nuclei were counterstained with DAPI and cells were analyzed by fluorescence microscopy. Scale bars: 10 µm. (B) Images from (A) were analyzed with ImageJ. Graph shows the ratio of mean fluorescence intensity (MFI) of nuclear to cytoplasmic GFP signal per cell. (Boxplot with Tukey whiskers; N=60, 54 cells; n=2). Statistical comparison by Mann-Whitney test: wt vs. NES1*: $p < 0.0001$.

Interestingly, in previous work, a part of the NES surrounding the serine residue on position 236 were identified to constitute a PKD phosphorylation consensus motif (Scholz et al. 2009). The phosphorylation of this site in immunopurified GFP-DLC1 by PKD1 was further validated experimentally in kinase assays *in vitro* (Rolf-Peter Scholz, IZI, University of Stuttgart, unpublished data). Phosphorylated amino acids within an NES have been reported to be able to alter nuclear export by affecting exportin recognition and binding. To probe a potential effect of NES phosphorylation in DLC1 nuclear export, phosphodeficient serine to alanine or phosphomimetic serine to aspartate or glutamate point mutations were introduced in GFP-tagged GAP-inactive DLC1. Localization of the muteins was again analyzed by immunofluorescence (Fig. 17A, B). However, all phosphomutants showed a mostly cytoplasmic localization in otherwise unstimulated cells, similar to the constructs with native NES. Nevertheless, subtle differences in export rates due to phosphodeficient or phosphomimetic mutation might not be immediately visible with this set-up and thus deserve future investigation.

In summary, a hydrophobic amino acid stretch within the serine-rich linker region between the SAM and the GAP domain of DLC1 could be identified as likely NES. Introduction of a targeted point mutation of this motif resulted in a predominantly nuclear localization, independent of the GAP activity. These constructs will thus serve as a valuable tool to unravel the role of DLC1 in the nucleus.

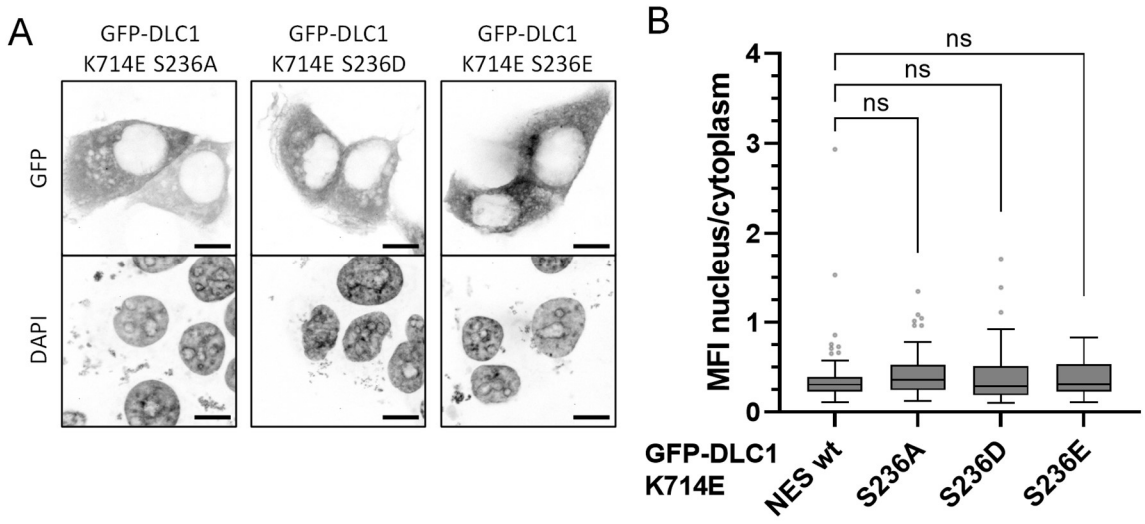


**Figure 17: Mutations of putative phosphorylation site in NES do not alter DLC1 localization.** (A) MCF7 cells were transfected with plasmids encoding the indicated constructs. After fixation, nuclei were counterstained with DAPI and cells were analyzed by fluorescence microscopy. (B) Images from (A) were analyzed with ImageJ. Graph shows the ratio of mean fluorescence intensity (MFI) of nuclear to cytoplasmic GFP signal per cell. For NES wt, cells analyzed represent the same samples as in Fig. 16. (Boxplot with Tukey whiskers; N=115, 62, 45, 36 cells; n=1). Statistical comparison by Kruskal-Wall test with Dunn's multiple comparisons test: NES wt vs. S236A: p= 0.1599; NES wt vs. S236D: p> 0.9999; NES wt vs. S236E: p=0.9116).

## 3.3 Regulation of localization and activity of DLC3 by a novel phosphorylation switch

### 3.3.1 An intrinsically disordered polybasic region in DLC3 is essential for membrane binding

Protein binding of negatively charged phospholipids is often mediated through adjacent clusters of basic amino acids separated by hydrophobic residues (Heo et al. 2006). To uncover potential membrane binding regions in DLC3, we made use of the modified hydrophobicity scale and algorithm described by Brzeska and colleagues (Brzeska et al. 2010).

The most prominent peak identified by the sequence analysis corresponds to a 23 amino acid stretch within the region of DLC3 linking the SAM and GAP domains (Fig. 18A, B). This region is rich in the basic amino acids arginine, lysine and histidine and is therefore referred to as polybasic region (PBR) hereafter.

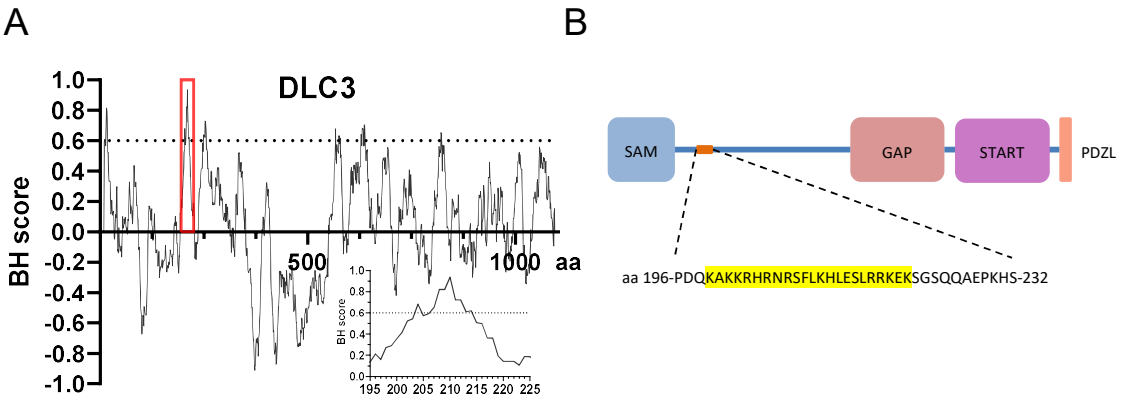


**Figure 18: Identification of a basic-hydrophobic-basic cluster in DLC3.** (A) BH plot of basic and hydrophobic residues in the DLC3 sequence using the scale developed by Brzeska et al. The red box marks the identified polybasic region from aa 199-221, magnified in the insert. (B) Schematic showing the sequence and position of the polybasic region in the linking region between the SAM and GAP domains of DLC3 (aa 199-221, marked yellow).

For the other family members DLC1 and DLC2, sequence analysis with the BH algorithm did not show a similar prominent peak in the N-terminal linker region (Fig. 19A,B). Rather, the region that showed the highest BH score in DLC1 and DLC2, respectively, corresponds to the previously described PBR directly adjacent to the GAP (Erlmann et al. 2009). Direct sequence comparison of the novel PBR showed that DLC3 contains five additional basic amino acids compared to the homologous regions in DLC1 and DLC2, respectively (Fig. 19C). Interestingly, this region in DLC1 was found to contain an additional hydrophobic amino acid and constitutes the NES newly described above. When comparing the PBR sequence with orthologous DLC3 sequences from other species, a high degree of conservation was observed for higher mammals (Table 18).

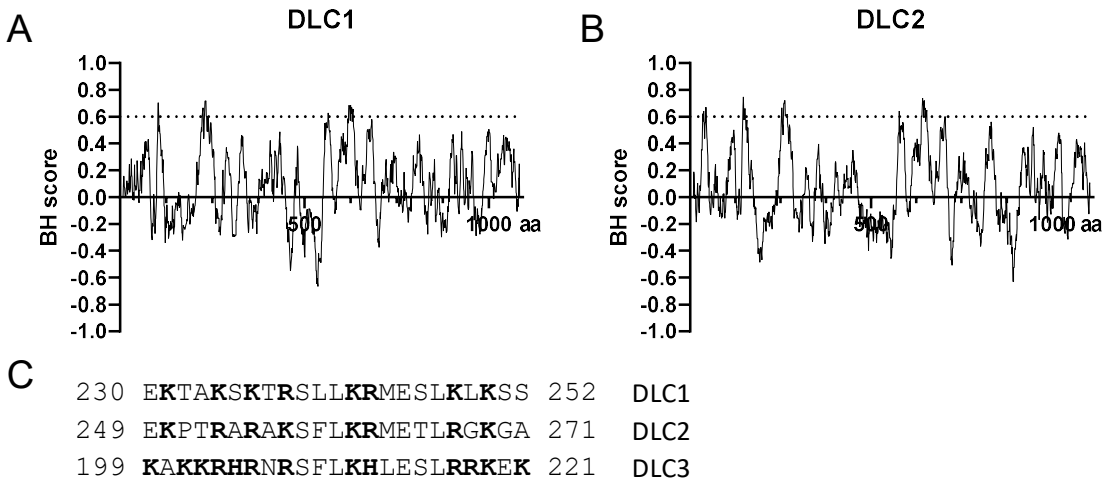


**Figure 19: The DLC3 PBR is more basic than the corresponding region in DLC1 and DLC2.** (A,B) BH plot of basic and hydrophobic residues in the DLC1 (A) and DLC2 (B) sequence using the scale developed by Brzeska et al.(C) Sequence comparison of the novel PBR in DLC3 with homologous regions of other DLC family members after alignment with BLAST. Basic amino acids are marked in bold.

**Table 18: The DLC3 PBR sequence is conserved among higher mammals.** Orthologous DLC3/STARD8 protein sequences from the indicated species were aligned with BLAST.

| Species | Aligned Sequence |
|---|---|
| *Homo sapiens* | 199 KAKKRHRNRSFLKHLESLRRKEK 221 |
| *Pan troglodytes* | 203 KAKKRHRNRSFLKHLESLRRKEK 225 |
| *Macaca mulatta* | 213 KAKKRHRNRSFLKHLESLRRKEK 235 |
| *Canis lupus* | 214 KAKKRH-SRSFLKHLDSLRWKEK 235 |
| *Mus musculus* | 195 KVKK-HYSRSFLKHLESLRRKEK 216 |
| *Rattus norvegicus* | 199 KVKK-HYSRSFLKHLESLRRKEK 220 |
| *Bos taurus* | 209 KTKK-HRSQSFLKHLESLRRKEK 230 |
| *Sus scrofa* | 215 KTKKHH-SRSFLKHLESLRRKEK 236 |
| *Heterocephalus glaber* | 119 KAKKHH-TRSFLKHLESLRRKEK 140 |
| *Ictidomys tridecemlineatus* | 209 KSKK-QRSRSFLKHLESLRRKEK 230 |
| *Gallus gallus* | 228 KPKKR-RSRSFLKRIESLRRKDK 249 |
| *Xenopus tropicalis* | 222 KTKKR-KTRGFLKRMESLRRREK 243 |
| *Danio rerio* | 237 KP-KRP-SRSFL------RRKE- 250 |

In recent years, protein regions that lack a stable secondary structure, referred to as unstructured or intrinsically disordered region (IDR), have gained increased attention with respect to membrane binding properties (Cornish et al. 2020). As no experimental structural data for DLC3 are available, *in silico* analyses with protein disorder prediction programs were performed. Applying the ANCHOR2 and IUPred3 algorithms on the DLC3 sequence, revealed high disorder scores for some parts of the linker region between the SAM and GAP domains. In particular, the highest scores were obtained around amino acid position 200, where the PBR was located, and for a larger segment from approximately amino acid position 400 to 550. (Fig. 20A). Further *in silico* analysis was performed using the recently developed artificial

intelligence program AlphaFold 2, a deep learning system to accurately predict protein structure. In the output models, the PBR was not folded into a secondary structure (Fig. 20B). Rather, the low pLDDT confidence scores obtained further pointed toward the PBR being disordered (Fig. 20C).

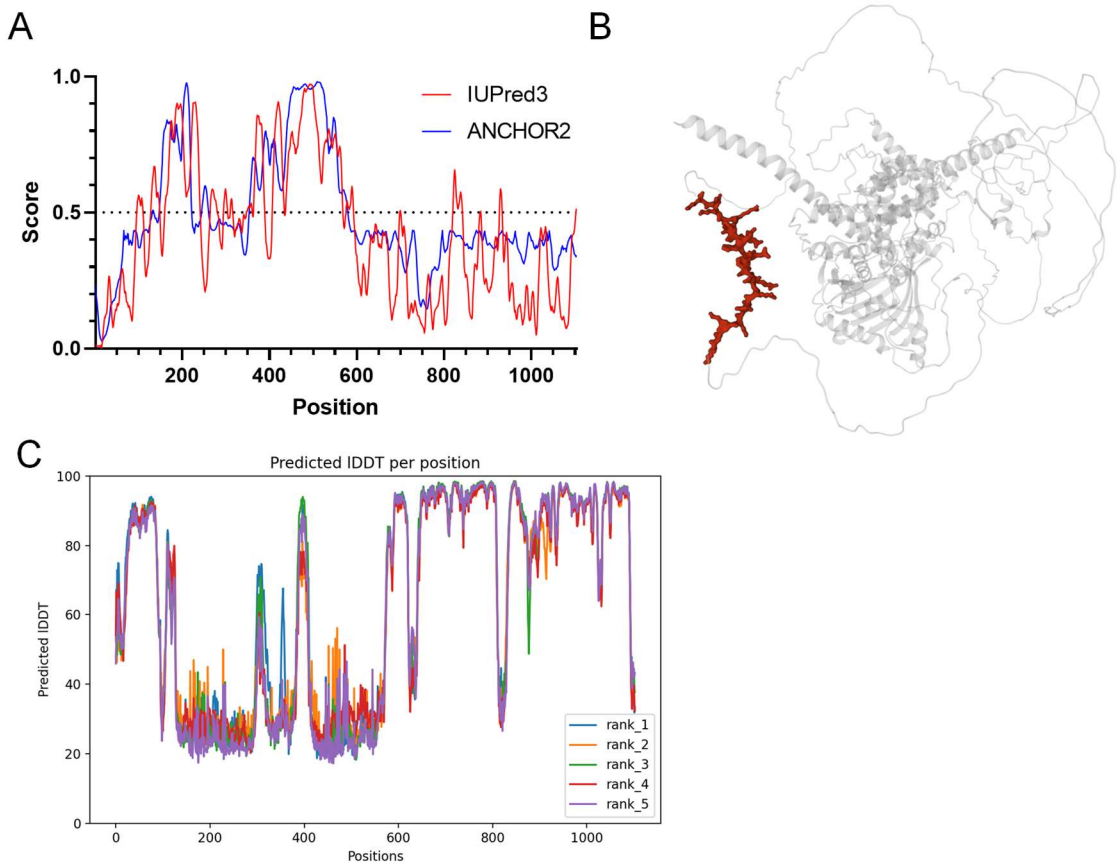


**Figure 20: Large regions of DLC3 are intrinsically disordered.** (A) Predicted disorder scores for the DLC3 amino acid sequence obtained with the IUPred3 and ANCHOR2 programs. (B) Unrelaxed rank 1 model of the predicted DLC3 structure using AlphaFold 2 depicted as cartoon representation, with the PBR (aa 199-221) depicted as red molecular surface representation. (C) pLDDT confidence scores of predicted DLC3 structures obtained with AlphaFold 2 unrelaxed model prediction.

Previously, recombinant N-terminal DLC3 fragments encompassing amino acids 2-232 were found to interact with negatively charged lipids, using lipid overlay assays, whereas fragments lacking the PBR did not (Braun 2015). To study the importance of the PBR in the context of the full-length protein, MCF7 cells stably expressing the GFP-tagged full length protein or a PBR deletion mutant (DLC3-ΔPBR), lacking amino acids 196 to 232, were generated. The GAP-inactive DLC3 K725E point mutant was used to prevent disruption of epithelial morphology (Hendrick et al. 2016). Fractionation experiments with these cells revealed an enrichment of the DLC3-ΔPBR protein in the supernatant fraction containing soluble cytosolic proteins compared to the full-length protein (Meyer 2019). Further, the subcellular distribution

was analyzed by immunofluorescence microscopy. The intact DLC3 protein accumulated at cell-cell contacts marked by E-Cadherin as previously described (Hendrick et al. 2016), while the DLC3-ΔPBR mutant displayed a significantly stronger cytosolic localization (Fig. 21A, B). Taken together, these data imply that DLC3 is able to associate with membranes through an intrinsically disordered polybasic region.

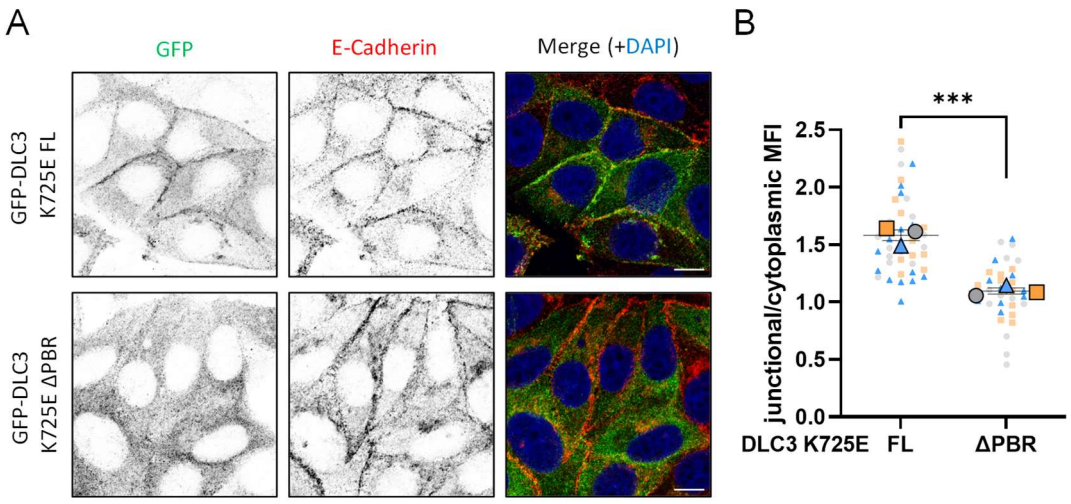


**Figure 21: Deletion of the PBR leads to decreased membrane association.** (A) GFP-DLC3 K725E full-length (FL) and ΔPBR localization in MCF7 cells stably expressing the proteins. Cells were stained for GFP (green) and E-Cadherin (red) with specific primary antibodies and AlexaFluor488- or AlexaFluor546- coupled secondary antibodies, nuclear counterstain with DAPI (blue). Images are maximum intensity projections of several confocal sections. Stainings and image acquisition were performed by Vivien Heller. Scale bars: 10 µm. (B) Analysis of images from (A). Graph shows the mean fluorescence intensity (MFI ± SEM) of the GFP signal at cell junctions versus the cytoplasmic GFP signal (n=3; N=43, 36 cells; unpaired t-test of means: p=0.0008).

### 3.3.2 The DLC3 PBR contains a phosphorylation switch regulating membrane association

IDRs are known to be prime targets for phosphorylation events (Iakoucheva et al. 2004) which change the electrostatic landscape and may also result in disorder-to-order transitions (Mittag et al. 2010). Thus, phosphorylation of the PBR could represent a regulatory mechanism for the interaction of DLC3 with negatively charged membranes. Initial sequence analyses using the prediction programs Scansite4.0 and NetPhos3.1 predicted two serine residues at position 208 and 215 to be phosphorylated with high stringency. To find out whether these serines within the PBR were indeed subject to phosphorylation, mass spectrometry experiments of full-length Flag-DLC3 isolated by immunoprecipitation from HEK293T cells overexpressing the construct were performed. In these samples, peptides with phosphorylated serine residues

corresponding to S208 and S215 could be detected (Fig. 22A, B), thus confirming that both sites can undergo phosphorylation *in cellulo*.

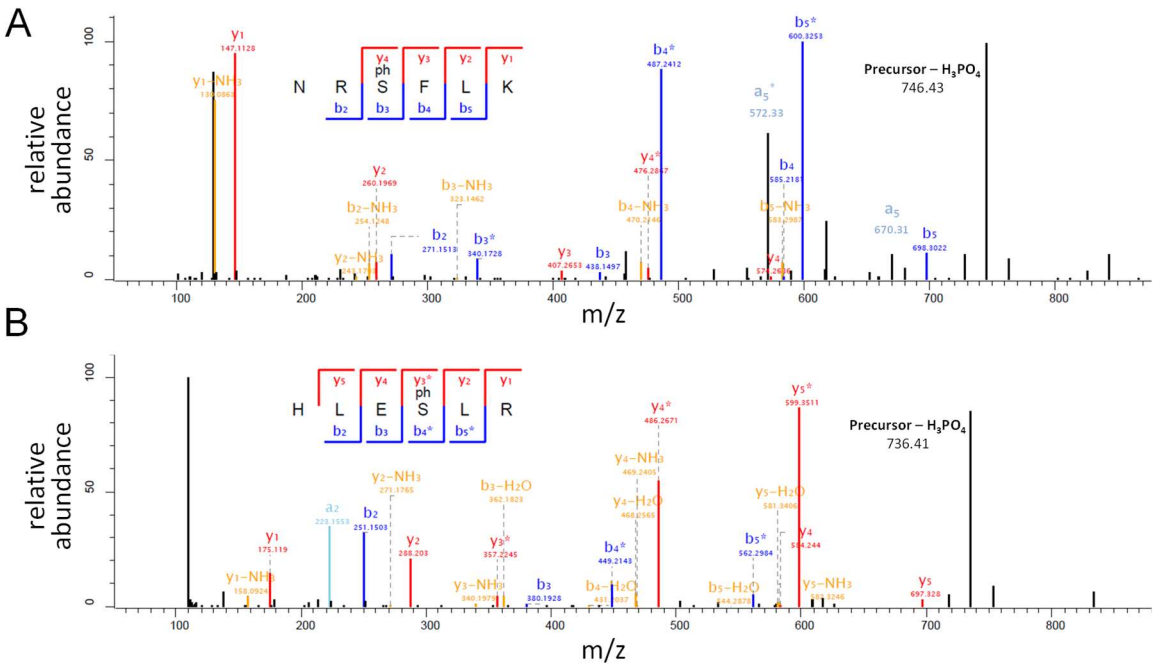


**Figure 22: Serines 208 and 215 of DLC3 are phosphorylation targets in cellulo.** Fragmentation mass spectra of the phosphopeptides NRpSFLK (A) and HLEpSLR (B) corresponding to amino acids 206-211 and 212-217 in DLC3, respectively, obtained after immunoprecipitation of FLAG-tagged DLC3 from HEK293T cells (n=1).

In work from collaborators, structural NMR studies were performed to investigate the interaction of short peptide sequences of the DLC3 PBR, either wild-type or with incorporated phosphoserines, with small unilamellar vesicles containing variable amounts of negatively charged phosphatidylserine as membrane mimetics. These data suggested that the phosphorylation could indeed reduce the interactions with negatively charged membranes (Hauth 2018). For *in cellulo* experiments, GAP-inactive GFP-DLC3 constructs harboring phosphodeficient serine to alanine mutations or phosphomimetic serine to aspartate mutations on serines 208 and 215, respectively, were transiently expressed in MCF7 cells. The introduction of phosphodeficient mutations did not appear to alter the localization of the protein at cell-cell contacts (Fig. 23A, B). However, the phosphomimetic PBR mutant constructs displayed a significant change towards a more soluble localization. Of note, in co-immunoprecipitation experiments, the phosphomimetic DLC3 PBR mutations did not interfere in the interaction of DLC3 with Scribble (Fig. 24), thus ruling out an indirect effect of the PBR domain on DLC3 membrane recruitment by the C-terminal PDZ ligand motif. This suggests a phosphorylation switch model with phosphorylation of the DLC3 PBR leading to displacement from the membrane.

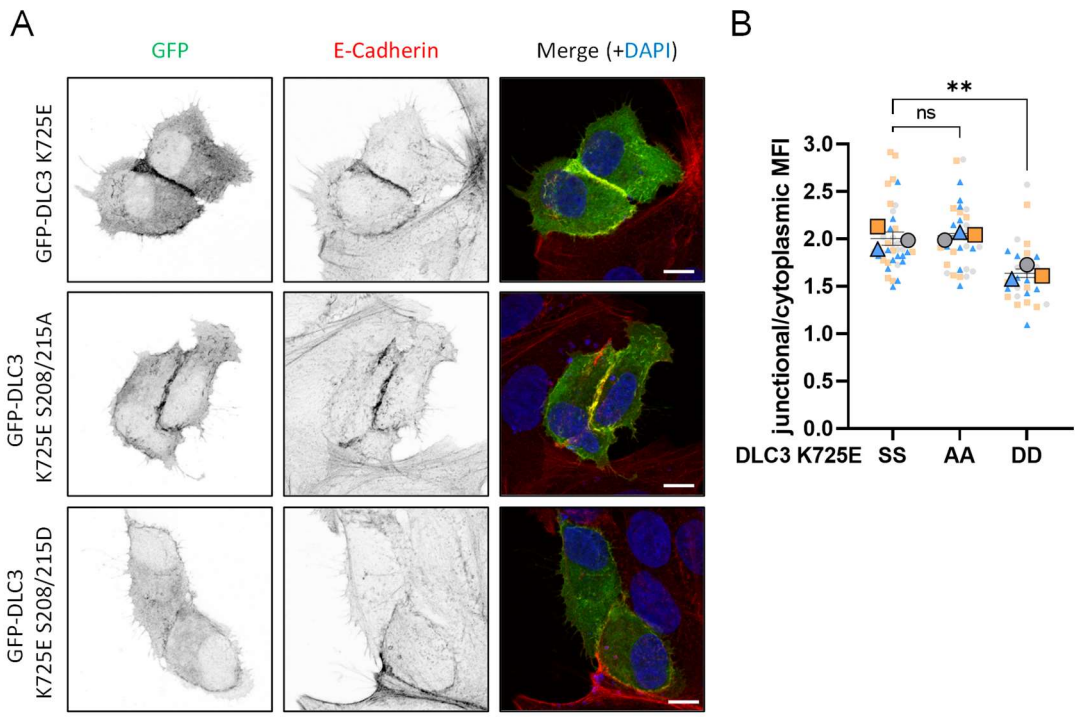


**Figure 23: Phosphomimetic PBR mutations decrease DLC3 membrane association.** (A) MCF7 cells were transfected with plasmids encoding the indicated GFP-DLC3 constructs. After fixation, cells were stained for GFP (green) and E-Cadherin (red) with specific primary antibodies and AlexaFluor488- or AlexaFluor546- coupled secondary antibodies, nuclear counterstain with DAPI (blue). Images are maximum intensity projections of several confocal sections. Stainings and image acquisition were performed by Corinna Kersten. Scale bars: 10 µm. (B) Graph shows the mean fluorescence intensity (MFI -/+ SEM) of the GFP signal at cell junctions versus the cytoplasmic GFP signal (n=3, N= 39, 33, 30); one-way ANOVA of means with Dunnett's post-test: WT vs. AA p=0.8765; WT vs. DD p=0.0037)

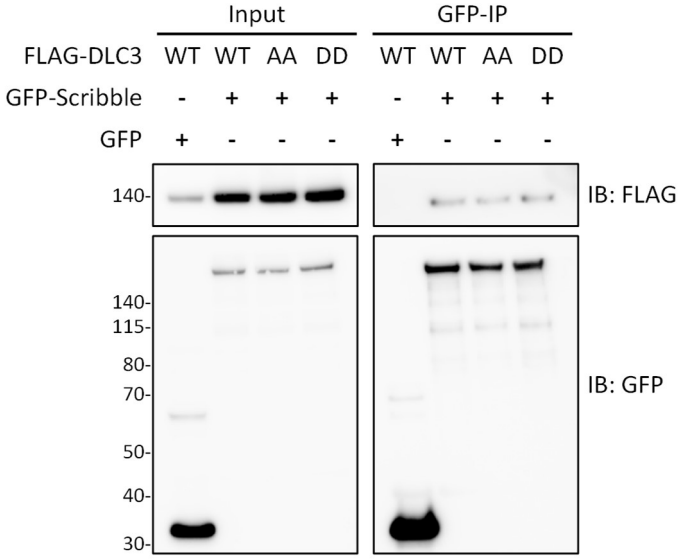


**Figure 24: Phosphomimetic DLC3 PBR mutations do not abolish Scribble binding.** HEK293T cells were transiently transfected with vectors encoding the indicated constructs. The next day, cells were lysed and immunoprecipitation with a GST-tagged anti-GFP nanobody pre-coupled to glutathione sepharose beads was performed. Cell lysates (Input) and precipitates (GFP-IP) were analyzed by immunoblotting using the indicated antibodies. Cropped blot showing co-immunoprecipitation signals is derived from blots with different exposure compared to input. Shown is a representative blot of two independent experiments.

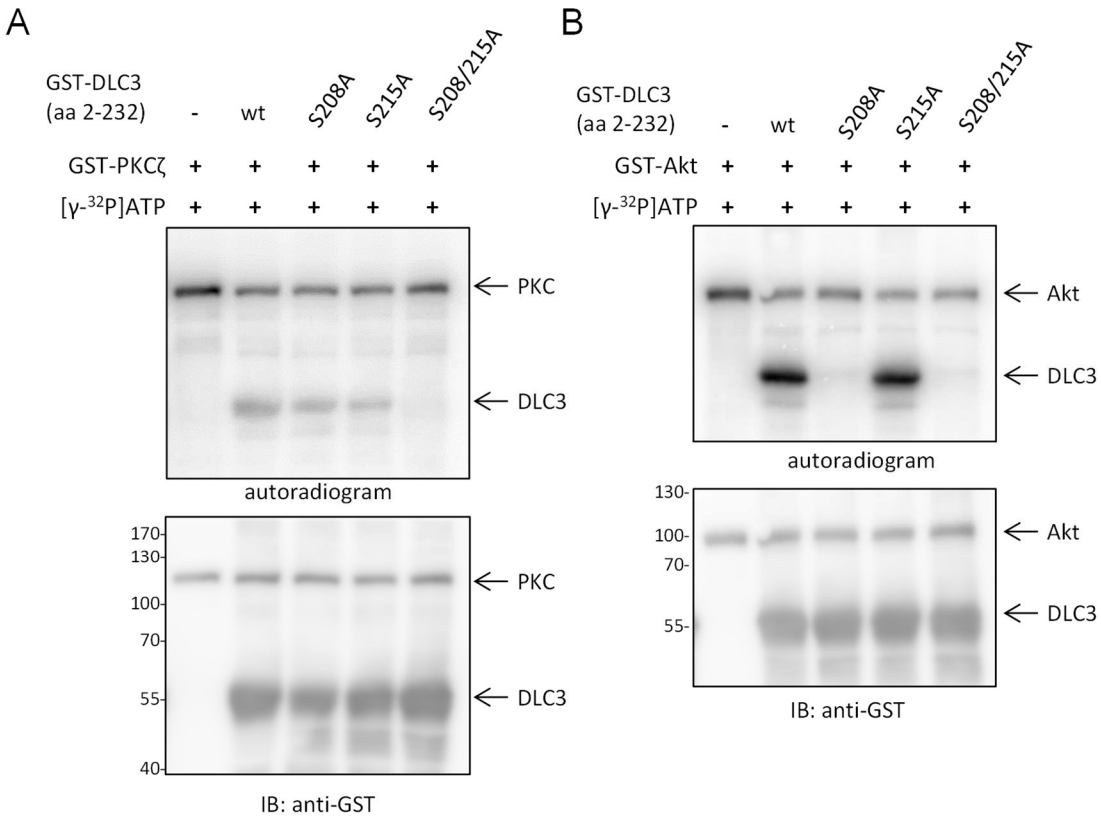


**Figure 25: aPKC and Akt can phosphorylate serine residues in the DLC3 PBR in vitro.** In-vitro kinase assay on purified N-terminal DLC3-GST fusion proteins with or without phosphodeficient serine to alanine muta-tions using radiolabeled ATP and recombinant GST-PKCζ (A) or GST-Akt (B). Proteins were separated by SDS-PAGE and transferred to membrane. Incorporation of radioactive phosphate was analyzed using a PhosphorImager (top panel), followed by immunoblotting with a GST-specific antibody (n=1).

Identification of upstream kinases controlling this phosphorylation switch and triggers for DLC3 phosphorylation would deepen our understanding of spatial Rho regulation. To start, *in silico* sequence analysis for kinase consensus substrate motifs was performed. The prediction programs Scansite 4.0 and NetPhos3.1 both predicted kinases of the protein kinase C family as most likely kinases responsible for the phosphorylation. Independently, the region encompassing the PBR has been predicted to be a target of phosphorylation through the aPKC subfamily (Bailey and Prehoda 2015). Since more than half of all proteins that are essential for regulating cell polarity have been characterized as aPKC substrates (Hong 2018), first, the ability of the kinase family member PKCζ to phosphorylate these residues was investigated *in vitro*. Whereas recombinant GST-tagged N-terminal DLC3 fragments were efficiently phosphorylated by PKCζ, fusion proteins with either S208 or S215 mutated to alanine incorporated markedly lower amounts of radiolabeled phosphate, while phosphorylation was completely abolished by mutating both residues simultaneously (Fig. 25A). Thus, both serines can be regarded as genuine aPKC phosphorylation sites. For S208, the next-best result predicting a responsible kinase was PKB/Akt, a well-known downstream kinase of EGFR activation. As DLC3 was shown to regulate EGFR trafficking (Braun et al. 2015),

phosphorylation by Akt as a feedback scenario might be a possibility. Therefore, further in vitro kinase assays were performed with recombinant Akt. For this kinase, the results showed a clear preference for phosphorylation of S208, as its mutation to alanine completely abolished the incorporation of radiolabeled phosphate (Fig. 25B). This suggests that only S208 but not S215 is a phosphorylation target of Akt.

Intriguingly, a number of cancer samples catalogued in the cBioPortal and COSMIC databases showed genomic mutations that result in the replacement of certain amino acid residues within the DLC3 PBR (Table 18). Some of these mutations might have the potential to directly alter the PBR electrostatic and structural properties. However, in the context of the newly proposed phosphorylation switch, the accumulation in substitutions of specific arginine residues directly upstream of S208 is particularly interesting (Fig. 26A). To recognize their substrates, basophilic kinases depend on critical arginine residues surrounding the target serine (Rust and Thompson 2011). These mutations could therefore perturb the recognition and phosphorylation of S208 in DLC3 by its upstream kinases. As a proof of concept, *in vitro* kinase assays were conducted with DLC3 fragments harboring mutations in R205. Indeed, phosphorylation by Akt was markedly reduced for the R205H mutation, and completely abolished for the R205C mutation, comparable to the phosphodeficient S208A variant (Fig. 26B). This implies that these mutations can alter the phosphoregulatory mechanism of DLC3 membrane association and thus potentially lead to an imbalance in Rho signaling that might contribute to tumor progression.

**Table 19: List of cancer-associated DLC3 PBR mutations**. Human cancer samples with STARD8 mutations resulting in amino acid substitutions in the DLC3 PBR from the cBioportal and COSMIC databases are shown. CO refers to the COSMIC sample ID, where available. Otherwise, the sample ID from the respective study in cBioportal is given. ICGC: International Cancer Genome Consortium

| Substitution | Tumor entity | Sample ID | Study |
|---|---|---|---|
| K201N | Uterus | TCGA-EO-A3B0-01 | TCGA PanCancerAtlas |
| R203C | Uterus | TCGA-B5-A3FA-01 | TCGA PanCancerAtlas |
| R203C | Breast | COSS1649378 (CO) | Nik-Zainal et al. 2016 |
| R203H | Prostate | COSS2467394 (CO) | Robinson et al. 2015 |
| R205C | Melanoma | Patient 62 | Liu et al. 2019 |
| R205C | Melanoma | MEL-JWCI-WGS-1 | Hodis et al. 2012 |
| R205C | Kidney | COSS2856950 (CO) | Singla et al. 2020 |
| R205C | Uterus | COSS2198308 (CO) | TCGA PanCancerAtlas |
| R205H | Endometrium | COSS2906931 (CO) | Li et al. 2021c |
| R205H | Ovary | COSS1475106 (CO) | TCGA PanCancerAtlas |
| R207H | Biliary tract | COSS2459748 (CO) | ICGC (BTCA-JP) |
| R207S | Melanoma | COSS2121765 (CO) | TCGA PanCancerAtlas |
| R218Q | Prostate | COSS2467362 (CO) | Robinson et al. 2015, |
| E220K | Skin | COSS2869816 (CO) | Bonilla et al. 2016 |
| K221R | Liver | COSS2340048 (CO) | TCGA PanCancerAtlas |

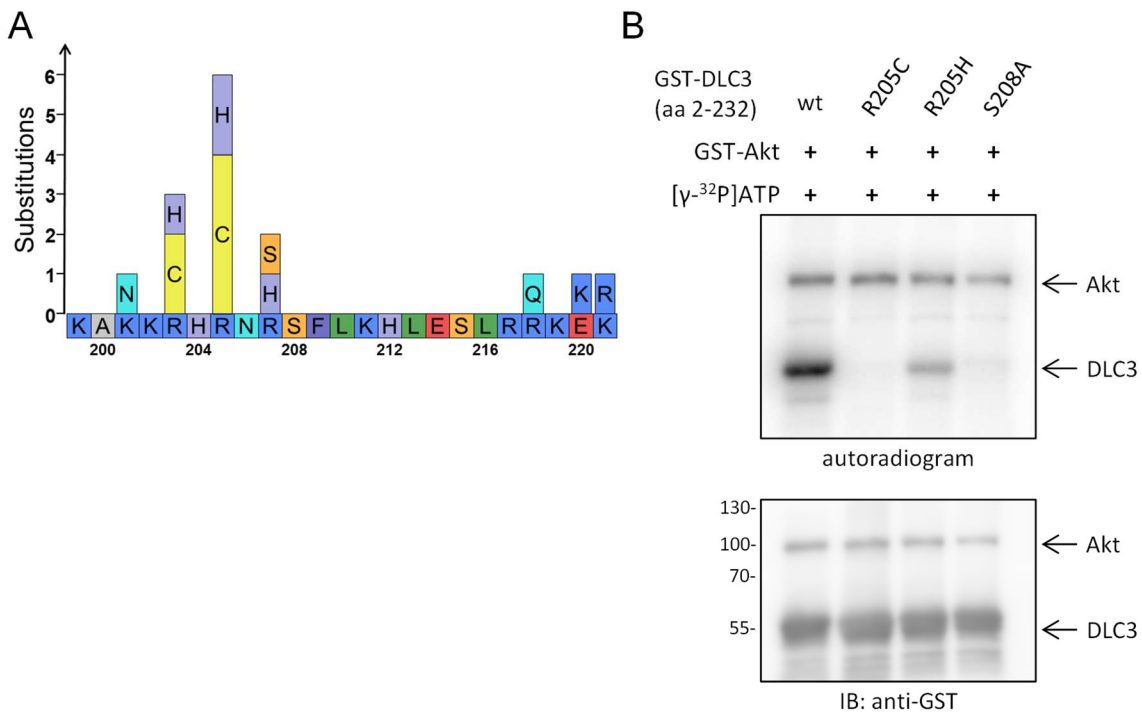


**Figure 26: Cancer-associated mutations can alter DLC3 PBR phosphorylation in vitro.** (A) Schematic of amino acid substitutions in the DLC3 PBR resulting from *STARD8* mutations in human cancer samples reported in the cBioportal and COSMIC databases. (B) In-vitro kinase assay on purified N-terminal DLC3-GST fusion proteins with or without cancer-associated substitution of arginine 205 or phosphodeficient serine to alanine mutation, respectively, using radiolabeled ATP and recombinant GST-Akt. Proteins were separated by SDS-PAGE and transferred to membrane. Incorporation of radioactive phosphate was analyzed using a PhosphorImager (top panel), followed by immunoblotting with a GST-specific antibody (n=1).

# 4 Discussion and outlook

Small GTPases of the Rho subfamily are key regulators of cytoskeletal remodeling and thus play a vital role in many important cellular processes such as cell motility, cell adhesion, cell polarity and polarized intracellular trafficking. Alteration of these functions through deregulated Rho signaling can facilitate cancer initiation and progression. Normally, Rho activity is tightly controlled in space and time through activating GEFs and inactivating GAP proteins. However, in cancer, expression of these regulators is often disturbed. Inactivation of RhoGAPs has been described as the most common alteration of Rho regulators (Lukasik et al. 2011). In particular, the DLC family of RhoGAP proteins has emerged as a potent class of tumor suppressors whose expression is frequently lost in various tumors. The underlying mechanisms have been best studied for DLC1 until now. The *DLC1* gene undergoes loss-of-heterozygosity at a comparable frequency to the master tumor suppressor *TP53* in lung, colon, breast, liver and pancreatic cancer (Xue et al. 2008). While additional transcriptional and post-transcriptional suppression of DLC1 expression is common in various cancers, such mechanisms play a lesser role in other tumor types, e.g. breast cancer. Therefore, functional inactivation of DLC proteins by posttranslational regulatory mechanisms such as degradation or mislocalization may provide an additional means to silence their GAP activity, but this remains largely unexplored. In this work, I investigated the proteostasis of DLC1 in breast cancer cell lines and uncovered new regulators of its proteasomal degradation. In addition, a previously unknown nuclear export motif in DLC1 was revealed whose mutation entraps the protein in the nucleus. In the last part, a unique membrane binding site in DLC3 and its regulation by phosphorylation was characterized.

## 4.1 DLC1 proteostasis in breast cancer

In breast cancer, loss of heterozygosity of the DLC1 gene also occurs relatively frequently in up to 50-60% of primary tumors (Xue et al. 2008). The remaining allele does not appear to be as severely affected by epigenetic transcriptional regulation as in other cancers, since promoter methylation occurs in breast cancer in only about 10% to one-third of cases (Teramoto et al. 2004; Seng et al. 2007). Moreover, no evidence of post-transcriptional suppression by miRNAs has yet been reported for DLC1 in breast cancer. Therefore, DLC1 expression might in principle be retained in a significant fraction of breast cancers but shut down by post-translational inactivation. Previous reports of DLC protein regulation mostly relied on single cell lines or overexpression models. Only recently, the expression of DLC1 protein was more systematically studied in panels of four breast cancer and NSCLC cell lines, five gastric cancer cell lines, and seven melanoma cell lines, respectively (Tripathi et al. 2017; Hinsenkamp et al. 2022; Yang et al. 2020). The cell line panel used in this work, comprising

15 BC cell lines of different subgroups, thus represents the most comprehensive resource on DLC1 protein expression in cell lines of a single tumor entity to date.

Low levels of DLC1 in most luminal A/B, HER2+, and in some triple negative breast cancer (TNBC) cell lines are in agreement with its presumed role as a tumor suppressor. In contrast, the robust DLC1 expression in several TNBC cell lines is surprising and raises questions about its role in these. TNBC represents 15-20% of all breast cancers and is defined by the deficiency of estrogen and progesterone receptors (ER/PR) and HER2 overexpression (Perou et al. 2000). Patients with TNBC cannot be treated with endocrine or anti-HER2 therapies and have a higher risk of metastasis and lower progression-free and overall survival rates (Foulkes et al. 2010; Liedtke et al. 2008). DLC1 is functionally inactivated after phosphorylation by Akt or Src, the latter being primed by Erk phosphorylation (Tripathi et al. 2017; Tripathi et al. 2019). Hyperactivation of the PI3K/AKT/mTOR pathway through mutations in the *PIK3CA*, *PTEN* or *AKT1* genes is a common feature in TNBC (Umemura et al. 2007; Costa et al. 2018; Bareche et al. 2018). Additionally, alterations in the MAPK signaling cascade were frequently reported (Rocca et al. 2022; Acosta-Casique et al. 2022). Thus, it seems plausible that in TNBC cell lines, the RhoGAP activity of highly expressed DLC1 is suppressed by aberrant phosphorylation and hence the protein is largely inactive. However, non-tumor suppressive functions, as have recently been suggested in metastatic melanoma, cannot be excluded (Yang et al. 2020).

In several breast cancer cells, low or barely detectable DLC1 protein levels were significantly increased after treatment with proteasome inhibitors. Together, the results of inhibition of protein synthesis, DUBs and proteasomal degradation clearly demonstrate a rapid turnover of DLC1 in breast cancer cells with a short half-life of only a few hours. In a recent systematic study using a proteomic approach, similar protein half-lives of DLC1 were determined with two and six hours in U2OS osteosarcoma and RPE1 retinal pigment epithelial cells, respectively (Li et al. 2021b). This is further in agreement with data obtained from the NSCLC cell lines H1703 and A549 (Kim et al. 2013; Tripathi et al. 2021). Moreover, the rapid turnover of DLC1 contrasts with the prolonged stability of other focal adhesion-associated or -integral proteins observed here and reported elsewhere (Visavadiya et al. 2016; Lee and Otto 1996). In general, rapid protein degradation allows cells to quickly respond to external stimuli by altering the protein abundance (Golan-Lavi et al. 2017; Li et al. 2021b). For DLC1, this is likely to be useful to cells in relatively fast-changing or fast-acting processes such as cell adhesion and cell migration. Recent reports of its molecular functions on focal adhesions have brought DLC1 into the spotlight as an essential component in the regulation of focal adhesion turnover (Kaushik et al. 2014; Haining et al. 2018; Dahal et al. 2022). In this line, my data shows a clear effect on focal adhesion morphology after a change in DLC1 abundance. This goes along with

a recent report establishing DLC1 as pivotal for collective migration and sprouting angiogenesis in response to substrate stiffening and VEGF stimulation downstream of YAP/TAZ in endothelial cells (van der Stoel et al. 2020).

How is DLC1 protein turnover regulated on the molecular level? The results obtained in this work confirm earlier studies from hepatocellular carcinoma cells showing that its degradation is brought about by the human 26S proteasome (Luo et al. 2011). In NSCLC and mesenchymal stem cells, the CRL4A-DDB1-FBXW5 RING-type ubiquitin ligase complex was described to regulate DLC1 ubiquitination and degradation (Kim et al. 2013; Tripathi et al. 2021). Using mass spectrometry and subsequent biochemical validation, I identified the HECT E3 ligase HECTD1 as novel DLC1 interactor involved in its degradation in breast cancer cells. The siRNA-mediated depletion of HECTD1 resulted in DLC1 stabilization and increased its abundance at focal adhesions. Subsequently, the mean length of focal adhesion increased, indicating decreased turnover of focal adhesion, and this effect was dependent on DLC1. In a previous report, HECTD1 was implicated in the regulation of adhesive structures by regulating PIPKIγ90 ubiquitination and degradation (Li et al. 2013). Similarly to my results, HECTD1 knockdown by shRNA increased focal adhesion stability in breast cancer cells. Mechanistically, this could be explained by the direct competition of PIPKIγ90 with β-integrin for talin binding or the local production of $PIP_2$, which results in defects in integrin-mediated adhesion and force coupling (Barsukov et al. 2003; Legate et al. 2011). Interestingly, $PIP_2$ binds to the PBR preceding the GAP domain in DLC1 and is required for its efficient RhoGAP activity (Erlmann et al. 2009). The resulting reduction in focal adhesion turnover is expected to result in reduced migration. However, in contrasting reports, homozygous inactivation of HECTD1 in murine embryonic fibroblasts and shRNA-mediated HECTD1 knockdown in T47D or MDA-MB-231 breast cancer cells was associated with increased cell migration and EMT (Shen et al. 2017; Duhamel et al. 2018). These studies identified the scaffolding protein IQGAP1 and the microtubule plus-end tracking protein ACF7 as the major downstream factors mediating the effects of HECTD1 inactivation or depletion, respectively. IQGAP1 itself has been suggested as a facilitator of correct DLC1 localization (Tanaka et al. 2019). In addition to the different cellular systems, interpretation of these results is complicated by the different means used to downregulate HECTD1, from knockdown by siRNA or shRNA to homozygous inactivating mutation. The development of tools that allow acute disruption of HECTD1 activity, such as optogenetic and degron-mediated deletion approaches or a specific inhibitor, could help to better understand the interdependencies between HECTD1 and its proposed substrates, as well as the impact on cellular functions.

Moreover, the stimuli that trigger DLC1 ubiquitination and the crosstalk between different ubiquitination pathways remains an open question. While no components of the CRL4A-DDB1-

FBXW5 complex were among the putative DLC1 interaction partners identified in the mass spectrometry results, the list included another cullin-RING ligase substrate receptor, DCAF7. Further research into the molecular mechanisms is required, as neither this nor any previous study could convincingly demonstrate direct ubiquitination of endogenous DLC1 *in cellulo* or recombinant DLC1 *in vitro*. In many cases, ubiquitination is a multistep process with spatial and temporal regulation, often requiring priming PTMs (Song and Luo 2019). Indeed, for DLC1 a recent publication showed that methylation of DLC1 by EZH2 greatly increases interaction with the CRL4A-DDB1-FBXW5 complex and subsequent ubiquitination (Tripathi et al. 2021). Thus, endogenous polyubiquitinated DLC1 species may not be present in high abundance at any point in the cell. Additionally, the attached ubiquitin moieties or other necessary priming PTMs might preclude detection in immunoblotting or immunoprecipitation with the widely used monoclonal anti-DLC1 antibody.

Moreover, the interaction of DLC1 with a deubiquitinating enzyme, USP7, was demonstrated for the first time in this work. My results point towards a role for USP7 in the stabilization of DLC1, as its inhibition rapidly reduced DLC1 protein levels and cells overexpressing USP7 showed reduced DLC1 ubiquitination. The USP7 inhibitors used in this study employ different modes of action: HBX 41108 has been reported to act in an allosteric and reversible manner, while analogs of P5091 have been shown to covalently bind to the catalytic centre (Colland et al. 2009; Pozhidaeva et al. 2017). Nevertheless, the possibility of off-target effects contributing to the observed downregulation of DLC1 cannot be fully excluded. USP7 has been studied extensively in the context of degradation of the master tumor suppressor p53. Here, it mediates the deubiquitination of the ubiquitin ligase Mdm2, whose stabilization facilitates degradation of p53 (Li et al. 2002; Li et al. 2004; Cummins and Vogelstein 2004). USP7-mediated deubiquitination has further been implicated in tumor progression through the stabilization of the oncogene N-myc and the mislocalization of the tumor suppressor PTEN (Tavana et al. 2016; Song et al. 2008). Besides deciphering the molecular mechanisms of DLC1 ubiquitination and deubiquitination, it will be crucial to distinguish direct effects of USP7 on DLC1 from secondary effects upon longer-term USP7 inhibition to understand the collective and interdependent contribution of different USP7 substrates to the disruption of DLC1 proteostasis during carcinogenesis. For example, p53 was implicated in DLC1 transcription whereas PTEN was shown to regulate DLC1 subcellular localization (Low et al. 2011; Wang et al. 2016; Cao et al. 2015). In recent years, USP7 inhibition has been proposed as a promising therapeutic strategy in cancer treatment (Oliveira et al. 2022). However, in light of the new results regarding the involvement of USP7 but also its substrates in the regulation of DLC1, these approaches should be carefully weighed depending on the context and require further investigation in future studies.

## 4.2 DLC1 nuclear localization

DLC1 is the only member of the DLC protein family for which a nuclear localization has been described. The first report showed cytoplasmic to nuclear translocation of overexpressed fluorescently tagged DLC1 in NSCLC and healthy lung epithelial cell lines of which a fraction later underwent apoptosis (Yuan et al. 2007). While small proteins up to 20-40 kDa can passively diffuse between the two compartments, larger proteins require an energy-dependent transport mechanism through the nuclear pore complex (Fried and Kutay 2003). This involves binding of importins to a nuclear localization signal (NLS) while binding of exportins to nuclear export signals (NES) leads to translocation of the protein back to the cytoplasm. The constant shuttling of DLC1 into and out of the nucleus was demonstrated by the treatment of MCF7 breast cancer cells or hepatoma cell lines expressing ectopic DLC1 with the exportin inhibitor leptomycin B, which trapped the protein in the nucleus (Scholz et al. 2009; Chan et al. 2011). A basic segment comprising amino acids from position 423 to 429 was identified as a major NLS of ectopic DLC1 in breast cancer cells, as protein harboring mutations in the key arginine residues at positions 428 and 429 accumulated less in the nucleus after Leptomycin B treatment (Scholz et al. 2009). Additionally, the region encompassing amino acids 600 to 700 was identified as a potential contributor to DLC1 nuclear localization using internal deletion mutants in hepatoma cells (Chan et al. 2011).

The identification of a NES in the present work provides the missing piece in the nucleocytoplasmic shuttling cycle of DLC1 and facilitates the study of export mechanism as well as its nuclear function, by introducing NES mutations entrapping the protein in the nucleus. The LocNES algorithm used here has previously shown higher sensitivity and precision compared to earlier NES prediction tools (Xu et al. 2015). Generally, NESs can be classified into six patterns, according to their conserved hydrophobic spacing (Kosugi et al. 2008). The bioinformatical prediction identified a hydrophobic cluster spanning amino acids 227 to 239, which harbors class 1a, class 1b, and class 3 NES consensus patterns, as the two top results (referred to as NES1). The next best predicted region, encompassing amino acids 59 to 69, had in parts been superficially investigated as a potential NES in the past (Chan et al. 2011). However, the previous study only used a deletion mutant that might have altered DLC1 folding or nuclear import capacity. Of the following predicted NES sequences, which scored considerably lower prediction values, the region from amino acid position 271 to 279 was previously examined by mutational analysis and ruled out as a functional NES (Theil 2008).

My results revealed a clear shift in DLC1 localization to the nucleus when key leucine residues in NES1 were mutated to alanine. Mutation of the N-terminal NES2 did not show any effect on localization on its own or in combination with NES1 mutations. Thus, the region spanning amino acids 227 to 239 can be regarded as a bona fide NES. These findings are in line with

previous reports of predominant nuclear localization of DLC1 deletion mutants of the first 300 amino acids that comprise the newly identified NES, while a deletion mutant of only the first 200 amino acids showed a cytoplasmic localization (Yuan et al. 2007; Chan et al. 2011). A previous study further claimed that DLC1 GAP-inactive or GAP deletion mutants would be sequestered in the cytoplasm and that the GAP domain would be required for nucleocytoplasmic shuttling (Yuan et al. 2007). However, while the absolute ratio of nuclear to cytoplasmic fluorescence intensity appeared somewhat lower in cells expressing GAP-inactive than in GAP-competent DLC1 muteins, a marked shift to a nuclear localization was observed for both proteins after the introduction of NES1 mutations. Thus, the GAP domain does not seem to be the major factor in determining nuclear import competency of DLC1. Nevertheless, GAP activity could influence DLC1 nucleocytoplasmic shuttling through an altered interactome and thus differential retention or secondary effects of downstream Rho signaling. Importantly, other work has further validated DLC1 constructs with different protein tags harboring the NES mutation identified in this work in different cell lines and could show differential binding to a putative nuclear interaction partner (Hahn 2021).

Until now, no specific stimulus triggering nuclear import or export, respectively, has been identified. In fact, it is unclear whether such stimuli exist at all, or whether DLC1 is translocation-competent *per se* and its localization is determined by retention in either compartment, e.g. through binding of FOXK1 in the nucleus or 14-3-3 proteins in the cytoplasm (Yang et al. 2020; Scholz et al. 2009). Besides obtaining a valuable tool to study nuclear functions of DLC1, identification of the NES region allows for the study of potential regulatory mechanisms that might be responsible for supporting its nuclear localization. In this context, phosphorylated amino acids within NESs have been reported to alter nuclear export rates. Phosphorylation of two serine residues in the NES of sphingosine kinase by PKD prompts its nuclear export (Ding et al. 2007). On the contrary, the NES function of human papilloma virus helicase E1 or p53 in response to DNA damage is disrupted by phosphorylation (Deng et al. 2004; Zhang and Xiong 2001). In preliminary data, serine 236 in the DLC1 NES has been identified as a potential target of PKD. Thus, PKD, in addition to its role in binding DLC1 to 14-3-3, may regulate nucleocytoplasmic shuttling of DLC1 at the level of protein export from the nucleus. However, for serine 236, neither the phosphodeficient substitution by alanine nor the phosphomimetic substitutions by aspartate or glutamate showed any striking effect on protein localization. The phosphomimetic mutations mimic the negative charge introduced by phosphorylation but might not fully recapitulate the canonical activity of the phosphorylated protein (Mohler and Rinehart 2019). Additionally, the mutations might only cause subtle differences in export rates that are masked by transient overexpression and thus require more detailed investigation in future experiments.

## 4.3 DLC3 membrane localization

Active Rho GTPases are generally anchored to membranes via their C-terminal prenyl group. Thus, localization in proximity to the membrane is crucial for RhoGAP proteins to regulate their target GTPase. For this purpose, many GAP proteins contain canonical lipid or membrane binding domains (Amin et al. 2016). In addition to the C-terminal START domain, all DLC family members harbor a conserved sequence enriched in basic amino acids directly preceding the RhoGAP domain. This PBR is responsible for the binding of $PIP_2$ and the interaction stimulates GAP activity for DLC1 (Erlmann et al. 2009). Over the past few years, our lab has uncovered several non-redundant functions for DLC3 that involve different membrane environments. At the plasma membrane, DLC3 activity is important for the maintenance of adherens junction integrity and cell polarity (Holeiter et al. 2012; Hendrick et al. 2016). Furthermore, DLC3 was found to associate with endomembrane compartments where the regulation of local Rho signaling controls endocytic recycling (Braun et al. 2015; Noll et al. 2019; Lungu et al. 2023). Recruitment to these sites is mediated by the interaction with either Scribble or SNX27 adaptor proteins, which bind to a unique C-terminal PDZ ligand motif (Hendrick et al. 2016; Noll et al. 2019). Now, the results from the present work point towards a differentially regulated and potentially DLC3-specific mechanism for membrane binding and detachment.

Sequence analysis of DLC3 with several structure and disorder prediction algorithms suggested that large parts of the understudied serine-rich linker region between SAM and GAP domain would not fold into a stable secondary structure. Although this region shows poor conservation among the DLC family members, with only around 30% and 40% sequence identity for DLC1 and DLC2, respectively, similar results were previously predicted for the DLC1 serine-rich region (Durkin et al. 2007a; Durkin et al. 2007b). Protein binding to negatively charged lipid bilayers is commonly mediated through electrostatic interactions of positively charged amino acid residues (Mulgrew-Nesbitt et al. 2006). Generally, IDRs show a composition bias towards charged amino acid residues (Romero et al. 2001). Together with their binding promiscuity and their low sequence complexity, this makes them particularly well-suited for multivalent electrostatic interactions necessary for membrane binding compared to folded domains (Cornish et al. 2020). In addition, IDRs can act as steric spacers to maintain a certain distance from the membrane, allowing the formation of protein complexes (Thomas et al. 2019). The clustering of basic together with hydrophobic amino acids was shown to be important for interaction with phosphoinositide species (Heo et al. 2006). Here, a second, N-terminal polybasic region with intermixed hydrophobic residues was identified within the serine-rich DLC3 region, spanning amino acids 199 to 221. The high degree of sequence identity of the PBR observed in DLC3 orthologues in higher mammalian species suggests an evolutionary conserved function. The PBR appears to be necessary for efficient localization of DLC3 at cell-cell contacts, as shown by immunofluorescence analysis of a deletion mutant. In

previous work, a region encompassing the PBR was necessary for binding of an N-terminal recombinant DLC3 fragment to lipids *in vitro* and for recruitment of the full-length protein to Rab8-positive recycling tubules *in cellulo* (Braun 2015). Peptides of the DLC3 PBR were further shown to be sufficient for the interaction with negatively charged small unilamellar vesicles as a membrane model (Hauth 2018). Together, these data point towards membrane binding capability of DLC3 mediated by its PBR.

While the new PBR is partially conserved for the other DLC proteins, it contains three additional basic arginine and lysine residues in DLC3. Moreover, two histidines are present in this region in DLC3, but absent in DLC1 and DLC2. Histidine has a pKa of about 6.5 in solution, which varies depending on the depth of burial within the protein and polar interactions with neighboring residues (Edgcomb and Murphy 2002). This means that many histidine residues are partially protonated at physiological pH and protonation inversely correlates with pH. The DLC3 PBR thus carries more than three extra net positive charges, suggesting that in DLC1 and DLC2, this region would not bind to negatively charged membranes equally well and might not play such a prominent role in membrane binding. In some proteins, the protonation of histidine serves as a pH sensor and can be considered a post-translational modification (Schönichen et al. 2013). Several GEFs show histidine-mediated pH-dependent regulation of activity or altered localization by binding to phosphoinositides via their pleckstrin homology (PH) domain. For the Ras- and Rap-specific GEF RasGRP1, altered signaling activity and plasma membrane recruitment were observed depending on a single histidine charge (Vercoulen et al. 2017). Dbs, a Dbl family RhoGEF that controls migration by activating Cdc42, was found to bind $PIP_2$ with higher affinity at lower pH (Frantz et al. 2007). Further, the recruitment of the ArfGEF Grp1 to endosomal phosphatidylinositol (3,4,5)-trisphosphate ($PIP_3$) is favored at decreasing pH (He et al. 2008). Additional examples of pH-sensitive targeting to endomembranes include proteins containing FYVE (Fab1p, YOTB, Vac1p, and EEA1) domains binding to $PIP_3$ or four-phosphate-adaptor protein 1 (FAPP1) interaction with phosphatidylinositol 4-phosphate at the Golgi (Lee et al. 2005; He et al. 2011). Protons leaking from the acidic lumen of endosomes can lower the local pH on the cytoplasmic membrane side (Lee et al. 2005). The resulting increase in histidine protonation and consequently in charge when recruited to endosomal membranes may stabilize membrane binding of the DLC3-PBR to these organelles. Migrating cells exhibit a pH gradient from front to rear, which could help to balance the previously reported membrane recruitment of DLC3 to the leading edge (Martin et al. 2011; Tarbashevich et al. 2015; Hendrick 2016). Finally, intracellular alkalinization as part of a pH gradient reversal commonly observed in malignant tumors might facilitate DLC3 mislocalization during cancer progression (Zheng et al. 2020).

Given the important role of DLC3 in the maintenance of apical-basal cell polarity and endosomal trafficking, a tight regulation of its membrane association and proximity to the target RhoGTPase is necessary. While membrane recruitment is regulated via the interaction with SNX27 and Scribble, a regulated detachment mechanism might also be required to avoid prolonged retention at the membrane through binding of the PBR. On the one hand, this seems essential to clear proteins that make their way to non-target membranes by diffusion rather than specific recruitment. On the other hand, this could play a role in dynamic processes such as the maintenance of Rho and Rac gradients during cell polarity and RhoB regulation during endocytic recycling, but also on a larger scale in the rapid repolarization of cells after cytokinesis or during cell migration. Protein phosphorylation is a fast and reversible post-translational modification ideally suited for this purpose. Specifically, IDRs were shown to be a major target for phosphorylation events (Iakoucheva et al. 2004). The addition of a negatively charged phosphate group changes the local electrostatic environment and can further lead to adoption of a more stable, ordered confirmation, both of which may result in impaired membrane binding (Mittag et al. 2010). Changes in membrane localization upon PBR phosphorylation have been shown for a number of cases, including the adaptor protein SH2B1β and the GTPase K-Ras (Maures et al. 2011; Bivona et al. 2006).

In the DLC3 PBR, two serine residues were predicted to be candidate phosphorylation targets by kinase motif analyses, and the possibility of phosphorylation of these sites was validated *in cellulo*. Furthermore, proteins harboring two phosphomimetic mutations showed decreased localization at the plasma membrane. Importantly, binding of this mutant to Scribble was maintained, indicating that the observed change in localization was not because of an impaired recruitment mechanism. Previously, peptides representing the phosphorylated PBR showed decreased interaction with negatively charged membrane model systems compared to their unphosphorylated form (Hauth 2018). Further functional experiments in MCF7 cells expressing GAP-competent PBR phosphomutants of DLC3 in an inducible manner revealed that the introduction of phosphomimetic mutations severely reduced the GAP activity towards RhoB compared to the wild-type protein (Cristiana Lungu, University of Stuttgart, unpublished data). This suggests a phosphorylation switch model for the spatial control of Rho signaling, whereby phosphorylation of the DLC3 PBR leads to displacement from the membrane and thus the attenuation of local GAP activity.

Based on kinase motif analysis, aPKC and Akt were predicted as putative kinases responsible for phosphorylation of the DLC3 PBR and validated by *in vitro* kinase assays. While these serve as valuable guidance towards assessing whether certain residues can be directly targeted by a given kinase, additional spatial and temporal regulation mechanisms are at play in cells. Thus, future *in cellulo* experiments will be necessary to validate whether both aPKC

and Akt are indeed upstream kinases responsible for DLC3 PBR phosphorylation. Many other polarity-associated proteins have been confirmed as aPKC substrates (Hong 2018). Moreover, PBR phosphorylation switches depending on aPKC have been reported for *C. elegans* LGL-1 and *D. melanogaster* Miranda polarity proteins (Visco et al. 2016; Hannaford et al. 2018). Therefore, the involvement of aPKC as the possible kinase for DLC3 PBR phosphorylation in a polarity context seems plausible. In addition, other RhoGAP proteins have been predicted as putative aPKC substrates and may thus underlay similar regulatory mechanisms (Bailey and Prehoda 2015). While aPKC may phosphorylate two serine residues in the PBR, the results from the *in vitro* kinase assays suggest that Akt phosphorylation can only take place on serine 208. As DLC3 has been implicated in trafficking of internalized EGFR and Akt is a major downstream kinase of EGFR (Braun et al. 2015), Akt phosphorylation of DLC3 might be part of a feedback mechanism in the context of endocytic recycling. However, it is unclear whether the phosphorylation of single residue within its PBR is sufficient to cause detachment of DLC3 from membranes or whether this would require a cooperative kinase. While phosphorylation of both serine residues was observed on distinct peptides in mass spectrometry, it further remains unknown if both phosphorylation events occur simultaneously or sequentially or whether they might be mutually exclusive. The development of phosphospecific antibodies might help to answer these questions *in cellulo*. Mapping of the surface charge of different biological membranes revealed the inner leaflet of the plasma membrane to be the most negatively charged, while internal membranes showed a lower electrostatic potential (Eisenberg et al. 2021). In future studies, localization analyses of single and double phosphomutants of DLC3, including endomembrane compartments, should shed more light on detailed regulatory mechanisms.

Regarding the role of DLC3 as a tumor suppressor, the discovery of the membrane-binding region and phosphorylation-dependent localization switch opens new perspectives on a potential functional inactivation of DLC3 during cancer development. Both aPKC and Akt are highly dysregulated in various tumor entities and may contribute to the displacement and impaired GAP function of DLC3 (Reina-Campos et al. 2019; Revathidevi and Munirajan 2019). Additionally, several mutations in the DLC3 PBR found in cancer samples might affect DLC3 function. While electrostatic interactions play a major role in their binding of membranes, evidence suggests some additional sequence specificity. Early studies showed drastic differences in the binding of basic peptides to negatively charged membranes based on the presence of either arginine or lysine (Mosior and McLaughlin 1992). Similarly, it was recently reported that the charge-neutral substitution of arginine to lysine residues in Rac1 can alter its lipid binding specificity (Maxwell et al. 2018). Moreover, most kinases require a certain sequence context for efficient phosphorylation. Specifically, phosphorylation of serine 208 by basophilic kinases in DLC3 might be impaired by the cancer-associated mutations of arginines

203, 205, and 207, as these kinases depend on critical arginine residues upstream of the target serine (Rust and Thompson 2011). As a proof of concept, I could show that DLC3 fragments harboring R205H and R205C substitutions were no longer efficiently phosphorylated by Akt *in vitro*. However, all the implications of disease-associated alterations in the DLC3 PBR sequence and phosphorylation status and their possible functional consequences are yet to be elucidated and will open new perspectives to investigate the role of DLC3 cellular functions in health and disease.

## 5 References


Acosta-Casique, A.; Montes-Alvarado, J. B.; Barragán, M.; Larrauri-Rodríguez, K. A.; Perez-Gonzalez, A.; Delgado-Magallón, A. et al. (2022): ERK activation modulates invasiveness and Reactive Oxygen Species (ROS) production in triple negative breast cancer cell lines. *Cellular signalling* 101, p. 110487.

Adam, L.; Vadlamudi, R. K.; McCrea, P.; Kumar, R. (2001): Tiam1 overexpression potentiates heregulin-induced lymphoid enhancer factor-1/beta -catenin nuclear signaling in breast cancer cells by modulating the intercellular stability. *The Journal of biological chemistry* 276 (30), pp. 28443–28450.

Ahmadian, M. R.; Stege, P.; Scheffzek, K.; Wittinghofer, A. (1997): Confirmation of the arginine-finger hypothesis for the GAP-stimulated GTP-hydrolysis reaction of Ras. *Nature structural biology* 4 (9), pp. 686–689.

Alan, J. K.; Lundquist, E. A. (2013): Mutationally activated Rho GTPases in cancer. *Small GTPases* 4 (3), pp. 159–163.

Allin, C.; Ahmadian, M. R.; Wittinghofer, A.; Gerwert, K. (2001): Monitoring the GAP catalyzed H-Ras GTPase reaction at atomic resolution in real time. *Proceedings of the National Academy of Sciences of the United States of America* 98 (14), pp. 7754–7759.

Alpy, F.; Tomasetto, C. (2005): Give lipids a START: the StAR-related lipid transfer (START) domain in mammals. *Journal of cell science* 118 (Pt 13), pp. 2791–2801.

Amin, E.; Jaiswal, M.; Derewenda, U.; Reis, K.; Nouri, K.; Koessmeier, K. T. et al. (2016): Deciphering the Molecular and Functional Basis of RHOGAP Family Proteins: A SYSTEMATIC APPROACH TOWARD SELECTIVE INACTIVATION OF RHO FAMILY PROTEINS. *The Journal of biological chemistry* 291 (39), pp. 20353–20371.

Anbazhagan, R.; Fujii, H.; Gabrielson, E. (1998): Allelic loss of chromosomal arm 8p in breast cancer progression. *The American journal of pathology* 152 (3), pp. 815–819.

Ankasha, S. J.; Shafiee, M. N.; Abdul Wahab, N.; Raja Ali, R. A.; Mokhtar, N. M. (2021): Oncogenic Role of miR-200c-3p in High-Grade Serous Ovarian Cancer Progression via Targeting the 3'-Untranslated Region of DLC1. *International journal of environmental research and public health* 18 (11).

Asnaghi, L.; Vass, W. C.; Quadri, R.; Day, P. M.; Qian, X.; Braverman, R. et al. (2010): E-cadherin negatively regulates neoplastic growth in non-small cell lung cancer: role of Rho GTPases. *Oncogene* 29 (19), pp. 2760–2771.

Atherton, P.; Stutchbury, B.; Wang, D.-Y.; Jethwa, D.; Tsang, R.; Meiler-Rodriguez, E. et al. (2015): Vinculin controls talin engagement with the actomyosin machinery. *Nature communications* 6, p. 10038.

Au, S. L.-K.; Wong, C. C.-L.; Lee, J. M.-F.; Wong, C.-M.; Ng, I. O.-L. (2013): EZH2-Mediated H3K27me3 Is Involved in Epigenetic Repression of Deleted in Liver Cancer 1 in Human Cancers. *PloS one* 8 (6), e68226.

Audebert, S.; Navarro, C.; Nourry, C.; Chasserot-Golaz, S.; Lécine, P.; Bellaiche, Y. et al. (2004): Mammalian Scribble forms a tight complex with the betaPIX exchange factor. *Current biology : CB* 14 (11), pp. 987–995.

Bailey, M. J.; Prehoda, K. E. (2015): Establishment of Par-Polarized Cortical Domains via Phosphoregulated Membrane Motifs. *Developmental cell* 35 (2), pp. 199–210.

Bareche, Y.; Venet, D.; Ignatiadis, M.; Aftimos, P.; Piccart, M.; Rothe, F.; Sotiriou, C. (2018): Unravelling triple-negative breast cancer molecular heterogeneity using an integrative multiomic analysis. *Annals of oncology : official journal of the European Society for Medical Oncology* 29 (4), pp. 895–902.

Barrio-Real, L.; Kazanietz, M. G. (2012): Rho GEFs and cancer: linking gene expression and metastatic dissemination. *Science signaling* 5 (244), pe43.

Barsukov, I. L.; Prescot, A.; Bate, N.; Patel, B.; Floyd, D. N.; Bhanji, N. et al. (2003): Phosphatidylinositol phosphate kinase type 1gamma and beta1-integrin cytoplasmic domain bind to the same region in the talin FERM domain. *The Journal of biological chemistry* 278 (33), pp. 31202–31209.

Bartolomé, R. A.; Molina-Ortiz, I.; Samaniego, R.; Sánchez-Mateos, P.; Bustelo, X. R.; Teixidó, J. (2006): Activation of Vav/Rho GTPase signaling by CXCL12 controls membrane-type matrix metalloproteinase-dependent melanoma cell invasion. *Cancer research* 66 (1), pp. 248–258.

Basak, P.; Leslie, H.; Dillon, R. L.; Muller, W. J.; Raouf, A.; Mowat, M. R. A. (2018): In vivo evidence supporting a metastasis suppressor role for Stard13 (Dlc2) in ErbB2 (Neu) oncogene induced mouse mammary tumors. *Genes, chromosomes & cancer* 57 (4), pp. 182–191.

Berger, M. F.; Hodis, E.; Heffernan, T. P.; Deribe, Y. L.; Lawrence, M. S.; Protopopov, A. et al. (2012): Melanoma genome sequencing reveals frequent PREX2 mutations. *Nature* 485 (7399), pp. 502–506.

Bhattacharya, S.; Chakraborty, D.; Basu, M.; Ghosh, M. K. (2018): Emerging insights into HAUSP (USP7) in physiology, cancer and other diseases. *Signal transduction and targeted therapy* 3, p. 17.

Binamé, F.; Bidaud-Meynard, A.; Magnan, L.; Piquet, L.; Montibus, B.; Chabadel, A. et al. (2016): Cancer-associated mutations in the protrusion-targeting region of p190RhoGAP impact tumor cell migration. *The Journal of cell biology* 214 (7), pp. 859–873.

Bishop, A. L.; Hall, A. (2000): Rho GTPases and their effector proteins. *The Biochemical journal* 348 Pt 2, pp. 241–255.

Bivona, T. G.; Quatela, S. E.; Bodemann, B. O.; Ahearn, I. M.; Soskis, M. J.; Mor, A. et al. (2006): PKC regulates a farnesyl-electrostatic switch on K-Ras that promotes its association with Bcl-XL on mitochondria and induces apoptosis. *Molecular cell* 21 (4), pp. 481–493.

Blom, N.; Sicheritz-Pontén, T.; Gupta, R.; Gammeltoft, S.; Brunak, S. (2004): Prediction of post-translational glycosylation and phosphorylation of proteins from the amino acid sequence. *Proteomics* 4 (6), pp. 1633–1649.

Bonilla, X.; Parmentier, L.; King, B.; Bezrukov, F.; Kaya, G.; Zoete, V. et al. (2016): Genomic analysis identifies new drivers and progression pathways in skin basal cell carcinoma. *Nature genetics* 48 (4), pp. 398–406.

Borchert, N.; Dieterich, C.; Krug, K.; Schütz, W.; Jung, S.; Nordheim, A. et al. (2010): Proteogenomics of Pristionchus pacificus reveals distinct proteome structure of nematode models. *Genome research* 20 (6), pp. 837–846.

Boureux, A.; Vignal, E.; Faure, S.; Fort, P. (2007): Evolution of the Rho family of ras-like GTPases in eukaryotes. *Mol Biol Evol* 24 (1), pp. 203–216.

Braun, A. C.; Hendrick, J.; Eisler, S. A.; Schmid, S.; Hausser, A.; Olayioye, M. A. (2015): The Rho-specific GAP protein DLC3 coordinates endocytic membrane trafficking. *Journal of cell science* 128 (7), pp. 1386–1399.

Braun, A. C.; Olayioye, M. A. (2015): Rho regulation: DLC proteins in space and time. *Cellular signalling* 27 (8), pp. 1643–1651.

Braun, Anja Catharina (2015): Regulation of endocytic membrane trafficking by the GTPase-activating protein Deleted in Liver Cancer 3 (DLC3). PhD thesis: Universität Stuttgart.

Brodu, V.; Casanova, J. (2006): The RhoGAP crossveinless-c links trachealess and EGFR signaling to cell shape remodeling in Drosophila tracheal invagination. *Genes & development* 20 (13), pp. 1817–1828.

Brzeska, H.; Guag, J.; Remmert, K.; Chacko, S.; Korn, E. D. (2010): An experimentally based computer search identifies unstructured membrane-binding sites in proteins: application to class I myosins, PAKS, and CARMIL. *The Journal of biological chemistry* 285 (8), pp. 5738–5747.

Campbell, J. D.; Alexandrov, A.; Kim, J.; Wala, J.; Berger, A. H.; Pedamallu, C. S. et al. (2016): Distinct patterns of somatic genome alterations in lung adenocarcinomas and squamous cell carcinomas. *Nature genetics* 48 (6), pp. 607–616.

Cao, X.; Kaneko, T.; Li, J. S.; Liu, A.-D.; Voss, C.; Li, S. S. C. (2015): A phosphorylation switch controls the spatiotemporal activation of Rho GTPases in directional cell migration. *Nature communications* 6, p. 7721.

Cao, X.; Voss, C.; Zhao, B.; Kaneko, T.; Li, S. S.-C. (2012): Differential regulation of the activity of deleted in liver cancer 1 (DLC1) by tensins controls cell migration and transformation. *Proceedings of the National Academy of Sciences of the United States of America* 109 (5), pp. 1455–1460.

Cereijido, M.; Contreras, R. G.; Shoshani, L. (2004): Cell adhesion, polarity, and epithelia in the dawn of metazoans. *Physiological reviews* 84 (4), pp. 1229–1262.

Chan, L.-K.; Ko, F. C. F.; Sze, K. M.-F.; Ng, I. O.-L.; Yam, J. W. P. (2011): Nuclear-targeted deleted in liver cancer 1 (DLC1) is less efficient in exerting its tumor suppressive activity both in vitro and in vivo. *PloS one* 6 (9), e25547.

Chau, J. E.; Vish, K. J.; Boggon, T. J.; Stiegler, A. L. (2022): SH3 domain regulation of RhoGAP activity: Crosstalk between p120RasGAP and DLC1 RhoGAP. *Nature communications* 13 (1), p. 4788.

Chen, L.; Hu, W.; Li, G.; Guo, Y.; Wan, Z.; Yu, J. (2019): Inhibition of miR-9-5p suppresses prostate cancer progress by targeting StarD13. *Cellular & molecular biology letters* 24, p. 20.

Chiapparino, A.; Maeda, K.; Turei, D.; Saez-Rodriguez, J.; Gavin, A.-C. (2016): The orchestra of lipid-transfer proteins at the crossroads between metabolism and signaling. *Progress in lipid research* 61, pp. 30–39.

Ching, Y.-P.; Wong, C.-M.; Chan, S.-F.; Leung, T. H.-Y.; Ng, D. C.-H.; Jin, D.-Y.; Ng, I. O.-L. (2003): Deleted in liver cancer (DLC) 2 encodes a RhoGAP protein with growth suppressor function and is underexpressed in hepatocellular carcinoma. *The Journal of biological chemistry* 278 (12), pp. 10824–10830.

Chiu, J.-H.; Wen, C.-S.; Wang, J.-Y.; Hsu, C.-Y.; Tsai, Y.-F.; Hung, S.-C. et al. (2017): Role of estrogen receptors and Src signaling in mechanisms of bone metastasis by estrogen receptor positive breast cancers. *Journal of translational medicine* 15 (1), p. 97.

Citterio, C.; Menacho-Márquez, M.; García-Escudero, R.; Larive, R. M.; Barreiro, O.; Sánchez-Madrid, F. et al. (2012): The rho exchange factors vav2 and vav3 control a lung metastasis-specific transcriptional program in breast cancer cells. *Science signaling* 5 (244), ra71.

Colland, F.; Formstecher, E.; Jacq, X.; Reverdy, C.; Planquette, C.; Conrath, S. et al. (2009): Small-molecule inhibitor of USP7/HAUSP ubiquitin protease stabilizes and activates p53 in cells. *Molecular cancer therapeutics* 8 (8), pp. 2286–2295.

Cornish, J.; Chamberlain, S. G.; Owen, D.; Mott, H. R. (2020): Intrinsically disordered proteins and membranes: a marriage of convenience for cell signalling? *Biochemical Society transactions* 48 (6), pp. 2669–2689.

Costa, R. L. B.; Han, H. S.; Gradishar, W. J. (2018): Targeting the PI3K/AKT/mTOR pathway in triple-negative breast cancer: a review. *Breast cancer research and treatment* 169 (3), pp. 397–406.

Cox, J.; Mann, M. (2008): MaxQuant enables high peptide identification rates, individualized p.p.b.-range mass accuracies and proteome-wide protein quantification. *Nature biotechnology* 26 (12), pp. 1367–1372.

Cox, J.; Neuhauser, N.; Michalski, A.; Scheltema, R. A.; Olsen, J. V.; Mann, M. (2011): Andromeda: a peptide search engine integrated into the MaxQuant environment. *Journal of proteome research* 10 (4), pp. 1794–1805.

Cui, H.; Liu, Y.; Jiang, J.; Liu, Y.; Yang, Z.; Wu, S. et al. (2016): IGF2-derived miR-483 mediated oncofunction by suppressing DLC-1 and associated with colorectal cancer. *Oncotarget* 7 (30), pp. 48456–48466.

Cummins, J. M.; Vogelstein, B. (2004): HAUSP is Required for p53 Destabilization. *Cell Cycle* 3 (6), pp. 687–690.

Dahal, N.; Sharma, S.; Phan, B.; Eis, A.; Popa, I. (2022): Mechanical regulation of talin through binding and history-dependent unfolding. *Science advances* 8 (28), eabl7719.

Dammann, R.; Strunnikova, M.; Schagdarsurengin, U.; Rastetter, M.; Papritz, M.; Hattenhorst, U. E. et al. (2005): CpG island methylation and expression of tumour-associated genes in lung carcinoma. *European journal of cancer (Oxford, England : 1990)* 41 (8), pp. 1223–1236.

Deng, W.; Lin, B. Y.; Jin, G.; Wheeler, C. G.; Ma, T.; Harper, J. W. et al. (2004): Cyclin/CDK regulates the nucleocytoplasmic localization of the human papillomavirus E1 DNA helicase. *Journal of virology* 78 (24), pp. 13954–13965.

Denholm, B.; Brown, S.; Ray, R. P.; Ruiz-Gómez, M.; Skaer, H.; Hombría, J. C.-G. (2005): crossveinless-c is a RhoGAP required for actin reorganisation during morphogenesis. *Development (Cambridge, England)* 132 (10), pp. 2389–2400.

Ding, G.; Sonoda, H.; Yu, H.; Kajimoto, T.; Goparaju, S. K.; Jahangeer, S. et al. (2007): Protein kinase D-mediated phosphorylation and nuclear export of sphingosine kinase 2. *The Journal of biological chemistry* 282 (37), pp. 27493–27502.

Dow, L. E.; Kauffman, J. S.; Caddy, J.; Zarbalis, K.; Peterson, A. S.; Jane, S. M. et al. (2007): The tumour-suppressor Scribble dictates cell polarity during directed epithelial migration: regulation of Rho GTPase recruitment to the leading edge. *Oncogene* 26 (16), pp. 2272–2282.

Du, X.; Qian, X.; Papageorge, A.; Schetter, A. J.; Vass, W. C.; Liu, X. et al. (2012): Functional interaction of tumor suppressor DLC1 and caveolin-1 in cancer cells. *Cancer research* 72 (17), pp. 4405–4416.

Duhamel, S.; Goyette, M.-A.; Thibault, M.-P.; Filion, D.; Gaboury, L.; Côté, J.-F. (2018): The E3 Ubiquitin Ligase HectD1 Suppresses EMT and Metastasis by Targeting the +TIP ACF7 for Degradation. *Cell reports* 22 (4), pp. 1016–1030.

Durkin, M. E.; Avner, M. R.; Huh, C.-G.; Yuan, B.-Z.; Thorgeirsson, S. S.; Popescu, N. C. (2005): DLC-1, a Rho GTPase-activating protein with tumor suppressor function, is essential for embryonic development. *FEBS letters* 579 (5), pp. 1191–1196.

Durkin, M. E.; Ullmannova, V.; Guan, M.; Popescu, N. C. (2007a): Deleted in liver cancer 3 (DLC-3), a novel Rho GTPase-activating protein, is downregulated in cancer and inhibits tumor cell growth. *Oncogene* 26 (31), pp. 4580–4589.

Durkin, M. E.; Yuan, B.-Z.; Zhou, X.; Zimonjic, D. B.; Lowy, D. R.; Thorgeirsson, S. S.; Popescu, N. C. (2007b): DLC-1:a Rho GTPase-activating protein and tumour suppressor. *Journal of cellular and molecular medicine* 11 (5), pp. 1185–1207.

Ebnet, K. (2008): Organization of multiprotein complexes at cell-cell junctions. *Histochemistry and cell biology* 130 (1), pp. 1–20.

Edgcomb, S. P.; Murphy, K. P. (2002): Variability in the pKa of histidine side-chains correlates with burial within proteins. *Proteins* 49 (1), pp. 1–6.

Eisenberg, S.; Haimov, E.; Walpole, G. F. W.; Plumb, J.; Kozlov, M. M.; Grinstein, S. (2021): Mapping the electrostatic profiles of cellular membranes. *Molecular biology of the cell* 32 (3), pp. 301–310.

Elbediwy, A.; Zihni, C.; Terry, S. J.; Clark, P.; Matter, K.; Balda, M. S. (2012): Epithelial junction formation requires confinement of Cdc42 activity by a novel SH3BP1 complex. *The Journal of cell biology* 198 (4), pp. 677–693.

Elias, J. E.; Gygi, S. P. (2007): Target-decoy search strategy for increased confidence in large-scale protein identifications by mass spectrometry. *Nature methods* 4 (3), pp. 207–214.

Ellenbroek, S. I. J.; Iden, S.; Collard, J. G. (2012): Cell polarity proteins and cancer. *Seminars in cancer biology* 22 (3), pp. 208–215.

Erdős, G.; Pajkos, M.; Dosztányi, Z. (2021): IUPred3: prediction of protein disorder enhanced with unambiguous experimental annotation and visualization of evolutionary conservation. *Nucleic acids research* 49 (W1), W297-W303.

Erlmann, P.; Schmid, S.; Horenkamp, F. A.; Geyer, M.; Pomorski, T. G.; Olayioye, M. A. (2009): DLC1 activation requires lipid interaction through a polybasic region preceding the RhoGAP domain. *Molecular biology of the cell* 20 (20), pp. 4400–4411.

Etienne-Manneville, S.; Hall, A. (2002): Rho GTPases in cell biology. *Nature* 420 (6916), pp. 629–635.

Fang, Y.; Zhu, X.; Wang, J.; Li, N.; Li, D.; Sakib, N. et al. (2015): MiR-744 functions as a proto-oncogene in nasopharyngeal carcinoma progression and metastasis via transcriptional control of ARHGAP5. *Oncotarget* 6 (15), pp. 13164–13175.

Farrar, C. T.; Halkides, C. J.; Singel, D. J. (1997): The frozen solution structure of p21 ras determined by ESEEM spectroscopy reveals weak coordination of Thr35 to the active site metal ion. *Structure* 5 (8), pp. 1055–1066.

Fernandez-Borja, M.; Janssen, L.; Verwoerd, D.; Hordijk, P.; Neefjes, J. (2005): RhoB regulates endosome transport by promoting actin assembly on endosomal membranes through Dia1. *Journal of cell science* 118 (Pt 12), pp. 2661–2670.

Fernandez-Zapico, M. E.; Gonzalez-Paz, N. C.; Weiss, E.; Savoy, D. N.; Molina, J. R.; Fonseca, R. et al. (2005): Ectopic expression of VAV1 reveals an unexpected role in pancreatic cancer tumorigenesis. *Cancer cell* 7 (1), pp. 39–49.

Fields, A. P.; Justilien, V. (2010): The guanine nucleotide exchange factor (GEF) Ect2 is an oncogene in human cancer. *Advances in enzyme regulation* 50 (1), pp. 190–200.

Fillingham, I.; Gingras, A. R.; Papagrigoriou, E.; Patel, B.; Emsley, J.; Critchley, D. R. et al. (2005): A vinculin binding domain from the talin rod unfolds to form a complex with the vinculin head. *Structure* 13 (1), pp. 65–74.

Foulkes, W. D.; Smith, I. E.; Reis-Filho, J. S. (2010): Triple-negative breast cancer. *The New England journal of medicine* 363 (20), pp. 1938–1948.

Frank, S. R.; Bell, J. H.; Frödin, M.; Hansen, S. H. (2012): A βPIX-PAK2 complex confers protection against Scrib-dependent and cadherin-mediated apoptosis. *Current biology : CB* 22 (19), pp. 1747–1754.

Frantz, C.; Karydis, A.; Nalbant, P.; Hahn, K. M.; Barber, D. L. (2007): Positive feedback between Cdc42 activity and H+ efflux by the Na-H exchanger NHE1 for polarity of migrating cells. *The Journal of cell biology* 179 (3), pp. 403–410.

Franz-Wachtel, M.; Eisler, S. A.; Krug, K.; Wahl, S.; Carpy, A.; Nordheim, A. et al. (2012): Global detection of protein kinase D-dependent phosphorylation events in nocodazole-treated human cells. *Molecular & cellular proteomics : MCP* 11 (5), pp. 160–170.

Fried, H.; Kutay, U. (2003): Nucleocytoplasmic transport: taking an inventory. *Cellular and molecular life sciences : CMLS* 60 (8), pp. 1659–1688.

Fu, X.; Liang, C.; Li, F.; Wang, L.; Wu, X.; Lu, A. et al. (2018): The Rules and Functions of Nucleocytoplasmic Shuttling Proteins. *International journal of molecular sciences* 19 (5).

Fukuhara, T.; Shimizu, K.; Kawakatsu, T.; Fukuyama, T.; Minami, Y.; Honda, T. et al. (2004): Activation of Cdc42 by trans interactions of the cell adhesion molecules nectins through c-Src and Cdc42-GEF FRG. *The Journal of cell biology* 166 (3), pp. 393–405.

Gao, J.; Aksoy, B. A.; Dogrusoz, U.; Dresdner, G.; Gross, B.; Sumer, S. O. et al. (2013): Integrative analysis of complex cancer genomics and clinical profiles using the cBioPortal. *Science signaling* 6 (269), pl1.

Garcia-Mata, R.; Boulter, E.; Burridge, K. (2011): The 'invisible hand': regulation of RHO GTPases by RHOGDIs. *Nature reviews. Molecular cell biology* 12 (8), pp. 493–504.

George, A. J.; Hoffiz, Y. C.; Charles, A. J.; Zhu, Y.; Mabb, A. M. (2018): A Comprehensive Atlas of E3 Ubiquitin Ligase Mutations in Neurological Disorders. *Frontiers in genetics* 9, p. 29.

Golan-Lavi, R.; Giacomelli, C.; Fuks, G.; Zeisel, A.; Sonntag, J.; Sinha, S. et al. (2017): Coordinated Pulses of mRNA and of Protein Translation or Degradation Produce EGF-Induced Protein Bursts. *Cell reports* 18 (13), pp. 3129–3142.

Golding, A. E.; Visco, I.; Bieling, P.; Bement, W. M. (2019): Extraction of active RhoGTPases by RhoGDI regulates spatiotemporal patterning of RhoGTPases. *eLife* 8.

Gong, X.; Didan, Y.; Lock, J. G.; Strömblad, S. (2018): KIF13A-regulated RhoB plasma membrane localization governs membrane blebbing and blebby amoeboid cell migration. *The EMBO journal* 37 (17).

Goodison, S.; Yuan, J.; Sloan, D.; Kim, R.; Li, C.; Popescu, N. C.; Urquidi, V. (2005): The RhoGAP protein DLC-1 functions as a metastasis suppressor in breast cancer cells. *Cancer research* 65 (14), pp. 6042–6053.

Goult, B. T.; Zacharchenko, T.; Bate, N.; Tsang, R.; Hey, F.; Gingras, A. R. et al. (2013): RIAM and vinculin binding to talin are mutually exclusive and regulate adhesion assembly and turnover. *The Journal of biological chemistry* 288 (12), pp. 8238–8249.

Guan, M.; Zhou, X.; Soulitzis, N.; Spandidos, D. A.; Popescu, N. C. (2006): Aberrant methylation and deacetylation of deleted in liver cancer-1 gene in prostate cancer: potential clinical applications. *Clinical cancer research : an official journal of the American Association for Cancer Research* 12 (5), pp. 1412–1419.

Guo, J.; Wang, X.; Guo, Q.; Zhu, S.; Li, P.; Zhang, S.; Min, L. (2022): M2 Macrophage Derived Extracellular Vesicle-Mediated Transfer of MiR-186-5p Promotes Colon Cancer Progression by Targeting DLC1. *International journal of biological sciences* 18 (4), pp. 1663–1676.

Habets, G. G.; Scholtes, E. H.; Zuydgeest, D.; van der Kammen, R. A.; Stam, J. C.; Berns, A.; Collard, J. G. (1994): Identification of an invasion-inducing gene, Tiam-1, that encodes a protein with homology to GDP-GTP exchangers for Rho-like proteins. *Cell* 77 (4), pp. 537–549.

Haga, R. B.; Ridley, A. J. (2016): Rho GTPases: Regulation and roles in cancer cell biology. *Small GTPases* 7 (4), pp. 207–221.

Hahn, Daniel (2021): Investigation of the interplay between the RhoGAP DLC1 and the epigenetic regulator CBX3. Bachelor thesis: Universität Stuttgart.

Haining, A. W. M.; Rahikainen, R.; Cortes, E.; Lachowski, D.; Rice, A.; Essen, M. von et al. (2018): Mechanotransduction in talin through the interaction of the R8 domain with DLC1. *PLoS biology* 16 (7), e2005599.

Hall, A. (1998): Rho GTPases and the actin cytoskeleton. *Science (New York, N.Y.)* 279 (5350), pp. 509–514.

Hanahan, D. (2022): Hallmarks of Cancer: New Dimensions. *Cancer discovery* 12 (1), pp. 31–46.

Hanahan, D.; Weinberg, R. A. (2000): The hallmarks of cancer. *Cell* 100 (1), pp. 57–70.

Hannaford, M. R.; Ramat, A.; Loyer, N.; Januschke, J. (2018): aPKC-mediated displacement and actomyosin-mediated retention polarize Miranda in Drosophila neuroblasts. *eLife* 7.

Hauth, Franziskus (2018): Molecular regulation of the RhoGAP protein DLC3 by a novel N-terminal polybasic region. Master thesis: Universität Stuttgart.

He, J.; Haney, R. M.; Vora, M.; Verkhusha, V. V.; Stahelin, R. V.; Kutateladze, T. G. (2008): Molecular mechanism of membrane targeting by the GRP1 PH domain. *Journal of lipid research* 49 (8), pp. 1807–1815.

He, J.; Scott, J. L.; Heroux, A.; Roy, S.; Lenoir, M.; Overduin, M. et al. (2011): Molecular basis of phosphatidylinositol 4-phosphate and ARF1 GTPase recognition by the FAPP1 pleckstrin homology (PH) domain. *The Journal of biological chemistry* 286 (21), pp. 18650–18657.

Healy, K. D.; Hodgson, L.; Kim, T.-Y.; Shutes, A.; Maddileti, S.; Juliano, R. L. et al. (2008): DLC-1 suppresses non-small cell lung cancer growth and invasion by RhoGAP-dependent and independent mechanisms. *Molecular carcinogenesis* 47 (5), pp. 326–337.

Heckman-Stoddard, B. M.; Vargo-Gogola, T.; McHenry, P. R.; Jiang, V.; Herrick, M. P.; Hilsenbeck, S. G. et al. (2009): Haploinsufficiency for p190B RhoGAP inhibits MMTV-Neu tumor progression. *Breast cancer research : BCR* 11 (4), R61.

Heering, J.; Erlmann, P.; Olayioye, M. A. (2009): Simultaneous loss of the DLC1 and PTEN tumor suppressors enhances breast cancer cell migration. *Experimental cell research* 315 (15), pp. 2505–2514.

Hendrick, J.; Franz-Wachtel, M.; Moeller, Y.; Schmid, S.; Macek, B.; Olayioye, M. A. (2016): The polarity protein Scribble positions DLC3 at adherens junctions to regulate Rho signaling. *Journal of cell science* 129 (19), pp. 3583–3596.

Hendrick, Janina (2016): Deleted in Liver Cancer 3 (DLC3) in the regulation of junctional Rho signaling and cell polarity. PhD thesis: Universität Stuttgart.

Heo, W. D.; Inoue, T.; Park, W. S.; Kim, M. L.; Park, B. O.; Wandless, T. J.; Meyer, T. (2006): PI(3,4,5)P3 and PI(4,5)P2 lipids target proteins with polybasic clusters to the plasma membrane. *Science (New York, N.Y.)* 314 (5804), pp. 1458–1461.

Herder, C.; Swiercz, J. M.; Müller, C.; Peravali, R.; Quiring, R.; Offermanns, S. et al. (2013): ArhGEF18 regulates RhoA-Rock2 signaling to maintain neuro-epithelial apico-basal polarity and proliferation. *Development (Cambridge, England)* 140 (13), pp. 2787–2797.

Hewitt, C.; Wilson, P.; McGlinn, E.; MacFarlane, G.; Papageorgiou, A.; Woodwards, R. T. M. et al. (2004): DLC1 is unlikely to be a primary target for deletions on chromosome arm 8p22 in head and neck squamous cell carcinoma. *Cancer letters* 209 (2), pp. 207–213.

Hinsenkamp, I.; Köhler, J. P.; Flächsenhaar, C.; Hitkova, I.; Meessen, S. E.; Gaiser, T. et al. (2022): Functional antagonism between CagA and DLC1 in gastric cancer. *Cell death discovery* 8 (1), p. 358.

Hodis, E.; Watson, I. R.; Kryukov, G. V.; Arold, S. T.; Imielinski, M.; Theurillat, J.-P. et al. (2012): A landscape of driver mutations in melanoma. *Cell* 150 (2), pp. 251–263.

Holeiter, G.; Bischoff, A.; Braun, A. C.; Huck, B.; Erlmann, P.; Schmid, S. et al. (2012): The RhoGAP protein Deleted in Liver Cancer 3 (DLC3) is essential for adherens junctions integrity. *Oncogenesis* 1, e13.

Holeiter, G.; Heering, J.; Erlmann, P.; Schmid, S.; Jähne, R.; Olayioye, M. A. (2008): Deleted in liver cancer 1 controls cell migration through a Dia1-dependent signaling pathway. *Cancer research* 68 (21), pp. 8743–8751.

Homma, Y.; Emori, Y. (1995): A dual functional signal mediator showing RhoGAP and phospholipase C-delta stimulating activities. *The EMBO journal* 14 (2), pp. 286–291.

Hong, Y. (2018): aPKC: the Kinase that Phosphorylates Cell Polarity. *F1000Res* 7, p. 903.

Hornstein, I.; Pikarsky, E.; Groysman, M.; Amir, G.; Peylan-Ramu, N.; Katzav, S. (2003): The haematopoietic specific signal transducer Vav1 is expressed in a subset of human neuroblastomas. *The Journal of pathology* 199 (4), pp. 526–533.

Hu, R.; Zhu, X.; Chen, C.; Xu, R.; Li, Y.; Xu, W. (2018): RNA-binding protein PUM2 suppresses osteosarcoma progression via partly and competitively binding to STARD13 3'UTR with miRNAs. *Cell proliferation* 51 (6), e12508.

Iakoucheva, L. M.; Radivojac, P.; Brown, C. J.; O'Connor, T. R.; Sikes, J. G.; Obradovic, Z.; Dunker, A. K. (2004): The importance of intrinsic disorder for protein phosphorylation. *Nucleic acids research* 32 (3), pp. 1037–1049.

Iden, S.; Collard, J. G. (2008): Crosstalk between small GTPases and polarity proteins in cell polarization. *Nature reviews. Molecular cell biology* 9 (11), pp. 846–859.

Itoh, M.; Tsukita, S.; Yamazaki, Y.; Sugimoto, H. (2012): Rho GTP exchange factor ARHGEF11 regulates the integrity of epithelial junctions by connecting ZO-1 and RhoA-myosin II signaling. *Proceedings of the National Academy of Sciences of the United States of America* 109 (25), pp. 9905–9910.

Jaffe, A. B.; Hall, A. (2005): Rho GTPases: biochemistry and biology. *Annual review of cell and developmental biology* 21, pp. 247–269.

Jin, X.; Yu, W.; Ye, P. (2022): MiR-125b enhances doxorubicin-induced cardiotoxicity by suppressing the nucleus-cytoplasmic translocation of YAP via targeting STARD13. *Environmental toxicology* 37 (4), pp. 730–740.

Joshi, R.; Qin, L.; Cao, X.; Zhong, S.; Voss, C.; Min, W.; Li, S. S. C. (2020): DLC1 SAM domain-binding peptides inhibit cancer cell growth and migration by inactivating RhoA. *The Journal of biological chemistry* 295 (2), pp. 645–656.

Ju, J. A.; Gilkes, D. M. (2018): RhoB: Team Oncogene or Team Tumor Suppressor? *Genes* 9 (2).

Jumper, J.; Evans, R.; Pritzel, A.; Green, T.; Figurnov, M.; Ronneberger, O. et al. (2021): Highly accurate protein structure prediction with AlphaFold. *Nature* 596 (7873), pp. 583–589.

Kakiuchi, M.; Nishizawa, T.; Ueda, H.; Gotoh, K.; Tanaka, A.; Hayashi, A. et al. (2014): Recurrent gain-of-function mutations of RHOA in diffuse-type gastric carcinoma. *Nature genetics* 46 (6), pp. 583–587.

Kandoth, C.; McLellan, M. D.; Vandin, F.; Ye, K.; Niu, B.; Lu, C. et al. (2013): Mutational landscape and significance across 12 major cancer types. *Nature* 502 (7471), pp. 333–339.

Karlsson, R.; Pedersen, E. D.; Wang, Z.; Brakebusch, C. (2009): Rho GTPase function in tumorigenesis. *Biochimica et biophysica acta* 1796 (2), pp. 91–98.

Kashkooli, L.; Rozema, D.; Espejo-Ramirez, L.; Lasko, P.; Fagotto, F. (2021): Ectoderm to mesoderm transition by down-regulation of actomyosin contractility. *PLoS biology* 19 (1), e3001060.

Katoh, Y.; Nozaki, S.; Hartanto, D.; Miyano, R.; Nakayama, K. (2015): Architectures of multisubunit complexes revealed by a visible immunoprecipitation assay using fluorescent fusion proteins. *Journal of cell science* 128 (12), pp. 2351–2362.

Kaushik, S.; Ravi, A.; Hameed, F. M.; Low, B. C. (2014): Concerted modulation of paxillin dynamics at focal adhesions by Deleted in Liver Cancer-1 and focal adhesion kinase during early cell spreading. *Cytoskeleton (Hoboken, N.J.)* 71 (12), pp. 677–694.

Kawai, K.; Kitamura, S.; Maehira, K.; Seike, J.; Yagisawa, H. (2010): START-GAP1/DLC1 is localized in focal adhesions through interaction with the PTB domain of tensin2. *Advances in enzyme regulation* 50 (1), pp. 202–215.

Kawai, K.; Kiyota, M.; Seike, J.; Deki, Y.; Yagisawa, H. (2007): START-GAP3/DLC3 is a GAP for RhoA and Cdc42 and is localized in focal adhesions regulating cell morphology. *Biochemical and biophysical research communications* 364 (4), pp. 783–789.

Kawai, K.; Seike, J.; Iino, T.; Kiyota, M.; Iwamae, Y.; Nishitani, H.; Yagisawa, H. (2009): START-GAP2/DLC2 is localized in focal adhesions via its N-terminal region. *Biochemical and biophysical research communications* 380 (4), pp. 736–741.

Kawai, K.; Yamaga, M.; Iwamae, Y.; Kiyota, M.; Kamata, H.; Hirata, H. et al. (2004): A PLCdelta1-binding protein, p122RhoGAP, is localized in focal adhesions. *Biochemical Society transactions* 32 (Pt 6), pp. 1107–1109.

Kim, S. H.; Li, Z.; Sacks, D. B. (2000): E-cadherin-mediated cell-cell attachment activates Cdc42. *The Journal of biological chemistry* 275 (47), pp. 36999–37005.

Kim, T. Y.; Healy, K. D.; Der, C. J.; Sciaky, N.; Bang, Y.-J.; Juliano, R. L. (2008a): Effects of structure of Rho GTPase-activating protein DLC-1 on cell morphology and migration. *The Journal of biological chemistry* 283 (47), pp. 32762–32770.

Kim, T. Y.; Jackson, S.; Xiong, Y.; Whitsett, T. G.; Lobello, J. R.; Weiss, G. J. et al. (2013): CRL4A-FBXW5-mediated degradation of DLC1 Rho GTPase-activating protein tumor suppressor promotes non-small cell lung cancer cell growth. *Proceedings of the National Academy of Sciences of the United States of America* 110 (42), pp. 16868–16873.

Kim, T. Y.; Jong, H.-S.; Song, S.-H.; Dimtchev, A.; Jeong, S.-J.; Lee, J. W. et al. (2003): Transcriptional silencing of the DLC-1 tumor suppressor gene by epigenetic mechanism in gastric cancer cells. *Oncogene* 22 (25), pp. 3943–3951.

Kim, T. Y.; Kim, I. S.; Jong, H. S.; Lee, J. W.; Kim, T. Y.; Jung, M.; Bang, Y. J. (2008b): Transcriptional induction of DLC-1 gene through Sp1 sites by histone deacetylase inhibitors in gastric cancer cells. *Experimental & molecular medicine* 40 (6), pp. 639–646.

Klebe, C.; Prinz, H.; Wittinghofer, A.; Goody, R. S. (1995): The kinetic mechanism of Ran--nucleotide exchange catalyzed by RCC1. *Biochemistry* 34 (39), pp. 12543–12552.

Ko, F. C. F.; Chan, L.-K.; Sze, K. M.-F.; Yeung, Y.-S.; Tse, E. Y.-T.; Lu, P. et al. (2013): PKA-induced dimerization of the RhoGAP DLC1 promotes its inhibition of tumorigenesis and metastasis. *Nature communications* 4, p. 1618.

Ko, F. C. F.; Chan, L.-K.; Tung, E. K.-K.; Lowe, S. W.; Ng, I. O.-L.; Yam, J. W. P. (2010): Akt phosphorylation of deleted in liver cancer 1 abrogates its suppression of liver cancer tumorigenesis and metastasis. *Gastroenterology* 139 (4), pp. 1397–1407.

Kosugi, S.; Hasebe, M.; Tomita, M.; Yanagawa, H. (2008): Nuclear export signal consensus sequences defined using a localization-based yeast selection system. *Traffic (Copenhagen, Denmark)* 9 (12), pp. 2053–2062.

Kreider-Letterman, G.; Carr, N. M.; Garcia-Mata, R. (2022): Fixing the GAP: The role of RhoGAPs in cancer. *European journal of cell biology* 101 (2), p. 151209.

Lawrence, M. S.; Stojanov, P.; Mermel, C. H.; Robinson, J. T.; Garraway, L. A.; Golub, T. R. et al. (2014): Discovery and saturation analysis of cancer genes across 21 tumour types. *Nature* 505 (7484), pp. 495–501.

Lazer, G.; Idelchuk, Y.; Schapira, V.; Pikarsky, E.; Katzav, S. (2009): The haematopoietic specific signal transducer Vav1 is aberrantly expressed in lung cancer and plays a role in tumourigenesis. *The Journal of pathology* 219 (1), pp. 25–34.

Lee, S. A.; Eyeson, R.; Cheever, M. L.; Geng, J.; Verkhusha, V. V.; Burd, C. et al. (2005): Targeting of the FYVE domain to endosomal membranes is regulated by a histidine switch. *Proceedings of the National Academy of Sciences of the United States of America* 102 (37), pp. 13052–13057.

Lee, S. W.; Otto, J. J. (1996): Differences in turnover rates of vinculin and talin caused by viral transformation and cell density. *Experimental cell research* 227 (2), pp. 352–359.

Legate, K. R.; Takahashi, S.; Bonakdar, N.; Fabry, B.; Boettiger, D.; Zent, R.; Fässler, R. (2011): Integrin adhesion and force coupling are independently regulated by localized PtdIns(4,5)2 synthesis. *The EMBO journal* 30 (22), pp. 4539–4553.

Leung, T. H.-Y.; Ching, Y.-P.; Yam, J. W. P.; Wong, C.-M.; Yau, T.-O.; Jin, D.-Y.; Ng, I. O.-L. (2005): Deleted in liver cancer 2 (DLC2) suppresses cell transformation by means of inhibition of RhoA activity. *Proceedings of the National Academy of Sciences of the United States of America* 102 (42), pp. 15207–15212.

Li, G.; Du, X.; Vass, W. C.; Papageorge, A. G.; Lowy, D. R.; Qian, X. (2011): Full activity of the deleted in liver cancer 1 (DLC1) tumor suppressor depends on an LD-like motif that binds talin and focal adhesion kinase (FAK). *Proceedings of the National Academy of Sciences of the United States of America* 108 (41), pp. 17129–17134.

Li, H.; Fung, K.-L.; Jin, D.-Y.; Chung, S. S. M.; Ching, Y.-P.; Ng, I. O.-L. et al. (2007): Solution structures, dynamics, and lipid-binding of the sterile alpha-motif domain of the deleted in liver cancer 2. *Proteins* 67 (4), pp. 1154–1166.

Li, J.; Bao, S.; Wang, L.; Wang, R. (2021a): CircZKSCAN1 Suppresses Hepatocellular Carcinoma Tumorigenesis by Regulating miR-873-5p/Downregulation of Deleted in Liver Cancer 1. *Digestive diseases and sciences* 66 (12), pp. 4374–4383.

Li, J.; Cai, Z.; Vaites, L. P.; Shen, N.; Mitchell, D. C.; Huttlin, E. L. et al. (2021b): Proteome-wide mapping of short-lived proteins in human cells. *Molecular cell* 81 (22), 4722-4735.e5.

Li, L.; Li, Y.-M.; Zhou, P.; Wang, X.-S.; Wang, G.-Y.; Zhao, X.-H. et al. (2016a): Abnormal expression of p190RhoGAP in colorectal cancer patients with poor survival. *American journal of translational research* 8 (10), pp. 4405–4414.

Li, L.; Yue, P.; Song, Q.; Yen, T.-T.; Asaka, S.; Wang, T.-L. et al. (2021c): Genome-wide mutation analysis in precancerous lesions of endometrial carcinoma. *The Journal of pathology* 253 (1), pp. 119–128.

Li, M.; Brooks, C. L.; Kon, N.; Gu, W. (2004): A dynamic role of HAUSP in the p53-Mdm2 pathway. *Molecular cell* 13 (6), pp. 879–886.

Li, M.; Chen, D.; Shiloh, A.; Luo, J.; Nikolaev, A. Y.; Qin, J.; Gu, W. (2002): Deubiquitination of p53 by HAUSP is an important pathway for p53 stabilization. *Nature* 416 (6881), pp. 648–653.

Li, X.; Zheng, L.; Zhang, F.; Hu, J.; Chou, J.; Liu, Y. et al. (2016b): STARD13-correlated ceRNA network inhibits EMT and metastasis of breast cancer. *Oncotarget* 7 (17), pp. 23197–23211.

Li, X.; Zhou, Q.; Sunkara, M.; Kutys, M. L.; Wu, Z.; Rychahou, P. et al. (2013): Ubiquitylation of phosphatidylinositol 4-phosphate 5-kinase type I γ by HECTD1 regulates focal adhesion dynamics and cell migration. *Journal of cell science* 126 (Pt 12), pp. 2617–2628.

Li, Z.; Wang, Y.; Liu, S.; Li, W.; Wang, Z.; Jia, Z. et al. (2022): MiR-200a-3p promotes gastric cancer progression by targeting DLC-1. *Journal of molecular histology* 53 (1), pp. 39–49.

Liao, Y.-C.; Si, L.; deVere White, R. W.; Lo, S. H. (2007): The phosphotyrosine-independent interaction of DLC-1 and the SH2 domain of cten regulates focal adhesion localization and growth suppression activity of DLC-1. *The Journal of cell biology* 176 (1), pp. 43–49.

Liedtke, C.; Mazouni, C.; Hess, K. R.; André, F.; Tordai, A.; Mejia, J. A. et al. (2008): Response to neoadjuvant therapy and long-term survival in patients with triple-negative breast cancer. *Journal of clinical oncology : official journal of the American Society of Clinical Oncology* 26 (8), pp. 1275–1281.

Lin, B.; Wang, Y.; Wang, Z.; Tan, H.; Kong, X.; Shu, Y. et al. (2014): Uncovering the rare variants of DLC1 isoform 1 and their functional effects in a Chinese sporadic congenital heart disease cohort. *PloS one* 9 (2), e90215.

Lin, L.; Liu, Y.; Pan, C.; Zhang, J.; Zhao, Y.; Shao, R. et al. (2019): Gastric cancer cells escape metabolic stress via the DLC3/MACC1 axis. *Theranostics* 9 (7), pp. 2100–2114.

Lin, Y.; Chen, N.-T.; Shih, Y.-P.; Liao, Y.-C.; Xue, L.; Lo, S. H. (2010): DLC2 modulates angiogenic responses in vascular endothelial cells by regulating cell attachment and migration. *Oncogene* 29 (20), pp. 3010–3016.

Lindsay, C. R.; Lawn, S.; Campbell, A. D.; Faller, W. J.; Rambow, F.; Mort, R. L. et al. (2011): P-Rex1 is required for efficient melanoblast migration and melanoma metastasis. *Nature communications* 2, p. 555.

Linnerz, T.; Bertrand, J. Y. (2021): Dlc1 controls cardio-vascular development downstream of Vegfa/Kdrl/Nrp1 signaling in the zebrafish embryo. *bioRxiv* (2021.02.11.430763).

Liu, D.; Schilling, B.; Liu, D.; Sucker, A.; Livingstone, E.; Jerby-Arnon, L. et al. (2019): Integrative molecular and clinical modeling of clinical outcomes to PD1 blockade in patients with metastatic melanoma. *Nature medicine* 25 (12), pp. 1916–1927.

Liu, H.; Liu, Y.; Sun, P.; Leng, K.; Xu, Y.; Mei, L. et al. (2020): Colorectal cancer-derived exosomal miR-106b-3p promotes metastasis by down-regulating DLC-1 expression. *Clinical science (London, England : 1979)* 134 (4), pp. 419–434.

Liu, H.; Ma, X.; Niu, N.; Zhao, J.; Lu, C.; Yang, F.; Qi, W. (2021): MIR-301b-3p Promotes Lung Adenocarcinoma Cell Proliferation, Migration and Invasion by Targeting DLC1. *Technology in cancer research & treatment* 20, 1533033821990036.

Liu, J. A.; Rao, Y.; Cheung, M. P. L.; Hui, M.-N.; Wu, M.-H.; Chan, L.-K. et al. (2017): Asymmetric localization of DLC1 defines avian trunk neural crest polarity for directional delamination and migration. *Nature communications* 8 (1), p. 1185.

Liu, S.; Li, Y.; Qi, W.; Zhao, Y.; Huang, A.; Sheng, W. et al. (2014): Expression of Tiam1 predicts lymph node metastasis and poor survival of lung adenocarcinoma patients. *Diagnostic pathology* 9, p. 69.

Lohia, M.; Qin, Y.; Macara, I. G. (2012): The Scribble polarity protein stabilizes E-cadherin/p120-catenin binding and blocks retrieval of E-cadherin to the Golgi. *PloS one* 7 (11), e51130.

Lord, S. J.; Velle, K. B.; Mullins, R. D.; Fritz-Laylin, L. K. (2020): SuperPlots: Communicating reproducibility and variability in cell biology. *The Journal of cell biology* 219 (6).

Low, J. S. W.; Tao, Q.; Ng, K. M.; Goh, H. K.; Shu, X.-S.; Woo, W. L. et al. (2011): A novel isoform of the 8p22 tumor suppressor gene DLC1 suppresses tumor growth and is frequently silenced in multiple common tumors. *Oncogene* 30 (16), pp. 1923–1935.

Lu, Y.; Zheng, W.; Rao, X.; Du, Y.; Xue, J. (2022): MicroRNA-9-5p Facilitates Lung Adenocarcinoma Cell Malignant Progression via Targeting STARD13. *Biochemical genetics* 60 (6), pp. 1865–1880.

Lukasik, D.; Wilczek, E.; Wasiutynski, A.; Gornicka, B. (2011): Deleted in liver cancer protein family in human malignancies (Review). *Oncology letters* 2 (5), pp. 763–768.

Lungu, C.; Meyer, F.; Hörning, M.; Steudle, J.; Braun, A.; Noll, B. et al. (2023): Golgi screen identifies the RhoGEF Solo as a novel regulator of RhoB and endocytic transport. *Traffic (Copenhagen, Denmark)* 24 (4), pp. 162–176.

Luo, H.; Luo, Q.; Yuan, Y.; Zhu, X.; Huang, S.; Peng, Z. et al. (2011): The intracellular stability of DLC1 is regulated by the 26S proteasome in human hepatocellular carcinoma cell line Hep3B. *Biochemical and biophysical research communications* 404 (1), pp. 279–283.

Martin, C.; Pedersen, S. F.; Schwab, A.; Stock, C. (2011): Intracellular pH gradients in migrating cells. *American journal of physiology. Cell physiology* 300 (3), C490-5.

Maures, T. J.; Su, H.-W.; Argetsinger, L. S.; Grinstein, S.; Carter-Su, C. (2011): Phosphorylation controls a dual-function polybasic nuclear localization sequence in the adapter protein SH2B1β to regulate its cellular function and distribution. *Journal of cell science* 124 (Pt 9), pp. 1542–1552.

Maxwell, K. N.; Zhou, Y.; Hancock, J. F. (2018): Rac1 Nanoscale Organization on the Plasma Membrane Is Driven by Lipid Binding Specificity Encoded in the Membrane Anchor. *Molecular and cellular biology* 38 (18).

Mertens, A. E. E.; Rygiel, T. P.; Olivo, C.; van der Kammen, R.; Collard, J. G. (2005): The Rac activator Tiam1 controls tight junction biogenesis in keratinocytes through binding to and activation of the Par polarity complex. *The Journal of cell biology* 170 (7), pp. 1029–1037.

Mészáros, B.; Simon, I.; Dosztányi, Z. (2009): Prediction of protein binding regions in disordered proteins. *PLoS computational biology* 5 (5), e1000376.

Meyer, Vivien (2019): Regulation of the RhoGAP protein DLC3 through membrane interaction and phosphorylation. Master thesis: Universität Stuttgart.

Milburn, M. V.; Tong, L.; deVos, A. M.; Brünger, A.; Yamaizumi, Z.; Nishimura, S.; Kim, S. H. (1990): Molecular switch for signal transduction: structural differences between active and inactive forms of protooncogenic ras proteins. *Science (New York, N.Y.)* 247 (4945), pp. 939–945.

Mirdita, M.; Schütze, K.; Moriwaki, Y.; Heo, L.; Ovchinnikov, S.; Steinegger, M. (2022): ColabFold: making protein folding accessible to all. *Nature methods* 19 (6), pp. 679–682.

Mittag, T.; Kay, L. E.; Forman-Kay, J. D. (2010): Protein dynamics and conformational disorder in molecular recognition. *Journal of molecular recognition : JMR* 23 (2), pp. 105–116.

Mohler, K.; Rinehart, J. (2019): Expression of authentic post-translationally modified proteins in organisms with expanded genetic codes. *Methods in enzymology* 626, pp. 539–559.

Mokarram, P.; Kumar, K.; Brim, H.; Naghibalhossaini, F.; Saberi-firoozi, M.; Nouraie, M. et al. (2009): Distinct high-profile methylated genes in colorectal cancer. *PloS one* 4 (9), e7012.

Mosior, M.; McLaughlin, S. (1992): Binding of basic peptides to acidic lipids in membranes: effects of inserting alanine(s) between the basic residues. *Biochemistry* 31 (6), pp. 1767–1773.

Mu, J.-W.; Zhou, X.-Y.; Wang, Q.-J.; Han, L.-H.; Jiao, J.-B. (2020): MicroRNA-141-3p promoted the progression of nasopharyngeal carcinoma through targeting DLC1. *European review for medical and pharmacological sciences* 24 (21), pp. 11105–11113.

Mulgrew-Nesbitt, A.; Diraviyam, K.; Wang, J.; Singh, S.; Murray, P.; Li, Z. et al. (2006): The role of electrostatics in protein-membrane interactions. *Biochimica et biophysica acta* 1761 (8), pp. 812–826.

Müller, P. M.; Rademacher, J.; Bagshaw, R. D.; Wortmann, C.; Barth, C.; van Unen, J. et al. (2020): Systems analysis of RhoGEF and RhoGAP regulatory proteins reveals spatially organized RAC1 signalling from integrin adhesions. *Nature cell biology* 22 (4), pp. 498–511.

Nagase, T.; Seki, N.; Ishikawa, K.; Tanaka, A.; Nomura, N. (1996): Prediction of the coding sequences of unidentified human genes. V. The coding sequences of 40 new genes (KIAA0161-KIAA0200) deduced by analysis of cDNA clones from human cell line KG-1. *DNA research : an international journal for rapid publication of reports on genes and genomes* 3 (1), pp. 17–24.

Nakagawa, M.; Fukata, M.; Yamaga, M.; Itoh, N.; Kaibuchi, K. (2001): Recruitment and activation of Rac1 by the formation of E-cadherin-mediated cell-cell adhesion sites. *Journal of cell science* 114 (Pt 10), pp. 1829–1838.

Nakajima, H.; Tanoue, T. (2011): Lulu2 regulates the circumferential actomyosin tensile system in epithelial cells through p114RhoGEF. *The Journal of cell biology* 195 (2), pp. 245–261.

Ng, D. C.-H.; Chan, S.-F.; Kok, K. H.; Yam, J. W. P.; Ching, Y.-P.; Ng, I. O.-L.; Jin, D.-Y. (2006): Mitochondrial targeting of growth suppressor protein DLC2 through the START domain. *FEBS letters* 580 (1), pp. 191–198.

Ngok, S. P.; Geyer, R.; Kourtidis, A.; Mitin, N.; Feathers, R.; Der, C.; Anastasiadis, P. Z. (2013): TEM4 is a junctional Rho GEF required for cell-cell adhesion, monolayer integrity and barrier function. *Journal of cell science* 126 (Pt 15), pp. 3271–3277.

Nik-Zainal, S.; Davies, H.; Staaf, J.; Ramakrishna, M.; Glodzik, D.; Zou, X. et al. (2016): Landscape of somatic mutations in 560 breast cancer whole-genome sequences. *Nature* 534 (7605), pp. 47–54.

Noll, B.; Benz, D.; Frey, Y.; Meyer, F.; Lauinger, M.; Eisler, S. A. et al. (2019): DLC3 suppresses MT1-MMP-dependent matrix degradation by controlling RhoB and actin remodeling at endosomal membranes. *Journal of cell science* 132 (11).

Noren, N. K.; Niessen, C. M.; Gumbiner, B. M.; Burridge, K. (2001): Cadherin engagement regulates Rho family GTPases. *The Journal of biological chemistry* 276 (36), pp. 33305–33308.

Notsuda, H.; Sakurada, A.; Endo, C.; Okada, Y.; Horii, A.; Shima, H.; Kondo, T. (2013): p190A RhoGAP is involved in EGFR pathways and promotes proliferation, invasion and migration in lung adenocarcinoma cells. *Int J Oncol* 43 (5), pp. 1569–1577.

Obenauer, J. C.; Cantley, L. C.; Yaffe, M. B. (2003): Scansite 2.0: Proteome-wide prediction of cell signaling interactions using short sequence motifs. *Nucleic acids research* 31 (13), pp. 3635–3641.

O'Brien, L. E.; Jou, T. S.; Pollack, A. L.; Zhang, Q.; Hansen, S. H.; Yurchenco, P.; Mostov, K. E. (2001): Rac1 orientates epithelial apical polarity through effects on basolateral laminin assembly. *Nature cell biology* 3 (9), pp. 831–838.

Oliveira, R. I.; Guedes, R. A.; Salvador, J. A. R. (2022): Highlights in USP7 inhibitors for cancer treatment. *Frontiers in chemistry* 10, p. 1005727.

Olsen, J. V.; Macek, B. (2009): High accuracy mass spectrometry in large-scale analysis of protein phosphorylation. *Methods in molecular biology (Clifton, N.J.)* 492, pp. 131–142.

Osmani, N.; Vitale, N.; Borg, J.-P.; Etienne-Manneville, S. (2006): Scrib controls Cdc42 localization and activity to promote cell polarization during astrocyte migration. *Current biology : CB* 16 (24), pp. 2395–2405.

Otani, T.; Ichii, T.; Aono, S.; Takeichi, M. (2006): Cdc42 GEF Tuba regulates the junctional configuration of simple epithelial cells. *The Journal of cell biology* 175 (1), pp. 135–146.

Papagrigoriou, E.; Gingras, A. R.; Barsukov, I. L.; Bate, N.; Fillingham, I. J.; Patel, B. et al. (2004): Activation of a vinculin-binding site in the talin rod involves rearrangement of a five-helix bundle. *The EMBO journal* 23 (15), pp. 2942–2951.

Parri, M.; Chiarugi, P. (2010): Rac and Rho GTPases in cancer cell motility control. *Cell communication and signaling : CCS* 8, p. 23.

Peng, D.; Ren, C.-P.; Yi, H.-M.; Zhou, L.; Yang, X.-Y.; Li, H.; Yao, K.-T. (2006): Genetic and epigenetic alterations of DLC-1, a candidate tumor suppressor gene, in nasopharyngeal carcinoma. *Acta biochimica et biophysica Sinica* 38 (5), pp. 349–355.

Peng, H.; Long, F.; Wu, Z.; Chu, Y.; Li, J.; Kuai, R. et al. (2013): Downregulation of DLC-1 gene by promoter methylation during primary colorectal cancer progression. *BioMed research international* 2013, p. 181384.

Perou, C. M.; Sørlie, T.; Eisen, M. B.; van de Rijn, M.; Jeffrey, S. S.; Rees, C. A. et al. (2000): Molecular portraits of human breast tumours. *Nature* 406 (6797), pp. 747–752.

Plaumann, M.; Seitz, S.; Frege, R.; Estevez-Schwarz, L.; Scherneck, S. (2003): Analysis of DLC-1 expression in human breast cancer. *Journal of cancer research and clinical oncology* 129 (6), pp. 349–354.

Porter, A. P.; Papaioannou, A.; Malliri, A. (2016): Deregulation of Rho GTPases in cancer. *Small GTPases* 7 (3), pp. 123–138.

Pozhidaeva, A.; Valles, G.; Wang, F.; Wu, J.; Sterner, D. E.; Nguyen, P. et al. (2017): USP7-Specific Inhibitors Target and Modify the Enzyme's Active Site via Distinct Chemical Mechanisms. *Cell chemical biology* 24 (12), 1501-1512.e5.

Qian, X.; Li, G.; Asmussen, H. K.; Asnaghi, L.; Vass, W. C.; Braverman, R. et al. (2007): Oncogenic inhibition by a deleted in liver cancer gene requires cooperation between tensin binding and Rho-specific GTPase-activating protein activities. *Proceedings of the National Academy of Sciences of the United States of America* 104 (21), pp. 9012–9017.

Qian, Y.; Zhang, Y.; Ji, H.; Shen, Y.; Zheng, L.; Cheng, S.; Lu, X. (2021): LINC01089 suppresses lung adenocarcinoma cell proliferation and migration via miR-301b-3p/STARD13 axis. *BMC pulmonary medicine* 21 (1), p. 242.

Qiao, F.; Bowie, J. U. (2005): The many faces of SAM. *Science's STKE : signal transduction knowledge environment* 2005 (286), re7.

Qin, J.; Li, Y.; Li, Z.; Qin, X.; Zhou, X.; Zhang, H.; Li, S. (2022): LINC00114 stimulates growth and glycolysis of esophageal cancer cells by recruiting EZH2 to enhance H3K27me3 of DLC1. *Clinical epigenetics* 14 (1), p. 51.

Qin, Y.; Capaldo, C.; Gumbiner, B. M.; Macara, I. G. (2005): The mammalian Scribble polarity protein regulates epithelial cell adhesion and migration through E-cadherin. *The Journal of cell biology* 171 (6), pp. 1061–1071.

Rappsilber, J.; Mann, M.; Ishihama, Y. (2007): Protocol for micro-purification, enrichment, pre-fractionation and storage of peptides for proteomics using StageTips. *Nature protocols* 2 (8), pp. 1896–1906.

Ratheesh, A.; Gomez, G. A.; Priya, R.; Verma, S.; Kovacs, E. M.; Jiang, K. et al. (2012): Centralspindlin and α-catenin regulate Rho signalling at the epithelial zonula adherens. *Nature cell biology* 14 (8), pp. 818–828.

Ravi, A.; Kaushik, S.; Ravichandran, A.; Pan, C. Q.; Low, B. C. (2015): Epidermal growth factor activates the Rho GTPase-activating protein (GAP) Deleted in Liver Cancer 1 via focal adhesion kinase and protein phosphatase 2A. *The Journal of biological chemistry* 290 (7), pp. 4149–4162.

Reina-Campos, M.; Diaz-Meco, M. T.; Moscat, J. (2019): The Dual Roles of the Atypical Protein Kinase Cs in Cancer. *Cancer cell* 36 (3), pp. 218–235.

Reiss, Y.; Goldstein, J. L.; Seabra, M. C.; Casey, P. J.; Brown, M. S. (1990): Inhibition of purified p21ras farnesyl:protein transferase by Cys-AAX tetrapeptides. *Cell* 62 (1), pp. 81–88.

Revathidevi, S.; Munirajan, A. K. (2019): Akt in cancer: Mediator and more. *Seminars in cancer biology* 59, pp. 80–91.

Robinson, D.; van Allen, E. M.; Wu, Y.-M.; Schultz, N.; Lonigro, R. J.; Mosquera, J.-M. et al. (2015): Integrative clinical genomics of advanced prostate cancer. *Cell* 161 (5), pp. 1215–1228.

Rocca, A.; Braga, L.; Volpe, M. C.; Maiocchi, S.; Generali, D. (2022): The Predictive and Prognostic Role of RAS-RAF-MEK-ERK Pathway Alterations in Breast Cancer: Revision of the Literature and Comparison with the Analysis of Cancer Genomic Datasets. *Cancers* 14 (21).

Rodriguez-Boulan, E.; Macara, I. G. (2014): Organization and execution of the epithelial polarity programme. *Nature reviews. Molecular cell biology* 15 (4), pp. 225–242.

Romero, P.; Obradovic, Z.; Li, X.; Garner, E. C.; Brown, C. J.; Dunker, A. K. (2001): Sequence complexity of disordered protein. *Proteins* 42 (1), pp. 38–48.

Rust, H. L.; Thompson, P. R. (2011): Kinase consensus sequences: a breeding ground for crosstalk. *ACS chemical biology* 6 (9), pp. 881–892.

Sabbir, M. G.; Wigle, N.; Loewen, S.; Gu, Y.; Buse, C.; Hicks, G. G.; Mowat, M. R. A. (2010): Identification and characterization of Dlc1 isoforms in the mouse and study of the biological function of a single gene trapped isoform. *BMC biology* 8, p. 17.

Sahai, E.; Marshall, C. J. (2002): RHO-GTPases and cancer. *Nature reviews. Cancer* 2 (2), pp. 133–142.

Sakata-Yanagimoto, M.; Enami, T.; Yoshida, K.; Shiraishi, Y.; Ishii, R.; Miyake, Y. et al. (2014): Somatic RHOA mutation in angioimmunoblastic T cell lymphoma. *Nature genetics* 46 (2), pp. 171–175.

Sanchez-Solana, B.; Wang, D.; Qian, X.; Velayoudame, P.; Simanshu, D. K.; Acharya, J. K.; Lowy, D. R. (2021): The tumor suppressor activity of DLC1 requires the interaction of its START domain with Phosphatidylserine, PLCD1, and Caveolin-1. *Molecular cancer* 20 (1), p. 141.

Sarkar, A. A.; Zohn, I. E. (2012): Hectd1 regulates intracellular localization and secretion of Hsp90 to control cellular behavior of the cranial mesenchyme. *The Journal of cell biology* 196 (6), pp. 789–800.

Scheffzek, K.; Ahmadian, M. R.; Kabsch, W.; Wiesmüller, L.; Lautwein, A.; Schmitz, F.; Wittinghofer, A. (1997): The Ras-RasGAP complex: structural basis for GTPase activation and its loss in oncogenic Ras mutants. *Science (New York, N.Y.)* 277 (5324), pp. 333–338.

Scholz, R.-P.; Gustafsson, J. O. R.; Hoffmann, P.; Jaiswal, M.; Ahmadian, M. R.; Eisler, S. A. et al. (2011): The tumor suppressor protein DLC1 is regulated by PKD-mediated GAP domain phosphorylation. *Experimental cell research* 317 (4), pp. 496–503.

Scholz, R.-P.; Regner, J.; Theil, A.; Erlmann, P.; Holeiter, G.; Jähne, R. et al. (2009): DLC1 interacts with 14-3-3 proteins to inhibit RhoGAP activity and block nucleocytoplasmic shuttling. *Journal of cell science* 122 (Pt 1), pp. 92–102.

Schönichen, A.; Webb, B. A.; Jacobson, M. P.; Barber, D. L. (2013): Considering protonation as a posttranslational modification regulating protein structure and function. *Annual review of biophysics* 42, pp. 289–314.

Schwanhäusser, B.; Busse, D.; Li, N.; Dittmar, G.; Schuchhardt, J.; Wolf, J. et al. (2011): Global quantification of mammalian gene expression control. *Nature* 473 (7347), pp. 337–342.

Seng, T. J.; Low, J. S. W.; Li, H.; Cui, Y.; Goh, H. K.; Wong, M. L. Y. et al. (2007): The major 8p22 tumor suppressor DLC1 is frequently silenced by methylation in both endemic and sporadic nasopharyngeal, esophageal, and cervical carcinomas, and inhibits tumor cell colony formation. *Oncogene* 26 (6), pp. 934–944.

Shen, X.; Jia, Z.; D'Alonzo, D.; Wang, X.; Bruder, E.; Emch, F. H. et al. (2017): HECTD1 controls the protein level of IQGAP1 to regulate the dynamics of adhesive structures. *Cell communication and signaling : CCS* 15 (1), p. 2.

Singla, N.; Xie, Z.; Zhang, Z.; Gao, M.; Yousuf, Q.; Onabolu, O. et al. (2020): Pancreatic tropism of metastatic renal cell carcinoma. *JCI insight* 5 (7).

Song, L.; Luo, Z.-Q. (2019): Post-translational regulation of ubiquitin signaling. *The Journal of cell biology* 218 (6), pp. 1776–1786.

Song, M. S.; Salmena, L.; Carracedo, A.; Egia, A.; Lo-Coco, F.; Teruya-Feldstein, J.; Pandolfi, P. P. (2008): The deubiquitinylation and localization of PTEN are regulated by a HAUSP-PML network. *Nature* 455 (7214), pp. 813–817.

Svensmark, J. H.; Brakebusch, C. (2019): Rho GTPases in cancer: friend or foe? *Oncogene* 38 (50), pp. 7447–7456.

Tanaka, M.; Osanai, T.; Homma, Y.; Hanada, K.; Okumura, K.; Tomita, H. (2019): IQGAP1 activates PLC-δ1 by direct binding and moving along microtubule with DLC-1 to cell surface. *FASEB bioAdvances* 1 (8), pp. 465–480.

Tang, F.; Zhang, R.; He, Y.; Zou, M.; Le Guo; Xi, T. (2012): MicroRNA-125b induces metastasis by targeting STARD13 in MCF-7 and MDA-MB-231 breast cancer cells. *PloS one* 7 (5), e35435.

Tarbashevich, K.; Reichman-Fried, M.; Grimaldi, C.; Raz, E. (2015): Chemokine-Dependent pH Elevation at the Cell Front Sustains Polarity in Directionally Migrating Zebrafish Germ Cells. *Current biology : CB* 25 (8), pp. 1096–1103.

Tate, J. G.; Bamford, S.; Jubb, H. C.; Sondka, Z.; Beare, D. M.; Bindal, N. et al. (2019): COSMIC: the Catalogue Of Somatic Mutations In Cancer. *Nucleic acids research* 47 (D1), D941-D947.

Tavana, O.; Li, D.; Dai, C.; Lopez, G.; Banerjee, D.; Kon, N. et al. (2016): HAUSP deubiquitinates and stabilizes N-Myc in neuroblastoma. *Nature medicine* 22 (10), pp. 1180–1186.

Teramoto, A.; Tsukuda, K.; Yano, M.; Toyooka, S.; Dote, H.; Doihara, H.; Shimizu, N. (2004): Less frequent promoter hypermethylation of DLC-1 gene in primary breast cancers. *Oncol Rep*.

Terry, S. J.; Zihni, C.; Elbediwy, A.; Vitiello, E.; Leefa Chong San, I. V.; Balda, M. S.; Matter, K. (2011): Spatially restricted activation of RhoA signalling at epithelial junctions by p114RhoGEF drives junction formation and morphogenesis. *Nature cell biology* 13 (2), pp. 159–166.

Theil, Anke (2008): Nucleocytoplasmic Shuttling of Deleted In Liver Cancer 1. Diploma thesis. Stuttgart: Universität Stuttgart.

Thomas, L. L.; van der Vegt, S. A.; Fromme, J. C. (2019): A Steric Gating Mechanism Dictates the Substrate Specificity of a Rab-GEF. *Developmental cell* 48 (1), 100-114.e9.

Tikoo, A.; Czekay, S.; Viars, C.; White, S.; Heath, J. K.; Arden, K.; Maruta, H. (2000): p190-A, a human tumor suppressor gene, maps to the chromosomal region 19q13.3 that is reportedly deleted in some gliomas. *Gene* 257 (1), pp. 23–31.

Tripathi, B. K.; Anderman, M. F.; Bhargava, D.; Boccuzzi, L.; Qian, X.; Wang, D. et al. (2021): Inhibition of cytoplasmic EZH2 induces antitumor activity through stabilization of the DLC1 tumor suppressor protein. *Nature communications* 12 (1), p. 6941.

Tripathi, B. K.; Anderman, M. F.; Qian, X.; Zhou, M.; Wang, D.; Papageorge, A. G.; Lowy, D. R. (2019): SRC and ERK cooperatively phosphorylate DLC1 and attenuate its Rho-GAP and tumor suppressor functions. *The Journal of cell biology* 218 (9), pp. 3060–3076.

Tripathi, B. K.; Grant, T.; Qian, X.; Zhou, M.; Mertins, P.; Wang, D. et al. (2017): Receptor tyrosine kinase activation of RhoA is mediated by AKT phosphorylation of DLC1. *The Journal of cell biology* 216 (12), pp. 4255–4270.

Tripathi, B. K.; Qian, X.; Mertins, P.; Wang, D.; Papageorge, A. G.; Carr, S. A.; Lowy, D. R. (2014a): CDK5 is a major regulator of the tumor suppressor DLC1. *The Journal of cell biology* 207 (5), pp. 627–642.

Tripathi, V.; Popescu, N. C.; Zimonjic, D. B. (2012): DLC1 interaction with α-catenin stabilizes adherens junctions and enhances DLC1 antioncogenic activity. *Molecular and cellular biology* 32 (11), pp. 2145–2159.

Tripathi, V.; Popescu, N. C.; Zimonjic, D. B. (2014b): DLC1 induces expression of E-cadherin in prostate cancer cells through Rho pathway and suppresses invasion. *Oncogene* 33 (6), pp. 724–733.

Ullmannova, V.; Popescu, N. (2006): Expression profile of the tumor suppressor genes DLC-1 and DLC-2 in solid tumors. *Int J Oncol*.

Umemura, S.; Yoshida, S.; Ohta, Y.; Naito, K.; Osamura, R. Y.; Tokuda, Y. (2007): Increased phosphorylation of Akt in triple-negative breast cancers. *Cancer science* 98 (12), pp. 1889–1892.

van der Stoel, M.; Schimmel, L.; Nawaz, K.; van Stalborch, A.-M.; Haan, A. de; Klaus-Bergmann, A. et al. (2020): DLC1 is a direct target of activated YAP/TAZ that drives collective migration and sprouting angiogenesis. *Journal of cell science* 133 (3).

Vercoulen, Y.; Kondo, Y.; Iwig, J. S.; Janssen, A. B.; White, K. A.; Amini, M. et al. (2017): A Histidine pH sensor regulates activation of the Ras-specific guanine nucleotide exchange factor RasGRP1. *eLife* 6.

Vetter, I. R.; Wittinghofer, A. (2001): The guanine nucleotide-binding switch in three dimensions. *Science (New York, N.Y.)* 294 (5545), pp. 1299–1304.

Vigil, D.; Cherfils, J.; Rossman, K. L.; Der, C. J. (2010): Ras superfamily GEFs and GAPs: validated and tractable targets for cancer therapy? *Nature reviews. Cancer* 10 (12), pp. 842–857.

Visavadiya, N. P.; Keasey, M. P.; Razskazovskiy, V.; Banerjee, K.; Jia, C.; Lovins, C. et al. (2016): Integrin-FAK signaling rapidly and potently promotes mitochondrial function through STAT3. *Cell communication and signaling : CCS* 14 (1), p. 32.

Visco, I.; Hoege, C.; Hyman, A. A.; Schwille, P. (2016): In vitro Reconstitution of a Membrane Switch Mechanism for the Polarity Protein LGL. *Journal of molecular biology* 428 (24 Pt A), pp. 4828–4842.

Vitiello, E.; Ferreira, J. G.; Maiato, H.; Balda, M. S.; Matter, K. (2014): The tumour suppressor DLC2 ensures mitotic fidelity by coordinating spindle positioning and cell-cell adhesion. *Nature communications* 5, p. 5826.

Wang, C.-S.; Zhang, X.-B.; Zhu, X.-T.; Chen, R.-S. (2022): NBR2/miR-561-5p/DLC1 axis inhibited the development of multiple myeloma by activating the AMPK/mTOR pathway to repress glycolysis. *Neoplasma* 69 (5), pp. 1165–1174.

Wang, D.; Qian, X.; Rajaram, M.; Durkin, M. E.; Lowy, D. R. (2016): DLC1 is the principal biologically-relevant down-regulated DLC family member in several cancers. *Oncotarget* 7 (29), pp. 45144–45157.

Wang, D.; Qian, X.; Sanchez-Solana, B.; Tripathi, B. K.; Durkin, M. E.; Lowy, D. R. (2020): Cancer-Associated Point Mutations in the DLC1 Tumor Suppressor and Other Rho-GAPs Occur Frequently and Are Associated with Decreased Function. *Cancer research* 80 (17), pp. 3568–3579.

Wang, J.; Tian, X.; Han, R.; Zhang, X.; Wang, X.; Shen, H. et al. (2014a): Downregulation of miR-486-5p contributes to tumor progression and metastasis by targeting protumorigenic ARHGAP5 in lung cancer. *Oncogene* 33 (9), pp. 1181–1189.

Wang, K.; Yuen, S. T.; Xu, J.; Lee, S. P.; Yan, H. H. N.; Shi, S. T. et al. (2014b): Whole-genome sequencing and comprehensive molecular profiling identify new driver mutations in gastric cancer. *Nature genetics* 46 (6), pp. 573–582.

Wells, C. D.; Fawcett, J. P.; Traweger, A.; Yamanaka, Y.; Goudreault, M.; Elder, K. et al. (2006): A Rich1/Amot complex regulates the Cdc42 GTPase and apical-polarity proteins in epithelial cells. *Cell* 125 (3), pp. 535–548.

Wen, X.; Wan, J.; He, Q.; Wang, M.; Li, S.; Jiang, M. et al. (2020): p190A inactivating mutations cause aberrant RhoA activation and promote malignant transformation via the Hippo-YAP pathway in endometrial cancer. *Signal transduction and targeted therapy* 5 (1), p. 81.

Wheeler, A. P.; Ridley, A. J. (2004): Why three Rho proteins? RhoA, RhoB, RhoC, and cell motility. *Experimental cell research* 301 (1), pp. 43–49.

Wherlock, M.; Mellor, H. (2002): The Rho GTPase family: a Racs to Wrchs story. *Journal of cell science* 115 (Pt 2), pp. 239–240.

Wildenberg, G. A.; Dohn, M. R.; Carnahan, R. H.; Davis, M. A.; Lobdell, N. A.; Settleman, J.; Reynolds, A. B. (2006): p120-catenin and p190RhoGAP regulate cell-cell adhesion by coordinating antagonism between Rac and Rho. *Cell* 127 (5), pp. 1027–1039.

Wilson, P. J.; McGlinn, E.; Marsh, A.; Evans, T.; Arnold, J.; Wright, K. et al. (2000): Sequence variants ofDLC1 in colorectal and ovarian tumours. *Hum. Mutat.* 15 (2), pp. 156–165.

Wong, C.-M.; Lee, J. M.-F.; Ching, Y.-P.; Jin, D.-Y.; Ng, I. O.-L. (2003): Genetic and epigenetic alterations of DLC-1 gene in hepatocellular carcinoma. *Cancer research* 63 (22), pp. 7646–7651.

Wong, C.-M.; Yam, J. W.-P.; Ching, Y.-P.; Yau, T.-O.; Leung, T. H.-Y.; Jin, D.-Y.; Ng, I. O.-L. (2005): Rho GTPase-activating protein deleted in liver cancer suppresses cell proliferation and invasion in hepatocellular carcinoma. *Cancer research* 65 (19), pp. 8861–8868.

Wong, L. H.; Čopič, A.; Levine, T. P. (2017): Advances on the Transfer of Lipids by Lipid Transfer Proteins. *Trends in biochemical sciences* 42 (7), pp. 516–530.

Wu, M.-H.; Chen, Y.-A.; Chen, H.-H.; Chang, K.-W.; Chang, I.-S.; Wang, L.-H.; Hsu, H.-L. (2014): MCT-1 expression and PTEN deficiency synergistically promote neoplastic multinucleation through the Src/p190B signaling activation. *Oncogene* 33 (43), pp. 5109–5120.

Wu, P. P.; Zhu, H. Y.; Sun, X. F.; Chen, L. X.; Zhou, Q.; Chen, J. (2015): MicroRNA-141 regulates the tumour suppressor DLC1 in colorectal cancer. *Neoplasma* 62 (5), pp. 705–712.

Wu, X.; Wang, W.; Wu, G.; Peng, C.; Liu, J. (2021): miR-182-5p Serves as an Oncogene in Lung Adenocarcinoma through Binding to STARD13. *Computational and mathematical methods in medicine* 2021, p. 7074343.

Wu, Z.; Li, Y.; Zhang, G. (2017): Downregulation of microRNA-301a inhibited proliferation, migration and invasion of non-small cell lung cancer by directly targeting DLC1. *Oncology letters* 14 (5), pp. 6017–6023.

Xu, D.; Marquis, K.; Pei, J.; Fu, S.-C.; Cağatay, T.; Grishin, N. V.; Chook, Y. M. (2015): LocNES: a computational tool for locating classical NESs in CRM1 cargo proteins. *Bioinformatics (Oxford, England)* 31 (9), pp. 1357–1365.

Xu, X.; Jin, D.; Durgan, J.; Hall, A. (2013): LKB1 controls human bronchial epithelial morphogenesis through p114RhoGEF-dependent RhoA activation. *Molecular and cellular biology* 33 (14), pp. 2671–2682.

Xu, X.; Zheng, S. (2020): MiR-887-3p Negatively Regulates STARD13 and Promotes Pancreatic Cancer Progression. *Cancer management and research* 12, pp. 6137–6147.

Xue, W.; Krasnitz, A.; Lucito, R.; Sordella, R.; Vanaelst, L.; Cordon-Cardo, C. et al. (2008): DLC1 is a chromosome 8p tumor suppressor whose loss promotes hepatocellular carcinoma. *Genes & development* 22 (11), pp. 1439–1444.

Xue, Y.-Z.; Wu, T.-L.; Wu, Y.-M.; Sheng, Y.-Y.; Wei, Z.-Q.; Lu, Y.-F. et al. (2013): DLC-1 is a candidate biomarker methylated and down-regulated in pancreatic ductal adenocarcinoma. *Tumour biology : the journal of the International Society for Oncodevelopmental Biology and Medicine* 34 (5), pp. 2857–2861.

Yamada, S.; Nelson, W. J. (2007): Localized zones of Rho and Rac activities drive initiation and expansion of epithelial cell-cell adhesion. *The Journal of cell biology* 178 (3), pp. 517–527.

Yang, X.; Hu, F.; Liu, J. A.; Yu, S.; Cheung, M. P. L.; Liu, X. et al. (2020): Nuclear DLC1 exerts oncogenic function through association with FOXK1 for cooperative activation of MMP9 expression in melanoma. *Oncogene* 39 (20), pp. 4061–4076.

Yang, X.; Popescu, N. C.; Zimonjic, D. B. (2011): DLC1 interaction with S100A10 mediates inhibition of in vitro cell invasion and tumorigenicity of lung cancer cells through a RhoGAP-independent mechanism. *Cancer research* 71 (8), pp. 2916–2925.

Yang, X.-Y.; Guan, M.; Vigil, D.; Der, C. J.; Lowy, D. R.; Popescu, N. C. (2009): p120Ras-GAP binds the DLC1 Rho-GAP tumor suppressor protein and inhibits its RhoA GTPase and growth-suppressing activities. *Oncogene* 28 (11), pp. 1401–1409.

Yau, T. O.; Leung, T. H. Y.; Lam, S.; Cheung, O. F.; Tung, E. K. K.; Khong, P. L. et al. (2009): Deleted in liver cancer 2 (DLC2) was dispensable for development and its deficiency did not aggravate hepatocarcinogenesis. *PloS one* 4 (8), e6566.

Yoo, H. Y.; Sung, M. K.; Lee, S. H.; Kim, S.; Lee, H.; Park, S. et al. (2014): A recurrent inactivating mutation in RHOA GTPase in angioimmunoblastic T cell lymphoma. *Nature genetics* 46 (4), pp. 371–375.

Yuan, B. Z.; Miller, M. J.; Keck, C. L.; Zimonjic, D. B.; Thorgeirsson, S. S.; Popescu, N. C. (1998): Cloning, characterization, and chromosomal localization of a gene frequently deleted in human liver cancer (DLC-1) homologous to rat RhoGAP. *Cancer research* 58 (10), pp. 2196–2199.

Yuan, B.-Z.; Jefferson, A. M.; Baldwin, K. T.; Thorgeirsson, S. S.; Popescu, N. C.; Reynolds, S. H. (2004): DLC-1 operates as a tumor suppressor gene in human non-small cell lung carcinomas. *Oncogene* 23 (7), pp. 1405–1411.

Yuan, B.-Z.; Jefferson, A. M.; Millecchia, L.; Popescu, N. C.; Reynolds, S. H. (2007): Morphological changes and nuclear translocation of DLC1 tumor suppressor protein precede apoptosis in human non-small cell lung carcinoma cells. *Experimental cell research* 313 (18), pp. 3868–3880.

Yuan, B.-Z.; Zhou, X.; Durkin, M. E.; Zimonjic, D. B.; Gumundsdottir, K.; Eyfjord, J. E. et al. (2003): DLC-1 gene inhibits human breast cancer cell growth and in vivo tumorigenicity. *Oncogene* 22 (3), pp. 445–450.

Zacharchenko, T.; Qian, X.; Goult, B. T.; Jethwa, D.; Almeida, T. B.; Ballestrem, C. et al. (2016): LD Motif Recognition by Talin: Structure of the Talin-DLC1 Complex. *Structure* 24 (7), pp. 1130–1141.

Zack, T. I.; Schumacher, S. E.; Carter, S. L.; Cherniack, A. D.; Saksena, G.; Tabak, B. et al. (2013): Pan-cancer patterns of somatic copy number alteration. *Nature genetics* 45 (10), pp. 1134–1140.

Zhan, L.; Rosenberg, A.; Bergami, K. C.; Yu, M.; Xuan, Z.; Jaffe, A. B. et al. (2008): Deregulation of scribble promotes mammary tumorigenesis and reveals a role for cell polarity in carcinoma. *Cell* 135 (5), pp. 865–878.

Zhang, G.; Li, J.; Zhou, H.; Xiao, H.; Li, Y.; Zhou, T. (2015): MicroRNA-106b promotes colorectal cancer cell migration and invasion by directly targeting DLC1. *Journal of experimental & clinical cancer research : CR* 34, p. 73.

Zhang, L.; Zhang, Y.; Zhu, H.; Sun, X.; Wang, X.; Wu, P.; Xu, X. (2019): Overexpression of miR-301a-3p promotes colorectal cancer cell proliferation and metastasis by targeting deleted in liver cancer-1 and runt-related transcription factor 3. *Journal of cellular biochemistry* 120 (4), pp. 6078–6089.

Zhang, Q.; Ying, J.; Zhang, K.; Li, H.; Ng, K. M.; Zhao, Y. et al. (2007): Aberrant methylation of the 8p22 tumor suppressor gene DLC1 in renal cell carcinoma. *Cancer letters* 249 (2), pp. 220–226.

Zhang, X.; Chen, W.; Guo, D.; Li, Y.; Zhao, Y.; Ren, M. et al. (2022): Circ_0003570 Suppresses the progression of hepatocellular carcinoma through miR-182-5p/STARD13 regulatory axis. *Biological procedures online* 24 (1), p. 14.

Zhang, Y.; Xiong, Y. (2001): A p53 amino-terminal nuclear export signal inhibited by DNA damage-induced phosphorylation. *Science (New York, N.Y.)* 292 (5523), pp. 1910–1915.

Zheng, L.; Xiang, C.; Li, X.; Guo, Q.; Gao, L.; Ni, H. et al. (2018): STARD13-correlated ceRNA network-directed inhibition on YAP/TAZ activity suppresses stemness of breast cancer via co-regulating Hippo and Rho-GTPase/F-actin signaling. *Journal of hematology & oncology* 11 (1), p. 72.

Zheng, N.; Shabek, N. (2017): Ubiquitin Ligases: Structure, Function, and Regulation. *Annual review of biochemistry* 86, pp. 129–157.

Zheng, T.; Jäättelä, M.; Liu, B. (2020): pH gradient reversal fuels cancer progression. *The international journal of biochemistry & cell biology* 125, p. 105796.

Zhong, D.; Zhang, J.; Yang, S.; Soh, U. J. K.; Buschdorf, J. P.; Zhou, Y. T. et al. (2009): The SAM domain of the RhoGAP DLC1 binds EF1A1 to regulate cell migration. *Journal of cell science* 122 (Pt 3), pp. 414–424.

Zhou, X.; Jiao, D.; Dou, M.; Zhang, W.; Lv, L.; Chen, J. et al. (2020): Curcumin inhibits the growth of triple-negative breast cancer cells by silencing EZH2 and restoring DLC1 expression. *Journal of cellular and molecular medicine* 24 (18), pp. 10648–10662.

Zhou, X.; Yang, X.-Y.; Popescu, N. C. (2010): Synergistic antineoplastic effect of DLC1 tumor suppressor protein and histone deacetylase inhibitor, suberoylanilide hydroxamic acid (SAHA), on prostate and liver cancer cells: perspectives for therapeutics. *Int J Oncol* 36 (4), pp. 999–1005.

# 6 Supplemental data

**Table S1: Candidate DLC1 protein interaction partners identified by mass spectrometry analysis.** Co-immunoprecipitating proteins with iBAQ control = 0 are ranked according to their iBAQ GFP-DLC1 value.

| Majority protein IDs | Protein names | Gene names | iBAQ control | iBAQ GFP-DLC1 |
|---|---|---|---|---|
| K7ELM7;K7EQS4;K7EKF4;K7EJI2;Q9BZJ4- | Solute carrier family 25 member 39 | SLC25A39 | 0 | 3006300 |
| E5RIP1;E5RJX2;P60866;P60866-2 | 40S ribosomal protein S20 | RPS20 | 0 | 1376400 |
| Q5VTE0;P68104;A0A087WV01;A0A087WVQ9;A0A2U3TZH3;Q0563 | Putative elongation factor 1-alpha-like 3;Elongation factor 1-alpha 1;Elongation factor 1-alpha 2 | EEF1A1P5;EEF1A1;EEF1A2 | 0 | 1350100 |
| D6RDY9;D6R9G9;D6RHG0;P78383 | Solute carrier family 35 member B1 | SLC35B1 | 0 | 1060500 |
| P0DMV8-2;P0DMV9;P0DMV8;A | | HSPA1A | 0 | 1012500 |
| G3V2C6 | | ITGA7 | 0 | 713460 |
| E5RJI3;Q8WUX9 | Charged multivesicular body protein 7 | CHMP7 | 0 | 712590 |
| P32455 | Interferon-induced guanylate-binding protein 1 | GBP1 | 0 | 707430 |
| Q96FJ2;P63167 | Dynein light chain 2, cytoplasmic;Dynein light chain 1, cytoplasmic | DYNLL2;DYNLL1 | 0 | 700290 |
| P61204-2;P84077;P61204;F5H | ADP-ribosylation factor 3;ADP-ribosylation factor 1 | ARF3;ARF1 | 0 | 445480 |
| P15531;P15531-2;E7ERL0;J3KPD9;Q3 | Nucleoside diphosphate kinase A;Nucleoside diphosphate | NME1;NME2;NME1- | 0 | 420520 |
| P17066;P48741 | Heat shock 70 kDa protein 6;Putative heat shock 70 kDa protein 7 | HSPA6;HSPA7 | 0 | 369080 |
| A6NL93;A6NEL0;P05114 | Non-histone chromosomal protein HMG-14 | HMGN1 | 0 | 335600 |
| G3V4M2;G3V5E8;A0A087WX10;P54803 | Galactocerebrosidase | GALC | 0 | 314970 |
| J3KRS3;F5H6L3;E7ERK8;Q17R89-2;Q17R89- | Rho GTPase-activating protein 44 | ARHGAP44 | 0 | 306280 |
| Q5JP53;P07437;Q5ST81;Q9BVA1;Q13885 | Tubulin beta chain;Tubulin beta-2B chain;Tubulin beta-2A chain | TUBB;TUBB2B;TUBB2A | 0 | 300430 |
| P42677;C9JLI6;H0YMV8;Q71UM5 | 40S ribosomal protein S27;40S ribosomal protein S27-like | RPS27;RPS27L | 0 | 294390 |
| C9JRZ6;F8WAR4;Q9NX63;A0A286YEX5 | MICOS complex subunit MIC19 | CHCHD3 | 0 | 261620 |
| Q16891-2;Q16891;H7C463;C9J | MICOS complex subunit MIC60 | IMMT | 0 | 233280 |
| A0A2R8Y7C0;P69905 | Hemoglobin subunit alpha | HBA1 | 0 | 225740 |
| C9J0E4;P01040 | Cystatin-A;Cystatin-A, N-terminally processed | CSTA | 0 | 207240 |

| | | | | |
|---|---|---|---|---|
| Q9NZT1 | Calmodulin-like protein 5 | CALML5 | 0 | 205420 |
| K7ERX7;P25705;K7ESA0;K7EQH4;K7EJP1;K | ATP synthase subunit alpha, mitochondrial | ATP5A1 | 0 | 190850 |
| Q9Y265-2;Q9Y265;E7ETR0 | RuvB-like 1 | RUVBL1 | 0 | 179340 |
| C9JMM0;B8ZZ43;S4R2Y4;Q13185 | Chromobox protein homolog 3 | CBX3 | 0 | 171640 |
| E5RIY1;P63151;P63151-2 | Serine/threonine-protein phosphatase 2A 55 kDa regulatory subunit B alpha | PPP2R2A | 0 | 164610 |
| E7EMB6;E5RIA4;E7ETB3;Q9ULA0- | Aspartyl aminopeptidase | DNPEP | 0 | 155800 |
| P25398 | 40S ribosomal protein S12 | RPS12 | 0 | 147300 |
| Q96HS1;F5GXG4;Q96HS1-2 | Serine/threonine-protein phosphatase PGAM5, mitochondrial | PGAM5 | 0 | 133630 |
| G3V3U4;G3V3I1;G3V295;G3V5Z7;P60900- | Proteasome subunit alpha type;Proteasome subunit alpha type-6 | PSMA6 | 0 | 125020 |
| B4DUR8;P49368-2;P49368 | T-complex protein 1 subunit gamma | CCT3 | 0 | 124230 |
| F8WF32;P04843 | Dolichyl-diphosphooligosaccharide--protein glycosyltransferase subunit 1 | RPN1 | 0 | 119430 |
| F8WEB6;A2IDB1;Q04917 | 14-3-3 protein eta | YWHAH | 0 | 113680 |
| B5MDF5;P62826;A0A087X0W0;B4DV51;F5H0 | GTP-binding nuclear protein Ran | RAN | 0 | 112230 |
| C9JL25;E7EXB4;E7ESH4;P10809-2;P10809 | 60 kDa heat shock protein, mitochondrial | HSPD1 | 0 | 105060 |
| P08238;Q58FF8 | Heat shock protein HSP 90-beta;Putative heat shock protein HSP 90-beta 2 | HSP90AB1; HSP90AB2P | 0 | 103360 |
| F5H2D5;A0A087WVW6;Q9UHV5-2;Q9UHV5- | Rap guanine nucleotide exchange factor-like 1 | RAPGEFL1 | 0 | 98872 |
| K7EM90;A0A2R8Y6G6;P06733-2;P06733 | Enolase;Alpha-enolase | ENO1 | 0 | 97539 |
| P60842;J3KT04;J3KS93;E7EMV8;J3KSN7;J3 | Eukaryotic initiation factor 4A-I;Eukaryotic initiation factor 4A-II | EIF4A1;EIF4A2 | 0 | 92602 |
| Q9Y230;Q9Y230-2;X6R2L4;M0R0Y3 | RuvB-like 2 | RUVBL2 | 0 | 91437 |
| P31944 | Caspase-14;Caspase-14 subunit p19;Caspase-14 subunit p10 | CASP14 | 0 | 81109 |
| P17096-2;P17096 | High mobility group protein HMG-I/HMG-Y | HMGA1 | 0 | 80481 |
| C9J712;C9J0J7;C9JQ45;G5E9Q6;P35080- | Profilin;Profilin-2 | PFN2 | 0 | 78405 |
| H7C2G2;Q93070 | Ecto-ADP-ribosyltransferase 4 | ART4 | 0 | 75248 |
| G3V5T6;H0YJ77;H0YJX6;O14744-4;O14744- | Protein arginine N-methyltransferase 5;Protein arginine N-methyltransferase | PRMT5 | 0 | 75006 |

| | | | | |
|---|---|---|---|---|
| C9J8M6;P33993-2;P33993 | DNA replication licensing factor MCM7 | MCM7 | 0 | 74505 |
| F8VPF3;F8W1R7;J3KND3;G8JLA2;G3V1V0; | Myosin light polypeptide 6;Myosin light chain 6B | PDE6H;MYL6B;MYL6 | 0 | 72695 |
| P30050-2;P30050 | 60S ribosomal protein L12 | RPL12 | 0 | 71453 |
| M0QY96;M0R2I7;M0QZM1;A0A087X0X3;P52 | Heterogeneous nuclear ribonucleoprotein M | HNRNPM | 0 | 67273 |
| H0YJM8;P28074-2;P28074;P28074-3 | Proteasome subunit beta type-5 | PSMB5 | 0 | 66559 |
| A0A087WT28 | | | 0 | 66319 |
| A0A2R8YDE6;Q9UBN7;Q9UBN7-2 | Histone deacetylase 6 | HDAC6 | 0 | 65671 |
| O60701-2;O60701;D6RHF4;E9 | UDP-glucose 6-dehydrogenase | UGDH | 0 | 65282 |
| P60174-4;P60174;P60174- | Triosephosphate isomerase | TPI1 | 0 | 63533 |
| P00390-5;P00390-4;P00390-2;P00390- | Glutathione reductase, mitochondrial | GSR | 0 | 59809 |
| P28072 | Proteasome subunit beta type-6 | PSMB6 | 0 | 56206 |
| Q5VVC8;P62913-2;P62913 | 60S ribosomal protein L11 | RPL11 | 0 | 53685 |
| P47929 | Galectin-7 | LGALS7 | 0 | 47519 |
| Q5JUP3;Q9BQI0-4;Q9BQI0- | Allograft inflammatory factor 1-like | AIF1L | 0 | 46568 |
| A0A087WWI6;P61962 | DDB1- and CUL4-associated factor 7 | DCAF7 | 0 | 41768 |
| P31947-2;P31947 | 14-3-3 protein sigma | SFN | 0 | 38494 |
| P38646 | Stress-70 protein, mitochondrial | HSPA9 | 0 | 36337 |
| F5H867;F5H0E2;H0YFS2;F5GZS6;J3KPF3;P | 4F2 cell-surface antigen heavy chain | SLC3A2 | 0 | 36179 |
| G3V1A4;E9PP50;E9PK25;P23528 | Cofilin-1 | CFL1 | 0 | 34691 |
| P27348;E9PG15 | 14-3-3 protein theta | YWHAQ | 0 | 34079 |
| P23526-2;P23526 | Adenosylhomocysteinase | AHCY | 0 | 33355 |
| P31946-2;P31946;Q4VY20;A0A | 14-3-3 protein beta/alpha;14-3-3 protein beta/alpha, N-terminally processed | YWHAB | 0 | 31813 |
| H0YIV0;P14625 | Endoplasmin | HSP90B1 | 0 | 28629 |
| Q5T6W2;P61978-3;P61978;P61978-2 | Heterogeneous nuclear ribonucleoprotein K | HNRNPK | 0 | 26009 |
| H7BY16;P19338 | Nucleolin | NCL | 0 | 25316 |

| | | | | |
|---|---|---|---|---|
| A0A0B4J269;Q13509;Q13509- | Tubulin beta-3 chain;Tubulin beta-6 chain | TUBB3;TUBB6 | 0 | 24929 |
| P05198 | Eukaryotic translation initiation factor 2 subunit 1 | EIF2S1 | 0 | 23121 |
| P12004 | Proliferating cell nuclear antigen | PCNA | 0 | 22145 |
| P49411 | Elongation factor Tu, mitochondrial | TUFM | 0 | 20524 |
| M0QY11;J3KQC8;Q6NX49 | Zinc finger protein 544 | ZNF544 | 0 | 19952 |
| H0YJW3;H9KV75;P12814-2;P12814;P12814- | Alpha-actinin-1 | ACTN1 | 0 | 17968 |
| P00338-4;P00338;P00338-3 | L-lactate dehydrogenase A chain | LDHA | 0 | 17942 |
| Q5H928;Q99714-2;Q99714 | 3-hydroxyacyl-CoA dehydrogenase type-2 | HSD17B10 | 0 | 17459 |
| P49454 | Centromere protein F | CENPF | 0 | 17284 |
| D6RJ96;A0A0A0MSM0;E9PDE8;Q92598- | Heat shock protein 105 kDa;Heat shock 70 kDa protein 4L | HSPA4L;HSPH1 | 0 | 16601 |
| Q9Y512 | Sorting and assembly machinery component 50 homolog | SAMM50 | 0 | 15170 |
| E5RHW4;O94905;E5RJ09;B0QZ43;O94905- | Erlin-2;Erlin-1 | ERLIN2;ERLIN1 | 0 | 14922 |
| E9PC52;Q16576 | Histone-binding protein RBBP7 | RBBP7 | 0 | 14873 |
| A0A087WWY3;Q60FE5;P21333-2;P21333 | Filamin-A | FLNA | 0 | 14212 |
| Q14247-3;Q14247;Q14247-2 | Src substrate cortactin | CTTN | 0 | 12935 |
| M0QXF2;M0R116;B1AKY9;A0A2R8YEY8;A0A0A0MT26;P05023-2;P05023-3;P13637;P50993;P05023-4;P05023;P13637-2;P13637-3;P20648 | Sodium/potassium-transporting ATPase subunit alpha-1;Sodium/potassium-transporting ATPase subunit alpha-3;Sodium/potassium-transporting ATPase subunit alpha-2;Potassium-transporting ATPase alpha chain 1 | ATP1A3;ATP1A2;ATP1A1;ATP4A | 0 | 12165 |
| P31153-2;P31153 | S-adenosylmethionine synthase isoform type-2 | MAT2A | 0 | 10644 |
| H0Y449;P67809 | Nuclease-sensitive element-binding protein 1 | YBX1 | 0 | 10565 |
| A0A0A0MTS7;Q8WZ42-5;Q8WZ42- | Titin | TTN | 0 | 7738 |
| P22735 | Protein-glutamine gamma-glutamyltransferase K | TGM1 | 0 | 7093.5 |
| Q92820 | Gamma-glutamyl hydrolase | GGH | 0 | 6816.4 |
| A0A0D9SF54;A0A0D9SGF6;Q13813- | Spectrin alpha chain, non-erythrocytic 1 | SPTAN1 | 0 | 6755.4 |

| | | | | |
|---|---|---|---|---|
| A0A087WVQ6;Q00610-2;Q00610 | Clathrin heavy chain 1 | CLTC | 0 | 4223.6 |
| A0A0D9SFE5;E9PBF6;P20700 | Lamin-B1 | LMNB1 | 0 | 3687.3 |
| F5H2X1;H3BND8;A0A669KBL1;Q93009-3;Q93009 | Ubiquitin carboxyl-terminal hydrolase;Ubiquitin carboxyl-terminal hydrolase 7 | USP7 | 0 | 3066.8 |
| A0A075B730;P58107 | Epiplakin | EPPK1 | 0 | 2837.9 |
| F5H6X6;Q14697 | Neutral alpha-glucosidase AB | GANAB | 0 | 2767.5 |
| P35579-2;P35579 | Myosin-9 | MYH9 | 0 | 2509.2 |
| G3V4V5;H0YJP0;A0A087X2H1;Q9ULT8 | E3 ubiquitin-protein ligase HECTD1 | HECTD1 | 0 | 2391.3 |
| V9GYZ6;P07814 | Bifunctional glutamate/proline--tRNA ligase;Glutamate--tRNA ligase;Proline--tRNA ligase | EPRS | 0 | 1425.3 |
| A0A087WUZ3;Q01082-3;Q01082-2;Q01082 | Spectrin beta chain, non-erythrocytic 1 | SPTBN1 | 0 | 1153.4 |

# 7 Appendix

## 7.1 Publications

This work was published in part in the following publications:

Frey Y, Franz-Wachtel M, Macek B, Olayioye MA. Proteasomal turnover of the RhoGAP tumor suppressor DLC1 is regulated by HECTD1 and USP7. *Sci Rep*. 2022;12(1):5036. doi:10.1038/s41598-022-08844-3

Frey, Y, Lungu, C, Meyer F, et al. Regulation of the DLC3 tumor suppressor by a novel phosphoswitch. *Submitted*

Frey, Y, Lungu, C, Olayioye, MA. The regulation of the DLC tumor suppressor family. *In preparation*

Further publications:

Noll B, Benz D, Frey Y, et al. DLC3 suppresses MT1-MMP-dependent matrix degradation by controlling RhoB and actin remodeling at endosomal membranes. *J Cell Sci*. 2019;132(11):jcs223172. doi:10.1242/jcs.223172

Jensch A, Frey Y, Bitschar K, et al. The tumor suppressor protein DLC1 maintains protein kinase D activity and Golgi secretory function. *J Biol Chem*. 2018;293(37):14407-14416. doi:10.1074/jbc.RA118.003787

Meier MA, Konopa A, Frey Y, et al. Filamin A acts as a key regulator of the tumor suppressor DLC1 and the transcriptional coactivator MKL1. *In preparation*

## 7.2 Acknowledgments

In the following, I would like to thank everyone who has contributed in any way to this work.

First and foremost, I owe my deepest gratitude to my supervisor Professor Monilola Olayioye for sparking and furthering my scientific enthusiasm and giving me the chance to work on several interesting research projects. Thank you for your continuous personal and scientific support during my PhD, for all the stimulating discussions, the encouragement and the often necessary patience over the years.

I would especially like to thank Professor Hesso Farhan for the support during the writing of this thesis and for accepting the obligation to act as second reviewer and Professor Jörn Lausen for taking over the chair of my examination committee.

I want to thank Professor Angelika Hausser for your kind enthusiasm for my projects, sharing of reagents, and fruitful discussions during and outside of the lab meetings.

I wish to thank Dr. Igor Barsukov, Professor Susanne Mühlich and Professor Nicole Radde for the successful collaborations and the insights I was able to gain into the respective fields of research. Further, I want to thank Professor Boris Macek and Dr. Mirita Franz-Wachtel from the Proteome Center Tübingen for the collaboration on the mass spectrometry analyses.

Many thanks go to Dr. Stephan Eisler and Melanie Noack from the Cellular Analytics platform of the SRCSB for excellent microscopy and FACS support.

A very big thank you goes to all the amazing people from the MoAH groups for their support and great working atmosphere and all IZIans for the supportive environment. Special kudos to my benchmates David, Ismael, Florian and Stella for all the fun we had inside and outside of the lab. Moreover, I would like to thank my undergraduate students Manuel, Lilia, Viviane, Vivien, and Corinna for their interest and their work, as well as for the mentoring experience.

Finally, my huge thanks go to my friends and family for continuously backing me up and supporting me throughout my studies.